[PPA] Post Publication addition

7 Stage 3 Signal Projection

The process of communication involves a mutual agreement on the meaning of words.
- Charles Halsted, 1993

7.1 Introduction

This chapter will develop the architecture, neural paths and neural circuits used to project neural signals over long distances (greater than one or two millimeters). These circuits employ phasic propagation techniques and generate the well-known action potentials. Because of their unique response waveforms and apparent ease of interpretation, the action potentials are most often recorded and discussed in the literature.

The reader is encouraged to review Sections 3.1.2 & 3.5 before proceeding in this chapter. Much of the mathematical background supporting this discussion has been condensed. The extended mathematical background and a more in-depth discussion are available in Chapter 14 of PBV, www.sightresearch.net/pdf/14Tertiary.pdf.

The neurons of stage 3 employ a variety of mechanisms not usually discussed in neuroscience texts or found in biological curricula. Section 7.1.4 will introduce this material and provide references for further study. A stage 3 neuron also employs a unique cytology that has not been adequately addressed in neuroscience texts. Section 7.2 will address these unique features.

The main body of this chapter will address three major areas:
• How an analog-based neuron (or even a Node of Ranvier) can be easily converted into a neuron generating individual pulses (a phasic neuron) (Section 7.3.1)
• How the axon of an analog neuron can be changed physiologically to efficiently propagate pulse-coded signals (Section 7.3.4).
• The encoding/decoding protocol used in the neural system (Section 7.4).

The chapter will close with a review and discussion of some statistical techniques used in the hearing literature (Section 7.5)

Virtually no information could be found in the biological literature discussing the operational reasons for the existence of the neurons associated with signal projection. However, when the neural system is examined *in-toto*, the reason is obvious. In larger animals, the distance between individual engines (particularly between the peripheral source and the central nervous system) can exceed several meters. The use of phasic signaling techniques (action potentials) results in faster signal projection over these distances at lower power consumption.

Although action potentials exhibit a lower attenuation as a function of distance than normally found in electrotonic circuits, their propagation distance is still limited to a few millimeters. To transmit a signal over greater distances, a method of signal (waveform) regeneration is required. This is the role of stage 3 neural circuits. Three forms of specialized Activa circuits are used within stage 3. The first two operate as one-shot pulse (re)generators. The first form is used to convert analog signals into phasic signals (action potential pulses). Within Nodes of Ranvier, the second form is used to faithfully regenerate these phasic signals. These regenerators are placed at intervals (typically two millimeters) along the phasic signal paths of each neural path within all nerves and commissure. At the

termination of a stage 3 signal path, a specialized stellite neuron (defined in the next section) is used to decode the phasic signals and regenerate an analog replica of the original analog signal.

Serial combinations of these circuits are used to create individual stage 3 signal projection circuits throughout the neural system. They are specialized in that they accept only analog signals at the input to stage 3 and generate analog signals at the output of stage 3. There is no performance limit as to how many Nodes of Ranvier may be connected in series within a single axon of a ganglion cell.

Rather than use functional names for stage 3 neurons, it has been common for the histologist to assign them fanciful names. This tendency to name stage 3 neurons based initially on morphology, rather than physiological function, has proliferated. Unfortunately, it has also retarded development of the field of research in both vision and hearing. For clarity, it is best to use functional terms like encoding neurons and decoding neurons rather than terms like pyramid cells and octopus cells.

Figure 7.1.1-1 shows the general architecture of hearing. As noted above, many of the major neural groups of hearing are separated by distances greater than two millimeters. These individual groups of neurons will generally be described as engines in this work. They have been assigned a wide variety of morphological names; spiral ganglia, lateral motor nucleus, lateral superior olive, superior colliculus, etc. In this work, groups of less than four million neurons will be considered a single engine. Groups of more than four million neurons will generally be considered to consist of multiple engines. The spiral ganglia, while consisting of multiple small groups of neurons, will be considered a single engine. The large cochlear nucleus, on the other hand, consists of a group of three physiologically well differentiated engines. Within an engine, the signal processing is performed predominantly (if not exclusively) in the analog domain. The output of a typical engine may consist of a few to as many as one thousand recognizable output signals. These output signals are initially in analog form and difficult to access in the laboratory. They are more easily recognized following their conversion to phasic form for propagation to other engines.

7.1.1 The “stellite neuron” versus the stellate neuron

The profuse generic use of the term stellate cell or stellate neuron in the neurosciences makes precise discussions of the role of such neurons impossible. The term stellate (from the Greek *stelula*, or star-like) was originally used in a histological context to describe a neuron with many protuberances (neurites and axons) that did not exhibit a specific organization. Based on the uncountable adjective, many, the term was used freely and soon other authors differentiated between large and small stellate cells and between stellate cells located in different laminates of cerebral tissue. Other cells were labeled stellate outside of the cerebral cortex. The term became common in the writings of both the histological and morphological communities.

Carpenter & Sutin have provided a chart comparing different staining techniques[1]. It is obvious that a morphological name based on appearance using one stain has little relevance to work using a different stain. Young, Robert & Shofner have discussed the difficulties of using a name for a neuron that is based on imprecise morphological characteristics[2]. Their footnote is worth repeating:

> “We use the term ‘stellate’ to refer to cells that are called stellate cells in Golgi studies and multipolar cells in Nissl studies. These seem to be the same cells. The term ‘stellate’ has been used generally in studies correlating morphology and physiology because HRP injection gives a Golgi-like image of the neurons.”

They go on to identify two different classes of “stellate cells” and three classes of “chopper cells.”

This work has repeatedly asserted a basic principle. The morphological shape of a neuron is not relatable to the physiological function of that neuron. Therefore, another term is needed to provide a distinct descriptor for a functionally defined decoding neuron as found throughout the neurological system. The term stellite neuron appears uniquely appropriate for this requirement. It is a word derived from the same Greek root, synthesized for use in the metals industry and not used elsewhere at this time. Yet, it sounds similar to the alternate term stellate. These terms will be defined as follows:

Stellate neuron– Any neurological cell exhibiting multiple protuberances lacking any obvious and more specifically definable physical arrangement. Frequently contrasted with the pyramid neuron as the two cell types dominating the cerebral cortex (a typical first order dichotomy).

Stellite neuron– A neurological cell used to decode action potential streams associated with stage 3 signal projection

in chordates (vertebrates). The input to a stellite neuron is a series of action potentials. The output of a stellite neuron is an electrotonic (analog) voltage.

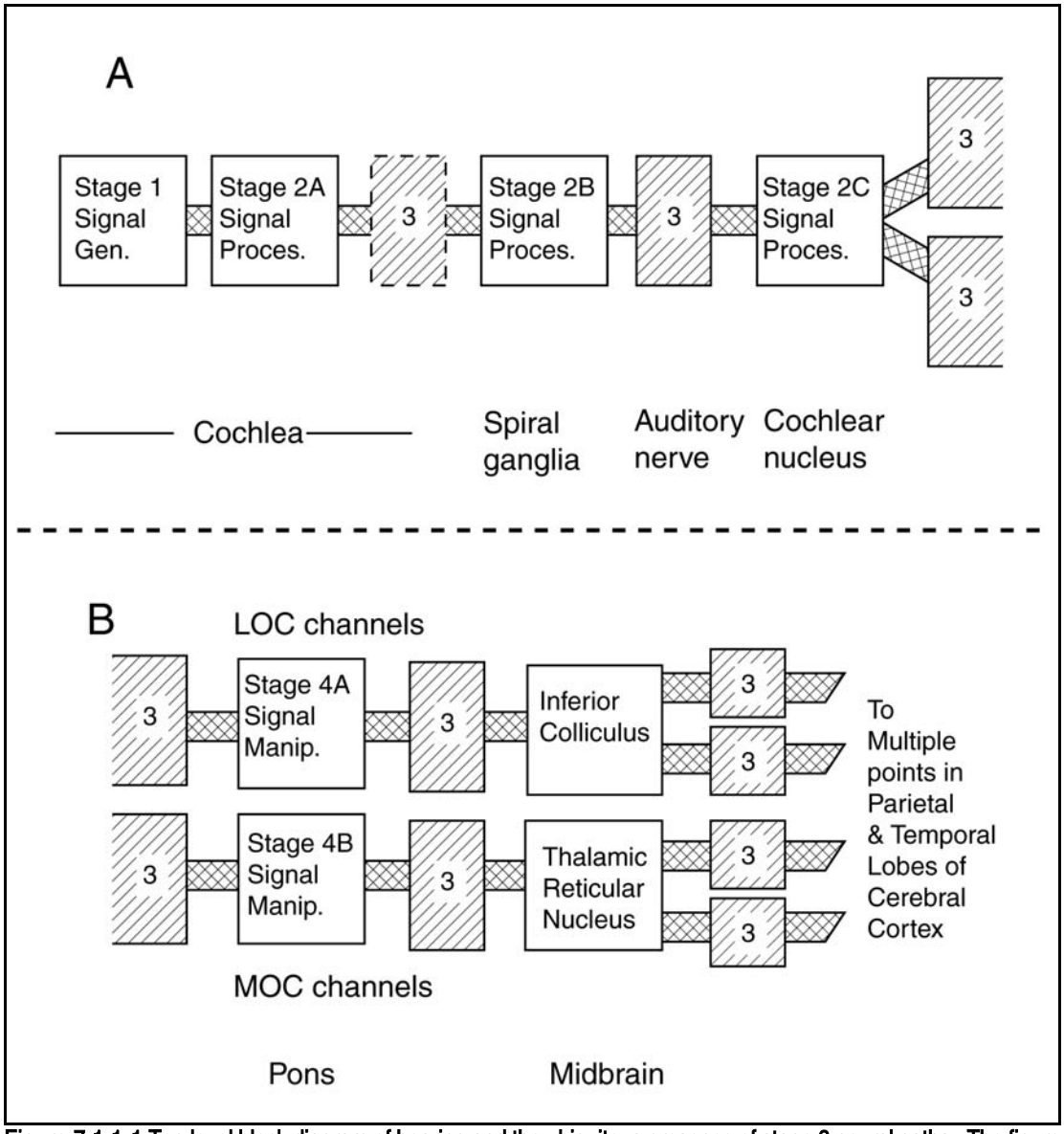

Figure 7.1.1-1 Top level block diagram of hearing and the ubiquitous presence of stage 3 neural paths. The figure is broken into two frames for clarity. Frame A is continued in frame B. Stage 3 neurons appear wherever signals must be propagated more than one or two millimeters. The cross-hatched paths represent the highly parallel circuits within an individual channel or nerve. The segments between stage 1 and stage 2A contain both Type N & B neurons. The segments between stage 2C and stage 4 contain multiple numbered signal types. LOC = channels originating within the lateral superior olive. MOC = channels originating within the medial superior olive.

The stellite neurons are usually found in laminate IV of the cerebral cortex and a similar laminate in other signal manipulation engines of the neurological system. They can be identified by the fact they are the termination point for the axons of ganglion neurons and interneurons arriving at an engine via either (inter-engine) projection nerves or (intra-engine) association nerves. These projection and association nerves may be called commissure in some contexts. The physical shape of a stellite neuron is not defined. However, they are frequently described as large stellate neurons when found in laminate IV.

A stellite neuron may be classified morphologically under a wide variety of names, including stellate neuron. However, only a stellate neuron functioning as defined above, and generating an analog output, can be considered a stellite neuron. The complement to the stellite neuron is generally described as a ganglion neuron. It accepts analog (electrotonic) signals at its inputs and generates a stream of one or more action potentials at its output. The ganglion neuron may incorporate multiple axon segments and Nodes of Ranvier within its overall morphological structure.

7.1.2 The "fundamental" stage 3 signaling path

It is frequently difficult to clearly separate the signal processing function associated with stage 2 and the signal projection function associated with stage 3 because of the morphological method of packaging the circuit elements of these stages within a single neuron. For purposes of this Chapter, the summing and differencing circuits of stage 2 found in the dendritic and poditic arborizations of encoding neurons will be considered elements of stage 2. Only the Activas within an encoding neuron (and the supporting elements connected to the terminals of these Activas) will be considered elements of stage 3.

Figure 7.1.2-1 shows the top level stage 3 signal path formed by a single pair of ganglion and stellite neurons within a larger nerve. All of the signals applied to the input of the stage 3 signal path are analog (electrotonic). Similarly, all of the output signals from the path are analog. The ensemble of neural paths at the entrance to a stage 3 segment forms a spatial pattern at a given instant of time. Similarly, the ensemble of neural paths at the exit forms a spatial pattern at a given instant. As noted previously, these two patterns may be grossly different. However, the elements of each signal path remain the same. Only the impedance values and battery potentials of those elements change. Between the ganglion conexus and the stellite conexus of a stage 3 segment, the signal is propagated as a phasic signal.

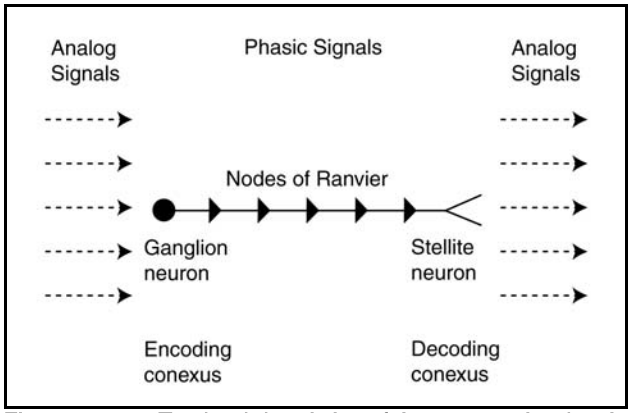

Figure 7.1.2-1 Top level description of the stage 3 signal path. Signals converge on the ganglion neuron as part of stage 2 signal processing or stage 4 signal manipulation. Signals fan out from the stellite neuron as part of the stage 4 signal manipulation.

Each of the neural paths within a signal propagation nerve consists of three critical components as shown in this figure. Each path can be described as consisting of a ganglion neuron that is used to encode the analog information into a phasic signal and a stellite neuron that is used to decode the phasic signal in order to recover the original analog signal. Often multiple Nodes of Ranvier (NoR) are found between a single pair of ganglion and stellite neurons. Each of these NoRs is used to regenerate the action potential pulse stream at regular intervals of between one and two millimeters.

Figure 7.1.2-2 shows the complete circuit diagram of a fundamental (or generic) stage 3 neural path. It begins with the receipt of a signal at the emitter (terminal E') of the first Activa in the first conexus of the chain. This conexus acts as the analog-to-phasic signal encoder. After encoding the signal at the collector of the Activa is propagated along the axon segment acting as a coaxial electrical cable. Just before the signal weakens to an unreliable amplitude, it encounters the next conexus that is designed to operate as a pulse signal regenerator. This regenerator circuit, morphologically described as a Node of Ranvier, recreates a full amplitude action potential exhibiting a finite delay. This action potential is propagated along the next axon segment. For long signal paths, the Node of Ranvier and its axon segment can be replicated as many times as required. The phasic signal delivered to the emitter of the decoding conexus, at G, will be a faithful reproduction of the original pulse train at F'. Its amplitude is unimportant. The critical fact is the relative time delay between adjacent pulses is preserved. As a result, the analog signal recovered at H is an adequate replica of the analog signal originally presented at E'.

A critical feature of this neural path has caused unnecessary errors in the literature. The Nodes of Ranvier introduce a fixed delay (typically between 0.5 and 1.0 ms) into the neural path as they regenerate the individual action potentials. The more NoRs associated with a given length of a neural path, the greater the fixed delay introduced into the path. When investigators attempt to calculate the velocity of neural signal propagation, they frequently overlook this delay and consider the total delay as representative of the velocity of propagation over a given distance. The resulting calculation correctly describes the average velocity of propagation (typically 44 m/sec). However, the instantaneous

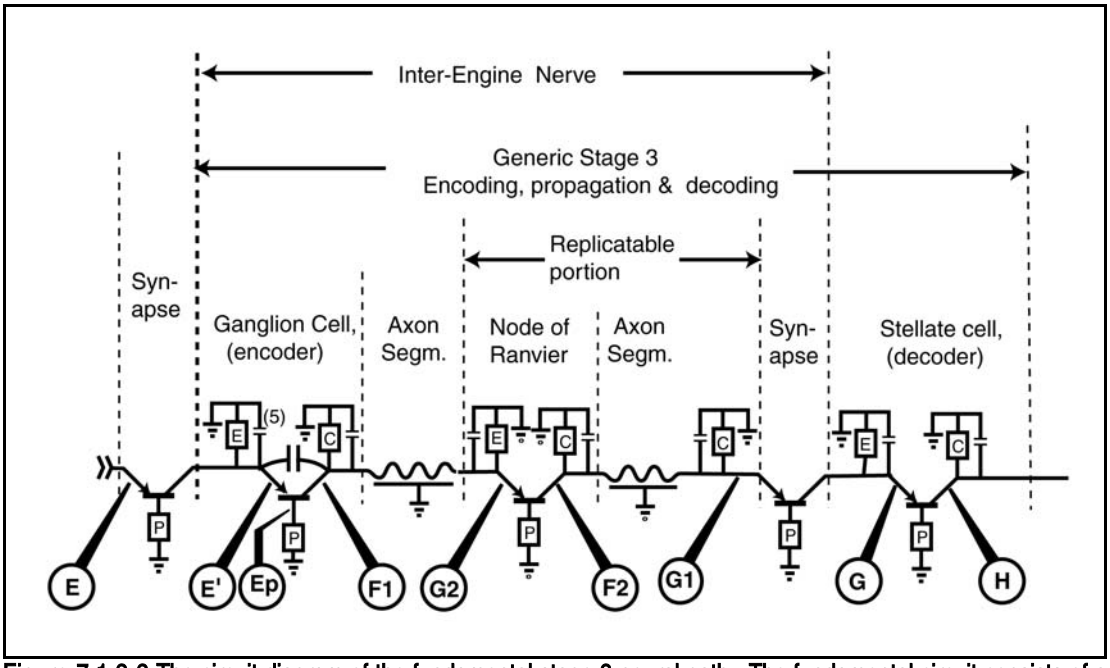

Figure 7.1.2-2 The circuit diagram of the fundamental stage 3 neural path. The fundamental circuit consists of a single encoding conexus, a single decoding conexus, and as many regenerative Nodes of Ranvier as required by the physical length of the circuit. The pulse stream delivered to node G is a faithful reproduction of the pulse stream delivered to node E'. See text.

velocity of neural signal propagation along an axon is considerably higher (typically 4400 m/sec). See Section 7.4.5.Stage 3 employs two distinct classes of encoding neurons, those which respond to monopolar input signals and generate trains of action potentials based on a "driven" oscillator, and those that respond to a bipolar input signal and generate trains of action potentials based on a "free-running" oscillator. The driven oscillators exhibit a rate of action potential generation equal to zero, in the absence of extraneous inputs. The free-running oscillators exhibit a nominal value near 30 pulses per second with a small standard deviation (in the absence of any input signal). Unfortunately, extraneous acoustic inputs are common in the hearing system (especially when closed auditory canal techniques are used). These extraneous signals frequently obscure features of the reported data, particularly when histographic techniques are used (Section 7.5).

The above representations can be used to draw the detailed circuit diagram associated with any neural path within the hearing modality. However, this task remains difficult because of the inherent complexity of the hearing circuitry required to satisfy a multitude of individual requirements. As an example, in the auditory nerve there are about three times more neurons than found in the complete array of sensory neurons. Many of the auditory nerve neurons exhibit responses far more complicated than those at the output of the sensory neurons[3].

7.1.3 Background

Most of the data related to stage 3 projection neuron signals in hearing have related to the auditory nerve emanating from the spiral ganglia. Frequently the signals from the IHC to the spiral ganglia are carried by neurons labeled type I and those from the OHC are carried by neurons labeled type II in the literature. To avoid later confusion, these afferent neuron types will be labeled type B (broadband) and type N (narrowband) respectively in this work. Following the auditory nerve, the various signal types, of which there are many, will be identified by type number using roman numerals.

Schwartz has reviewed the morphological characteristics of the neurons of the spiral ganglia[4]. She has provided statistical data on the size of these neurons in the albino rat. She has also divided them into two morphological classifications. The first consists of larger myelinated neurons with the second consisting of smaller unmyelinated neurons. No discussion was presented concerning the spontaneous rate of action potential generation between these

two classes. A figure is presented attempting to interpret the data available concerning the innervation of the sensory neurons over time. The idea that the two types of primary, auditory neurons have two different peripheral innervation patterns was refined by Kiang et al, in 1982. Brown & Ledwith have discussed two classes of afferent neurons as well as two classes of efferent neurons related to the spiral ganglia based on morphology[5].

Evans noted that the action potential pulse trains he measured in the guinea pig frequently extended beyond the duration of the stimulus[6]. He noted that Tasaki (1954) had observed the same phenomenon. Besides the obvious delays related to the location of the neurons accessed, the reason for these delayed peaks will become obvious during the discussion in this chapter.

As noted by Geisler[7], the dynamic range of signals following stage 1 within the auditory system "are functionally limited to approximately two orders of magnitude." This work uses a slightly larger and more specific value of 200:1. In the case of stage 3 signals, this range is expressed as a difference in action potential pulse rates, not pulse amplitudes. Recognition of this dynamic range limit has a major impact on the interpretation of many neural "tuning curves" (Section 4.6.2).

The number of neurons within the auditory nerve throughout the phylogenic tree gives a coarse estimate of the importance of hearing in a specific species. Harrison & Howe have given a table of values for a dozen representative species[8]. As expected, the number of neurons in the auditory nerve of man (a "visual species") is far below that of the animals known to use hearing extensively. Various investigators give 25,000 to 31,000 neurons in man. Porpoises and some whales exceed 210,000. The distribution of neurons within the auditory nerve of a given species has not been documented well. Brown & Ledwith have described the neurons in the auditory nerve of the mouse[9]. Their data is all based on morphology.

7.1.4 Types of coding used in hearing and other sensory systems

In neural signaling, the separate concepts of coding and modulation play major roles. It will be important to differentiate between the coding techniques occurring naturally within biological hearing and the modulation techniques employed in laboratory instrumentation to explore the hearing modality. It will also be important to differentiate between the simple (cochleotopic and largely serial) coding used within the PNS and the more sophisticated, and abstract, (largely parallel) coding used within the CNS. The forms and characteristics of these processes are defined at a very basic level in this section.

The methods used to project signals over relatively long distances within neurological systems are not those commonly discussed in elementary communications texts. As a result, attempts to adopt the more common schemes in the hearing literature have not borne fruit and the discussions of coding and modulation have been primarily conceptual[10]. The techniques used are very sophisticated and highly tailored to the requirement. To appreciate the individual features and subtleties of neurological signal projection, a background in the more common forms of modulation is required.

The intent of this section is to uniquely define the operational and mathematical relationships associated with the generic transfer functions used within stage 3 Signal Projection. There are three. The first is the transfer function relating an analog waveform, typically produced as the generator waveform at the axon of a sensory neuron, to the action potential at the output of an encoding (ganglion) neuron. The second is the transfer function associated with the decoding/demodulation mechanisms of hearing (and vision if not all of neurology) that recovers the previously encoded information in analog form. This is accomplished in a functionally defined decoding (stellite) neuron. The third is the transfer function associated with the pulse regeneration circuit generally known by the morphological designation, Node of Ranvier.

7.1.4.1 Terminology specific to coding/modulation

Coding and modulation are words frequently used in the vernacular. It is important to develop a specific definition of these terms for use in this Chapter. The following definitions are in general agreement with those of Panter. For a broad review of encoding/modulation theory, his text is recommended[11].

Modulation may generally be defined as the process whereby a message is transformed from its original form into a signal that is more suitable for transmission over the medium available between the source location and the intended receiving point. The transformation generally replaces one symbol (or minimum identifiable element) in the original form for one symbol (or minimum identifiable characteristic) in the modulated signal.

Coding is a more sophisticated technique than modulation. Coding is the process of converting each message symbol

or amplitude into a number of symbols (that are uniquely related to both each other and the original symbol) in the resultant coded signal. Converting a specific analog voltage into an eight, sixteen or thirty-two bit pulse stream is an obvious example of coding. Converting a specific analog voltage into a specific frequency relative to a reference frequency is a clear case of modulation. However, there are a large variety of intermediate situations that do not lend themselves to such clear differentiation.

Serial symbol transmission involves the sequential transmission of information-bearing symbols over a single transmission channel. This is the type of information transmission generally associated with the peripheral neural system. This mode involves a very low overhead but is not very fault-tolerant unless redundant signal paths are used to project a pattern of signals (such as a spatial visual pattern or a musical chord within the hearing system).

Parallel symbol transmission involves the sequential transmission of sets of information bearing symbols over multiple parallel transmission channels. All symbols of a given set are transmitted simultaneously. There are indications that many signals transmitted within the central nervous system employ parallel symbol transmission. Under specific conditions, this mode of transmission is very fault-tolerant. However, it can occasionally project ludicrously false information when a fault occurs.

7.1.4.2 Specific background related to coding/modulation

The hearing literature contains virtually no material discussing the potential forms of encoding used in that modality. One early paper is essentially lost[12]. Since about 1950, the conventional wisdom has been that the primary method of signal transmission in hearing has employed frequency modulation. The term was used generically. Unfortunately, this was a superficial assumption that has prevented further advancement in the field. This assumption is not supported here.

Modulation and encoding techniques are used whenever a signal is not in ideal form for projection over the medium separating the originating location and the desired receiving location. While the terms modulation and encoding are frequently used interchangeably, they are distinct in the discipline of information transfer, both being variants of a term that can be described using the label, angle modulation.

> It is unfortunate that the broadcast designation "frequency modulation" does not apply strictly to the actual type of modulation used in that service. Broadcast radio employs phase modulation of an oscillator by a stimulus waveform that has had its high frequencies boosted by a pre-emphasis circuit with a time constant of 75 microseconds. The result is a hybrid output that exhibits true phase modulation for low frequency input frequencies, but frequency modulation for high input frequencies. In the absence of such pre-emphasis, both regular FM radio stations and stage 3 neural circuits of the free-running type employ phase modulation.

The nominal goals in neurological signaling channels are four. First, provide the best possible estimate of when a stimulus first appears. Second, provide an adequate estimate of the intensity of the stimulus. Third, avoid introducing noise into the channel to the greatest possible extent. Fourth, achieve the above goals at the least possible energy cost. The primary purpose of encoding/modulating the signals in the stage 3 circuits of the neurological system is to improve propagation efficiency over distances larger than 1–2 millimeters. Power consumption savings amounting to several orders of magnitude are achieved in this way.

The signals to be projected over the channels of the typical neural system fall into two distinct categories. First, monopolar amplitude signals characterized by a distinct start time. Second, bipolar amplitude signals where the start time is less important than in the monopolar case. While there are data supporting the use of bipolar signaling in hearing (Hind et al. with the squirrel monkey[13]) the predominant form of analog signaling in the peripheral hearing system is monopolar.

Having specified these goals and characteristics, it becomes easy to focus on which methods of coding/modulation are likely to be used in neurological signaling and which are not. The basic biological hearing system requires a signaling system that is energy efficient, provides the earliest possible indication of danger, and can quantify that danger. All other features are essentially add-ons to satisfy an ecological requirement. To meet the above requirement, the hearing system has adopted the signaling method common to all neurological systems and used by all other sensory modalities. It employs pulse position encoding in the specific form of time-delay encoding (TDE). This coding mechanism is ideally suited to meeting the above primary requirements. It does not send any pulses until a threat arises. It sends a first pulse as soon as the sensed signal exceeds a low threshold. It sends subsequent pulses with a time delay that is inversely proportional to the strength of the signal generated by the threat.

While the type of encoding used in hearing is often assumed to be frequency modulation, it is not. The TDE method

of encoding is remarkably easy to implement, circuit-wise. A very important feature of time-delay encoding, not found in frequency modulated encoding, is the ability to transmit both continuous analog information and the precise starting time of an impulse type stimulus. This second feature is key to extracting source location information from the signals received at the cortex.

The action potential is the observable result of the mechanism used to implement TDE in hearing. The action potential is generated by a driven (aperiodic) reflex oscillator operating in the switching mode. These circuits generate pulses with a pulse-to-pulse interval that is inversely proportional to the analog signal applied to their control terminal. As a result, the output pulse train is described as of the TDE type. While a series of pulses generated in this manner may appear to the unaided eye to be frequency modulated, *the typical action potential pulse stream is not frequency modulated*. Section 7.3.4 will develop these facts in more detail.

Specialized neurons are used to implement the signal encoding and decoding functions. Two functional classes of ganglion cells but only one functional class of stellite cell are normally used. The ganglion cells only vary in their electrolytic bias and therefore cannot be reliably differentiated based on morphology. They are best differentiated by the local topology where they are found. A beauty of the design architecture of the neural system is that only one class of decoding (stellite) neuron is needed to recover all of the signals carried within stage three signal paths.

7.1.4.3 Signals associated with summing and differencing channels

The encoding neurons frequently operate in a dual stage 2/stage 3 mode. Besides generating action potentials, they frequently perform analog signal processing at their inputs. This signal processing can sum analog signals from multiple sources as well as take the difference between such analog signals. Gelfand provided a caricature of the action potential stream generated in the auditory nerve in response to a variable amplitude stimulus[14]. While reasonable, it only illustrates the summation case. Figure 7.1.3-1 expands on the Gelfand figure and describes the signals found in both differencing and summing channels *in-vivo*. The SR of the summing circuit would typically be zero *in-vitro*. The SR of the differencing circuit is typically its nominal pulse rate in the absence of stimulation, but it may vary due to extraneous stimulation *in-vivo*.

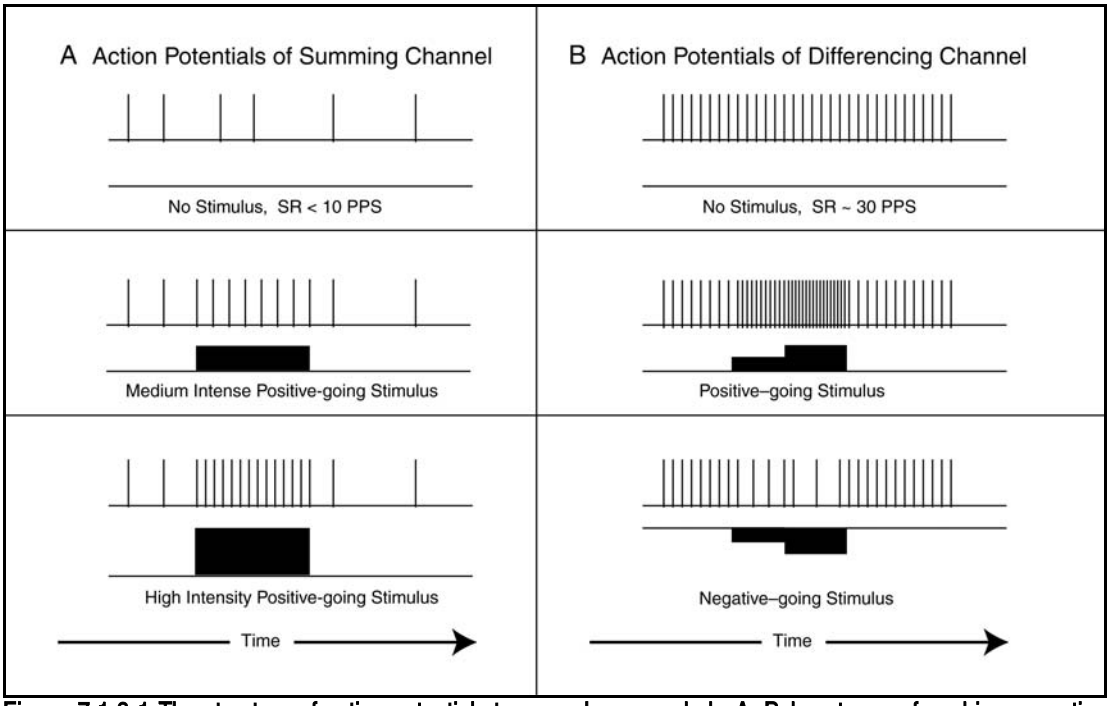

Figure 7.1.3-1 The structure of action potential streams when encoded. A; Pulse streams found in summation channels generally associated with parasol type ganglion neurons. The neuron responds only to positive-going monopolar waveforms. The pulse interval decreases linearly in response to the amplitude of a positive-going analog input signal. B; Pulse streams found in differencing channels generally associated with midget ganglion neurons. The neuron responds to bipolar input waveforms. The pulse interval decreases linearly in response to positive-going analog signals and increases linearly in response to negative going analog signal. Pulse frequencies change as the inverse of the pulse interval.

7.2 The morphology, cytology and topology of stage 3 projection neurons

As shown in Figure 7.1.2-2, the generic neural signaling path can be described morphologically. It consists of a series of electrolytic amplifiers and their associated components forming a discrete circuit (or conexus) separated by electrical conduits. Each conexus can act as an analog amplifier or as a phasic pulse generator depending on the values of its electrical components and the applied biases. To understand the neural signal path at a more detailed level, it is necessary to measure and understand the electrical characteristics of each of these amplifiers and conduits. The electrical properties are addressed in the next section.

Abbas & Miller have provided a top level morphology of the neural signaling path in 2004 that is similar to that above[15]. However, they did not develop the electrolytic semiconducting features of the overall circuitry. Nor did they explore the transmission line properties of the internodal segments which they treated as simple RC circuits. Lacking that development, their circuitry remains a chain of two-terminal nodal and internodal segments. The nodal elements consist of the primitive concept of a neuron developed in a series of papers by Huxley and Hodgkin in the 1950's[16]. Abbas & Miller provide a series of references to more complex models and focus on the signaling nodes as stochastic rather than deterministic circuits.

> For completeness, it is important to note the neuron examined by Huxley and Hodgkin was not a stage 3 signal projection neuron. It was a special type not found in the neurons of *Mammalia.* The type is normally found in the command generation portion of the stage 6 motor neurons. Their giant axon (a few cm long by one mm diameter), probably of the Atlantic squid *Loligo pealei* (< 60 cm in length), is part of a pair of neurons used in bilateral *Mollusca,* and possibly other animals that use a swimming motion, involving multiple muscles along each of their sides operating sequentially for purposes of locomotion. Section 10.3.7 of "Processes in Biological Vision" discusses this specialized type of nerve in greater detail.

Abbas & Miller did note the major difference in the capacitances of the nodes and internodes. This feature is of critical

importance to the propagation characteristics of the neural system. "The specific internodal capacitance and conductance (per unit length) were orders of magnitude smaller than the nodal values." They noted that myelination contributed greatly to this difference in capacitance. However, they did not recognize the fact that the myelination brought the reactance due to the capacitance per unit length down to the level of the reactance due to the inductance per unit length. When the two reactances are similar, the internodes become non-dispersive and nearly lossless with respect to the propagated signal.

Yost has given the most recent textbook interpretation of the ganglion (encoding) neuron within the auditory system[17]. His figure emphasizes the morphology of the cell. His use of the term neurolemma to describe a membrane exterior to the myelin sheath will not be used here. In accordance with this work, the phasic signal is transported along the neuron by propagation, and not by Yost's designation, conduction.

7.2.1 The morphology and cytology of the stage 3 neuron

As noted earlier in this work, the physical shape of a stage 3 neuron has little relationship to its function. The encoding neurons of hearing vary in morphology just as they do in vision. The encoding neurons of the PNS tend to be simple neurons traditionally described as bipolar. They generally have a neurite input structure separated from an axonal output structure by a soma. However, most of the soma is not functional with respect to signaling. Hence, it is sometimes placed farther from the signal path, resulting in a morphological structure that is called monopolar (based on the single structure emanating from the soma). The functional parts of the neuron remain the neurite input structure separated from the axonal output structure by a conexus containing an Activa. When generating action potentials from analog inputs, these neurons are functionally described as ganglion neurons. In the context of hearing, neurons of this type are most frequently associated with the spiral ganglia (groups of afferent neurons at peripheral locations generating action potentials). However, they are present at the output of every engine of the neural system when it is desired to transmit signals to another engine more than two millimeters away.

The encoding neurons of the CNS tend to be more complex in structure than those of the PNS and are frequently labeled pyramid cells. This is particularly true when the neurite input structure is clearly divided into a dendritic structure at the apex of the pyramid, a poditic structure at the edges of the base of the pyramid, and a single axon emanating from the middle of the base. Other investigators identify these neurons using names such as globular, star-shaped (stellate) or other less descriptive terms. Functionally, the encoding neurons are all ganglion neurons generating action potentials.

Decoding neurons are not known to exist in the PNS of hearing prior to the cochlear nucleus. However, they may be found in the spiral ganglia based on the significant difference between the count of neurons going into and coming out of that element. Decoding neurons are largely concentrated in the middle laminates of CNS tissue. Stellite neurons (as defined here) are typically spherical with only one major input and a multitude of potential outputs. The one major input may consist of multiple synapses from multiple branches of a single axon (except in the case of stellite neurons performing coincidence detection between axon signals from multiple neurons). The stellite neurons are difficult to identify at the cytological level because of their similarity to so many similarly shaped neurons. They are more easily identified by their location within the layers of the neural matrix at the termination of myelinated axons from ganglion neurons of remote engines (via nerves or commissure). By definition, they receive action potential streams at their input and provide analog signals at their outputs.

The encoding neurons frequently exhibit a larger hillock than do the neurons described in Chapter 3. The purpose of the larger hillock is to provide the large capacitance required to support monopulse oscillation. A second feature is described in Figure 7.2.1-1. It shows the static details of the axon segment found within a stage 3 signal propagation neuron. Any electrical charge injected into the axon from the power source or the synapse on the right proceeds to the outer perimeter of the axoplasm by electrostatic repulsion. Note the extreme thinness of the region occupied by the charge, typically 0.002 microns, a thickness even less than that of the lemma enclosing the charge. The dashed electric field lines suggest the bulk of the axoplasm is electrostatic. The changes in potential are concentrated in the terminal areas. The myelin sheath is shown in caricature along the lower edge of the axon segment instead of surrounding its full circumference. The sheath is interrupted in the post junction and pre junction regions. The myelin sheath typically increases the thickness of the combined myelin and plasmalemma, and decreases the capacitance of that package, by a factor of 100:1, except in the junction regions.

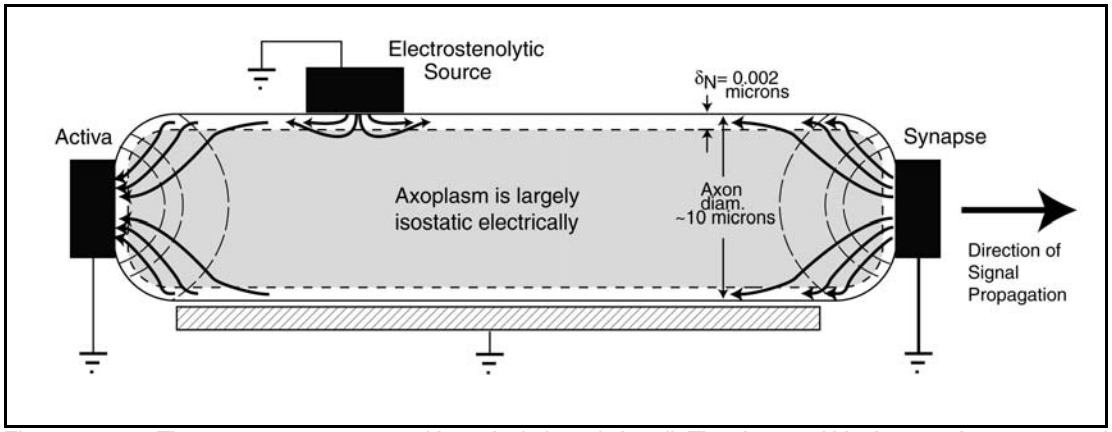

Figure 7.2.1-1 The axon segment as a multi-terminal electrolytic cell. The charge within the axon is concentrated along the external lemma by electrostatic repulsion. The bulk of the axoplasm is at a common potential. A majority of lateral charge motion is associated with the thin layer adjacent to the lemma. A myelin sheath is shown along the bottom of the axon but omitted from the top for clarity. The curved arrows represent the flow of electrons. See text.

The dynamic operation of this complex structure is addressed in Section 7.4.4.

The decoding (stellite) neurons also exhibit a large hillock but do not employ a myelinated axon. In this case, the capacitance provided by the hillock is even larger than in the encoding neurons. The capacitance is sized to generate an RC network of appropriate time constant. Functionally, the resulting decoding neuron represents a diode in series with an RC integrating circuit. Its output is a reproduction of the analog signal applied to the encoding neuron delayed by an interval calculated from the distance from the encoding neuron divided by the average propagation velocity of the channel between the two neurons.

7.2.2 A defining morphological feature of a stage 3 ganglion neuron

A defining morphological feature of a functionally defined ganglion cell is its multiple serial sections, each section containing a Node of Ranvier and a myelinated axon segment. As noted earlier, the purpose of this feature is energy conservation in signaling neurons significantly more than two millimeters long. As noted in this work, a Node of Ranvier may occur before or after the soma of a ganglion neuron.

In the past, the conventional wisdom, expressed by many authors, was that the axon of most neurons consisted of a continuous core with the signal propagated along the axon in a continuously decaying manner. The purpose of the Nodes of Ranvier was essentially unknown and the purpose of the myelin sheath was usually related in vague language to the insulation surrounding an electrical cable. More recently, it has been recognized that the signal traveling along an axon is regenerated at each Node (with the mode of signal transmission described as saltatory) and that the axon actually consists of semi-independent regions connected at the nodes, in the manner of a string of sausages. An early electron micrograph from Ottoson[18], reproduced as Figure 7.2.1-2, illustrates the physical separation of the axon segments. Similar figures can be found in Figure 2-6, 2-18, 2-19 & 2-20 of Waxman et al[19]. It is extremely difficult to obtain a good electron micrograph of a Node of Ranvier in cross section that includes the minute active area, the Activa. While difficult to confirm from a single image, study of a group of images confirms that the core of the axon is not continuous at the node, there is a juxtaposition of membrane walls. The active region of the Node, the area of the Activa, is approximately 200 Angstrom wide and 100 Angstrom in height (generally a diameter). The width dimension is made up of the two lemma and the hydronium-liquid-crystal between them. The overall width and diameter of the Node are considerably larger because of the supporting elements involved.

The functional details of this arrangement are discussed in Section 3.6. An important characteristic of this configuration is the break (or window) in the myelin sheath at each Node of Ranvier (not necessarily visible in micrographs selected to illustrate other features). This break provides chemical access to the lemma of the two axon segments for purposes of electrostenolysis as well as electrical contact between the poditic terminal of the Node and the surrounding interneural matrix. With this topology and circuitry in mind, portions of Tasaki's[20] text on the effects of pharmacological treatments become clearer. He notes that the effect of an anesthetic on the myelinated portion of a neuron is virtually nil. It is only when it is applied to the area of a Node of Ranvier (or other terminal area) that the anesthetic has an impact.

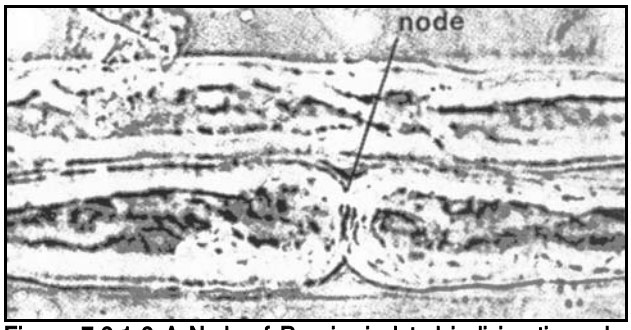

Figure 7.2.1-2 A Node of Ranvier isolated in living tissue by dissection. The internal synapse between the two segments of the axon is clearly seen. It is also clear that the point of contact is extremely small and that this region has direct electrical contact with the medium surrounding the nerve at this "void" in the myelin sheath. From Ottoson, 1953.

7.3 The physiology and operation of stage 3 pulse and hybrid neurons

The neurons of stage 3 are concerned with the transmission (projection) of neural signals over distances too great to be accomplished effectively by analog signaling. They are found in all mammalian, and generally all chordate signal paths of more than two millimeters. Stage 3 neurons are the main constituents of the bundles of neurons known morphologically as nerves in the PNS and commissure within the CNS.

As described superficially in Figure 7.1.2-2, the fundamental stage 3 signal path consists of an initial neuron capable of encoding an analog signal into a phasic pulse stream using time delay encoding, generally one or more regenerative circuits, represented morphologically by Nodes of Ranvier, and a final neuron capable of decoding the phasic pulse stream and recovering the desired analog signal information. In some cases, multiple decoding neurons are used to recover other different pieces of information relative to the same original analog waveform. Generally, there is one synapse between the final axon segment of the last regenerator circuit and each decoding neuron. In the following discussion, the physiological encoding neuron will be defined morphologically as a ganglion neuron and the physiological decoding neuron (the stellite neuron) will be defined morphologically as a stellate neuron.

A unique feature of the stage 3 neurons is the common occurrence of a string of physiologically distinct regenerative circuits being morphologically associated with the encoding circuit for purposes of homeostasis. The resulting morphologically identified ganglion neuron may be more than one meter long.

A second unique feature that makes understanding the auditory system more difficult is the reported and documented occurrence of the encoding circuit, and possibly several regenerative circuits, prior to the soma of a neuron. These active circuits have been labeled "beads" in the histology of the cochlea. The regenerative circuits described above should be described morphologically as Nodes of Ranvier wherever they occur, in accordance with their functional role.

To simplify the exposition, this section will develop the physiology of the Node of Ranvier before discussing the ganglion and stellite neurons.

This section will continue to describe the operation of neural circuits using only electrolytic mechanisms. The only chemical processes involved will be the electrostenolytic processes providing the electrical potentials required for the operation of the active circuits.

Until quite recently, it has been difficult to record signals from within a neuron except using patch-clamp techniques contacting the axoplasm. The majority of the available data has been acquired by placing probes in the interneural matrix adjacent to the axons, and occasionally the dendrites of stage 3 neurons. Siegel demonstrated the feasibility of achieving a patch-clamp condition on the dendrite synapsing with the axoplasm of a sensory neuron of hearing in 1992[21]. This confirmed the practicality of measuring the voltage potentials within a dendrite and was compatible with measuring the current through the synapse leading to that dendrite. His recordings frequently showed the signal as it was transferred across the synapse along with artifacts from the orthodromic neuron acting as a stage 3 encoder.

Steriade et al. have addressed the difficulty of interpreting neuronal oscillations in neural circuits of the brain without claiming any understanding of the underlying mechanisms[22]. They suggested the problem is the lack of a formal mathematical base for these mechanisms. An underlying theoretical framework is more important. The section will develop and demonstrate the applicability of such a framework. The suggestion of Goldbeter & Moran that a set of differential equations based on phase plane analysis can describe the oscillations of a neuron is correct. However, their supposition that the phase plane used is derivable from an autocatalytic (chemical) mechanism appears unproven[23]. Their resulting hypotheses, involving contorted chemistry, are not needed when the basic physics of the situation is examines as in Chapter 3.

7.3.1 The generic stage 3 phasic neurons as relaxation oscillators

The previous investigation by this author of the physiology of the visual system documented the role of the Node of Ranvier as a regenerative repeater typically found orthodromic to the soma of its neuron[24]. The physiology of the hearing modality supports an expanded role for the Node of Ranvier. As noted earlier, it appears that within the cochlea, a conexus equivalent to a Node of Ranvier can occur before the soma of the neuron. It also appears that the first of these equivalent NoRs can act as an encoding conexus instead of a regenerative repeater. While more experimental verification is warranted, these findings are consistent with the generic form of the neuron presented in Chapter 3.

This section will focus on the forms of the regenerative repeater most easily identified morphologically. In their most common form, these circuits generate a single positive-going monopulse waveform in response to a positive-going monopulse stimulus exceeding a threshold level.

7.3.1.1 The interneuron and Node of Ranvier as regenerators

The physiology of the Node of Ranvier, the synapse and any fully embedded conexus are nearly the same. The difference between them is primarily in their morphological association with the adjacent neurons. The synapse forms a distinct demarcation between the morphology of two neurons while the Node of Ranvier is largely encapsulated within one neuron (except for electrolytic access to the surrounding extra-neural matrix). The fully embedded conexus cannot be recognized morphologically. Only electron microscopy can identify its cytological organization and biasing.

Figure 7.3.1-1 provides a more detailed look at a single generic junction between two neural conduits. For purposes of this section, the nucleus and soma of the interneuron will be ignored. They are shown only to supply context. As shown, the figure represents the Node of Ranvier between two axon segments. By changing the axon segment on the left to a dendrite, and adjusting the biases, the same configuration can be considered a monopolar neuron.

Frame A shows the basic conexus associated with any junction in the neural system in circuit diagram form. It consists of a single Activa and its supporting electrolytic circuit elements, connected into the pre and post junction conduits and the surrounding electrolytic environment.

Frame B provides a composite caricature of both the morphological and electrolytic features of the typical conexus amid the pre and post junction conduits and the environment. The shaded areas represent molecularly asymmetrical, Type 2, plasmalemma. The unshaded areas of the lemma are of Type 1. The small electrical networks represent the fundamental electrical properties of the Type 2 lemma in the respective shaded areas.

Frame C provides a more integrated view of the generic stage 3 neural junction. The nomenclature has been generalized from that used earlier to more appropriately describe the stage 3 neuron. The small circuit diagrams of the asymmetrical lemmas forming junctions with adjacent conduits have been replaced with their more concise form, an active electrolytic semiconductor device, the Activa. This notation highlights the functional nature of the typical junction. It is to provide unidirectional transfer (with or without amplification) of the electrical signal propagating along the neural path. This unidirectional feature is established by the electrical biases applied to the otherwise bidirectional Activa.

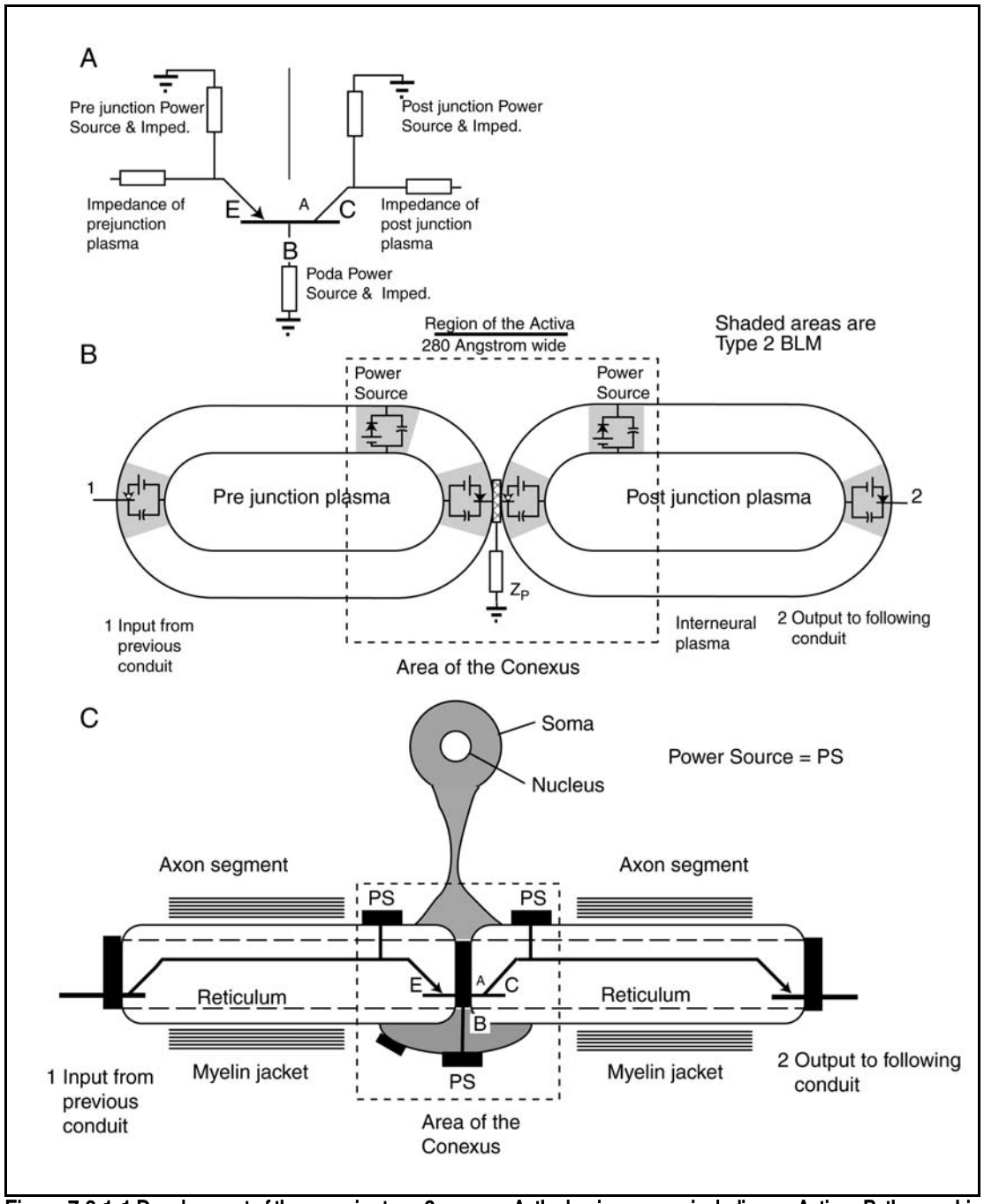

Figure 7.3.1-1 Development of the generic stage 3 neuron. A; the basic conexus including an Activa. B; the graphic representation of a typical stage 3 junction between two conduits. C; a more schematic description of a typical stage 3 conexus between two conduits. If the nucleus and soma are ignored, the circuit is typical of a Node of Ranvier. Note the diode symbology at the two extreme ends of the figure. The input diode on the left (half of the Activa symbol) typically forms the collector portion of the preceding junction. The output diode on the right (half of the Activa symbol) typically forms the emitter portion of the orthodromic junction. See text.

Several critical features of the stage 3 conexus are shown in frame C. The regions of the axon segment immediately adjacent to the conexus are not covered by myelin. These regions support the electrostenolytic processes providing

power to the conexus (and labeled PS). They also form large value capacitances, due to the extreme thinness of the lemma, when needed to support relaxation oscillation by the conexus. Farther from the conexus, the myelin encloses the axon segment and prevents any of the external matrix fluids from contacting the lemma. This action insures the capacitance per unit distance is orders of magnitude lower than it would be for the unwrapped lemma. This major reduction in the capacitance per unit length is critical to the propagation of the action potentials of stage 3 along the conduit (See Section 7.4.5).

The symbols at the extreme ends of the two conduits represent the "functional diodes" associated with the synaptic junctions at those locations. The diode symbol on the left represents the post junction diode (associated with the collector of the conexus at that location). This diode is typically part of the Activa forming the synapse and is reverse biased. The diode symbol on the right represents the pre junction diode normally associated with the synapse at that location. This diode is typically forward biased. In patch-clamp experiments, it frequently acts as a nonlinear resistance in shunt with the other impedances associated with the plasma of the axon segment. This shunt element frequently degrades the electrical performance of the post junction circuitry, resulting in a voltage-current characteristic that approaches a straight line instead of the ideal exponential curve. Both diodes are morphological parts of either another regenerative NoR or of a synapse.

7.3.1.2 The detailed circuitry and operation of the Node of Ranvier

The circuitry of the conexus within the Node of Ranvier is typical of any man-made common-base semiconductor (transistor) circuit. Such circuits have been used commercially for many years[25]. The only difference is that the neural circuit is formed of liquid-crystalline-state semiconductor materials instead of solid-state semiconductor materials. The common-base circuit is particularly subject to oscillation and this susceptibility has been widely used in practice. The susceptibility arises if the impedance of the base (or poda) circuit is high and a significant reactive impedance is found at one of several potential locations in the circuit. The following paragraphs will explore these situations using Figure 7.3.1-2.

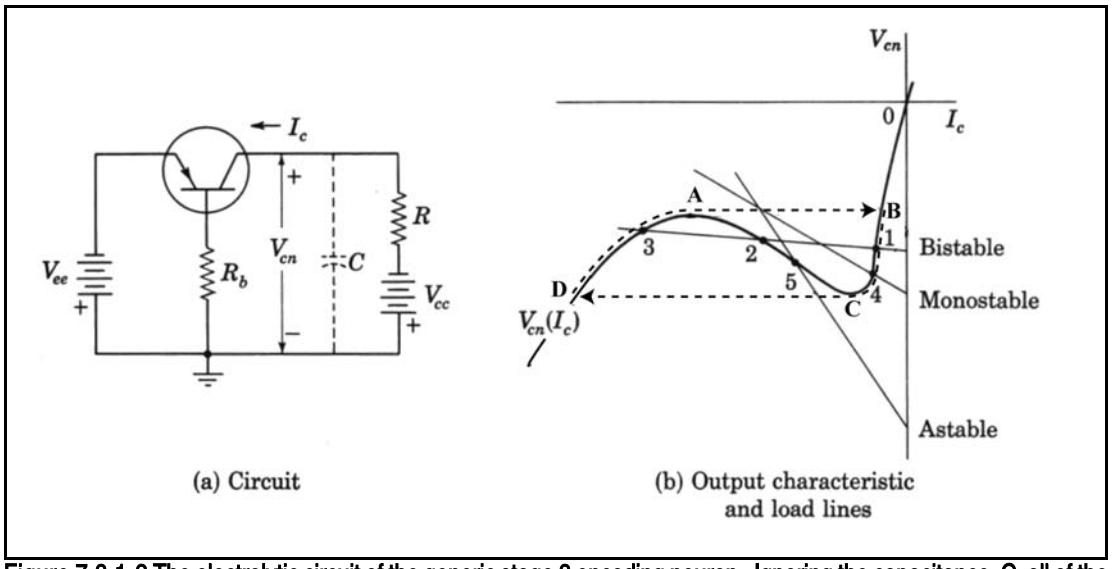

Figure 7.3.1-2 The electrolytic circuit of the generic stage 3 encoding neuron. Ignoring the capacitance, C, all of the dashed lines and the letters in frame (b), the circuit shows the nominal circuit with feedback between the input and output circuits provided by the common-base resistance, R_b. As shown, the circuit can operate bistatically, monostatically or astably depending on the load impedance, R, and the bias potential V_{ee}. The circuit can change its operating point along the curve $V_{cn}(I_c)$ very rapidly (limited only by the current capacity and stray capacitance of the circuit elements). If a capacitor, C, is added to the collector circuit, the switching performance of the circuit is controlled by that capacitor. See text. Adapted from Gray, 1954.

The following discussion is brief and purely pedagogical. For more details concerning the potential oscillation of common-base active circuits, a more specific text should be consulted. These circuits, consisting of only resistive and capacitive impedances and an active device exhibiting positive internal feedback, are usually described as relaxation oscillators. At a more fundamental level, they are described as switching oscillators as shown in frame (b). This

switching character is key to understanding the action potential generated by a neuron (Section 7.3.1).

If the conexus in the above figure contains a resistive impedance, R_b, between its base connection and the surrounding medium (electrical ground), the overall device will exhibit a degree of positive *internal* feedback which is controlled by the value of that impedance. This internal feedback will introduce a unique characteristic into the *input impedance*, the *output impedance* and the *transfer impedance* of the neuron. Frame (b) illustrates this feature. The voltage-current characteristic of the output (collector) circuit, $V_{cn}(I_c)$, exhibits a significant deviation from a straight line. It is important to note the unusual impedance in the region of the deviation. The portion of this curve sloping down and to the right can be defined as a region of negative (dynamic) impedance--a clear indication of the presence of an active electronic device since no conventional passive impedance can exhibit such a characteristic.

Three load lines are shown representing different values of the resistance, R, and different values of the supply voltage, V_{cc}. If the load resistance, R, and the collector supply voltage, V_{cc}, are selected appropriately, the circuit can be made to operate monostably (operating about a stable quiescent point, 4), bistably (switching between two fixed operating points, 1 & 3, when stimulated) or astably (continuously switching between two operating points, A & C) as shown.

Only one voltage-current characteristic is shown. However, this characteristic is also a function of the bias applied to the emitter circuit. Changing the net potential at the emitter has the effect of changing the effective collector supply potential, V_{cc}. This results in the intersection of the load lines with the ordinate moving up or down but the slope of the load lines remaining fixed.

The above circuit with the load line labeled monostable is conditionally stable. The axoplasm will remain at a specific voltage with a small current passing through the collector of the Activa as described by point 4 indefinitely. However, if the load line should be momentarily moved down to where the load line intersects the voltage-current characteristic in the negative region, the circuit will become unstable. The locus of operation will move from point C to point D very rapidly and then proceed to point A before jumping to point B and then returning to the stable point at 4. This behavior is due to the capacitance between the collector and the local ground of the collector circuit. The potential across a capacitor cannot change instantly. However, the current flowing into or out of a capacitor can change instantly. As a result, the horizontal dashed lines indicate changes in current flow that can occur without any voltage change. On the other hand, the voltage can change between points D & A and B & 4 as the current discharges or charges the capacitor potential. During interval D to A, the rate of voltage change is controlled by the size of the capacitance and the current capability of the Activa. During the interval B to 4, the rate of voltage change is controlled by the size of the capacitance, the resistance R and the current capability of the voltage source V_{cc}. For a given circuit, the time for the operating point to traverse the locus one time is equal to the time interval between D & A plus the time interval from B to 4. The primary factor controlling this interval is the capacitance, C.

The above circuit with the load line labeled Astable is unstable. If any small perturbation of the nominal voltage across the capacitance, C, at point 5 occurs (even due to Brownian motion), the current will proceed to point C, jump to point D, proceed to point A, jump to point B, proceed back to point C and repeat the sequence indefinitely. Here again the time for the operating point to traverse the entire locus is given by the time interval required to travel from D to A plus the time interval required to travel from B to C. The primary factor controlling this interval is again the capacitance, C.

7.3.2 The Action Potential (AP) vs pseudo action potentials

The concept of an action potential arose from the observation that the axon of many easily accessed neurons exhibited a uniquely shaped output pulse. While these pulses frequently occurred in groups, the structure of the groupings were difficult to interpret.

> It is important to differentiate between the waveform recorded at the pedicle of a sensory neuron, and called the generator potential and the pulse waveform known as the action potential. While the generator potential may be pulse-shaped, that characteristic is a result of the stimulus used.

The action potential is intimately associated with the stage 3 projection neurons of *Chordata* and is generally assumed to be unique to *Chordata*. It is closely associated with the long neurons forming the neural chord within the backbone, and other long neural pathways, in those species. It can be considered necessary in any large animal with a central nervous system.

The occurrence, but not the unique shape of the action potential has been extensively investigated. The individual action potential contains very little information. However, groups of these pulses *represent* the fundamentally analog

information projected between engines of the neural system. These groups are generated by ganglion neurons typically near the output of a given engine and decoded by stellite neurons typically near the input region of a second engine. Action potentials are the temporal responses of the encoding neurons of stage 3.

The true action potential consists of a pulse with distinctly different leading and trailing edges. The leading edge is straighter than an exponential response because it is formed by an active circuit including feedback. The majority of the leading edge is a straight line when voltage is plotted versus time. This is because the circuit forming it acts as a constant current source charging a capacitor. The trailing edge of the true action potential is fundamentally an exponential curve since it is formed by the charge stored on a capacitor leaking off through a nominally resistive impedance. Variations occur among these waveform elements in practical situations.

A pulse, believed to be similar to an action potential in the 1940's, had been observed in several cephalopods of the Order *Mollusca*. Based on this observation, Hodgkin & Huxley investigated the source of the assumed action potential associated with the giant axon of the squid *Loligo*. Following their work, Mueller & Rudin attempted to fabricate synthetic (symmetrical!) bilayer membranes exhibiting the same properties as those described for the axolemma of Loligo[26]. While the work of this team is exemplary, their activities were premature. They did not recognize the different forms of lemma that are known today and most of their advertised action potentials were products of their test set and protocols (their fig. 1). When they explored more complex membranes formed of natural biological material[27], they obtained more interesting results, including the natural breakdown potential of biological bilayers (sphingomyelin), the effect of doping these bilayers and apparently monostable and bistable oscillations.

7.3.2.1 Details of the generic action potential waveform

There is considerable difference between the *in-vivo* chordate action potentials and the waveforms measured and interpreted by Hodgkin & Huxley, Mueller & Rudin and others. While Hodgkin & Huxley based their analysis on the difference between two currents that existed for the entire duration of their pseudo-action potential, a true action potential is formed by currents that are switched on and off at the peak of the pulse.

Figure 7.3.2-1 shows the features of the action potential generated at a Node of Ranvier. The left and right scales of the figure are not directly related. Schwarz & Eikhof[28] have presented a similar figure recorded from a single myelinated rat nerve fiber. Action potential generators are typically biased so that they are in the cutoff condition under quiescent conditions. The axoplasm-to-ground potential is near –155 mV, and the dendrite-to-podite potential is typically near –10 mV. [An axoplasm potential of –140 mV is shown to agree with the reported measurements.] For dendrite-to-podite potentials of between –10 and 0 mV, the circuit operates in a linear amplifier mode. The axoplasm potential will vary by small amounts in direct response to changes in the dendrite to podite potential. However, if the dendrite-to-podite potential becomes positive, the gain of the circuit becomes greater than one and the circuit goes into an oscillatory mode. Current will begin to flow from the axoplasm through the Activa. This current will cause the axon potential to become more positive and the podite potential to become more negative. The more negative podite potential reinforces the dendrite-to-podite potential difference and causes still more current to flow out of the axoplasm. During the resulting rapid positive-going change in the axoplasm potential, the Activa acts like a constant current drain that discharges the axoplasm capacitance. The leading edge of the output waveform rises nearly linearly until the axoplasm potential approaches the saturation level of the device (axoplasm potential of about –10 mV). Upon reaching saturation, the current through the Activa collector circuit goes to zero. Meanwhile, the stimulus has already declined. As a result, the quiescent dendrite-to-podite potential becomes reestablished and the Activa goes into cutoff. The axoplasm capacitance is now recharged from the electrical power supply acting as a constant potential source in series with a resistance.

The axoplasm potential follows an exponential curve during this recharging cycle. Depending on the temperature of the specimen, the axoplasm potential follows the curve marked T_0 or T_1. The shape of the axoplasm potential as a function of time has been given the name action potential. Good instrumentation is required to record the detailed shapes of its rise and fall and the discontinuity near its positive peak. The recording problem is exacerbated if the electrical probe used to record the waveforms is not properly compensated to insure a flat frequency response. If the probe is not compensated, an overshoot (where the apparent potential of the axoplasm becomes positive) is frequently recorded. This condition is pathological due to the protocol.

7.3.2.2 The effect of temperature on the action potential

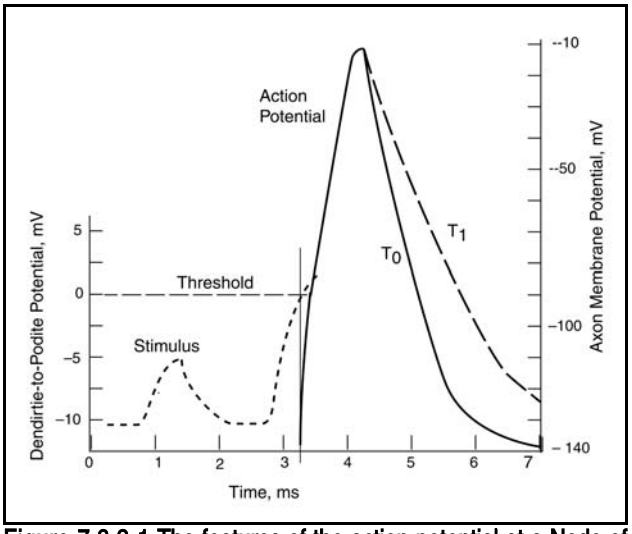

Figure 7.3.2-1 The features of the action potential at a Node of Ranvier. The stimulus is shown dotted and uses the scale on the left. The first stimulus pulse does not cause the generation of an action potential. The second stimulus exceeds the amplitude threshold and does cause an action potential to be generated. There is a significant delay between the peak of the stimulus and the peak of the action potential.

Temperature has a very distinct impact on the shape of the action potential. The effect on the leading and trailing edges are distinctly different. They both are based on a common capacitance that does not change significantly with temperature. The leading edge time constant is also determined by the collector-to-base resistance of the Activa within the neuron when conducting. This value is virtually independent of temperature. As a result, the leading edge of the action potential does not change significantly for temperatures within the biological range. The trailing edge time constant is determined by the load impedance of the collector (axon) circuit. This impedance is dominated by the impedance of the electrostenolytic power source and the impedance of the associated vascular supply system. These components are highly dependent on the temperature of the organism. As a result, the trailing edge time constant is strongly affected by the temperature. Figure 7.3.2-2 shows the effect of temperature on the action potential of the rat from figure 1 of Schwarz & Eikhof[29]. While not shown in detail, note the slower rise of the voltage prior to the beginning of the action potential at 20C. This suggests the time constant of the dendrite-to-base circuit was also temperature dependent. The time constant of this dendritic circuit is also dominated by the parameters of its electrostenolytic source and the vascular supply.

> The effects of temperature on the action potential reported by Schwarz & Eikhof provide strong support for the switching current mechanism proposed here and strong repudiation (falsification) of the current difference theory of Hodgkin & Huxley.

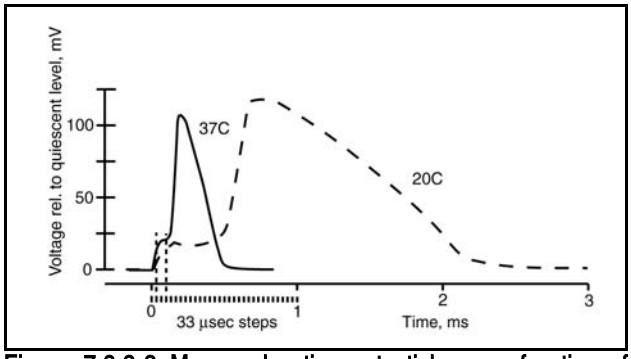

Figure 7.3.2-2 Measured action potentials as a function of temperature for rat motor neurons. The 37C response was elicited by a 30 μsec current pulse. The 20C response was elicited by a 100 μsec current pulse. From Schwarz & Eikhof, 1987

A variety of pseudo action potentials appear in various conceptual papers in the hearing literature. The most famous of these was proposed by Huxley & Hodgkin and discussed above[30]. Another example is the activating function defined by Rattay and discussed in considerable detail in Zeng, Popper & Fay[31]. The continuous mathematical form of this activating function is significantly different from that of the actual, switching-generated, action potential.

Mueller & Rudin, working in the 1960's, used the generic term action potential to describe virtually any pulse response, whether driven or not and whether related to the nervous system or not[32, 33]. They were working to emulate a biological membrane through reconstitution from recovered biological material or synthesis from stock materials. They proposed that the action potential was generated by a two-terminal neuron employing a "tunnel diode" mechanism (a popular newly discovered electronic device during that period). While this approach cannot be ruled out a priori, it involves an asymmetrical membrane that has been "heavily doped" in the semiconductor sense of the term. The literature of the biological membrane has not previously or subsequently reported such heavy doping. The use of the tunnel diode concept also requires the presence of resonant circuits, in addition to the diode, to shape the resulting voltage profile to resemble an action potential. No such resonant circuits have been identified

in real biological membranes.

None of the above approaches defined any role for the neurites of the neuron, although Hodgkin & Huxley reported considerable experimental difficulty unless all vestiges of the neurites were removed from the soma of their neuron. Such "spontaneous activity" related to the presence of the neurites clearly indicated their importance in the overall operation of the neuron.

7.3.3 Electrical operating conditions in the absence of feedback

The description of the switching regenerative repeaters provides a baseline for describing all action potential pulse generating neurons. Assuming the internal Activa is biased into the active state, the critical parameter is the emitter to base potential, $V_E - V_B$. If the emitter-to-base potential is significantly negative, the device is in cutoff, no current flows through the collector circuit and the axoplasm potential will be at its supply potential, nominally –154 mV. As $V_E - V_B$ becomes positive, current will begin to flow through the collector circuit and the axoplasm potential will begin to move toward zero potential. As the $V_E - V_B$ potential becomes more positive, the current through the collector circuit will increase and the axoplasm potential will continue to become more positive until a saturation condition is reached (maximum collector current and minimum axoplasm potential). Saturation occurs when the collector-to-ground potential reaches the base-to-ground potential. This condition occurs when both potentials are approximately –20 mV in observed neurons. Under this condition, the $V_E - V_B$ potential is typically +30 mV and the emitter-to-ground potential is about +10 mV.

Stage 3 neurons operate under large signal conditions and the pulse generation circuits spend a majority of their time in the cutoff condition. Thus, thermal noise at their input terminals is not normally a significant consideration. Noise in the emitter circuit rising to the threshold potential for the circuit can cause the generation of action potentials. The Poisson statistics of the noise stimuli recorded by Kiang (1965, pp 93) suggest these signals were generated in just this way. Below-threshold noise in the emitter circuit can add to the applied excitation and thereby cause a marginal advancement or delay in when the emitter-to-base potential reaches threshold. This can cause a similar marginal advance or delay in when the action potential is generated.

7.3.4 The encoding (ganglion) neurons

The physically dominant neurons of stage 3, signal projection, are those used to generate and regenerate action potentials. These neurons are known as ganglion cells in the neural systems of both vision and hearing. Ganglion neurons, by whatever name, are introduced as a matter of power efficiency at the expense of some time delay. In the auditory system, they are typically found at the output of the OHC and IHC neurons and at the output of every signal processing and signal manipulation engine of the system.

7.3.4.1 Operation of the ganglion neuron

The Node of Ranvier is typically used to regenerate at full amplitude the phasic waveform of a reduced-amplitude action potential applied to its input. It accomplishes this on an individual pulse basis. The same circuit can be used in an alternate mode; the generation of one or more phasic pulses in response to the application of a sustained electrotonic (analog) waveform at its input. This is the role of the ganglion neuron.

Consider the circuit for a Node of Ranvier described in Figure 7.3.1-2 under different operating conditions. Let the circuit be incorporated into a neuron and let a constant voltage be applied to the dendrite of the neuron. If this voltage is slightly higher than the threshold for the neuron, the neuron will be unstable and generate a single action potential followed by a refractory period while the emitter-to-base voltage, $V_E - V_B$, is more negative than its quiescent value. However, because of the potential applied to the dendrite, the emitter-to-base voltage will attempt to return to a voltage slightly higher than its quiescent voltage. When it exceeds its threshold value, another single action potential will be generated. This cycle will be repeated as long as the voltage at the dendrite is above the threshold value. Under this condition, the stream of action potentials will be continuous and exhibit a uniform pulse-to-pulse interval characteristic of the circuit elements associated with the Activa within the neuron.

Now consider the same circuit within a neuron but apply a slowly rising ramp voltage to its dendrite. The circuit will operate as above only every time it attempts to return to its quiescent value, that value will be incrementally higher than on the previous cycle due to the voltage applied to the dendrite. As a result, the threshold voltage of the circuit will be achieved incrementally sooner and the pulse-to-pulse interval will be incrementally shorter. The result will be an initial pulse followed by a series of pulses of incrementally shorter pulse-to-pulse interval. This is the fundamental operating mode of the electrotonic signal encoding neurons of the neurological system. These neurons have been defined functionally as ganglion neurons in this work.

The ganglion neurons can encode any electrotonic waveform having frequency components below the maximum action potential pulse frequency that it can generate. This maximum frequency is on the order of 200-500 Hz but can be as high as 1000 Hz for certain ganglion neurons associated with the source location circuits of hearing.

The data of Golding & Oertel recorded using a current-type axonal patch-clamp shows the operation of the encoding ganglion neuron in considerable detail when interpreted in the context of the Electrolytic Theory of the Neuron[34]. Their waveforms support the theory presented in Section 7.3 very well.

7.3.4.2 Characteristics of ganglion neurons

Since the performance of the ganglion neuron is a function of the emitter-to-base potential, this neuron can be driven by potentials applied to either its dendritic or poditic terminals. The combinations of circuit elements associated with the synapse and dendrite, and the synapse and podite, can be complex circuits. These circuits may act as differentiators or integrators. In some cases, the dendritic input is known to combine these mechanisms to form complicated lead-lag networks. For consistency, this work considers such networks as stage 2 networks at the input to stage 3 encoders.

Ganglion neurons exhibit several time delays. Each of the input circuits exhibits a delay due to the diffusion time of current along the length of the neurite. Upon reaching the capacitance associated with each Activa emitter and base, there is a time required to charge the RC network to the threshold potential associated with that terminal. The total time required for the circuit to reach threshold is the intrinsic latency of the ganglion neuron. After achieving threshold, there is a finite time required for the action potential of the collector circuit to reach peak amplitude. The intrinsic latency plus this additional delay equals the clinical latency of the circuit at the collector terminal.

To provide the necessary capacitance to achieve the unstable condition required to create action potentials, the cytological area associated with the collector of the neuron is typically enlarged. This area is normally described as the hillock region.

Although the above discussion brings to mind the conventional ganglion neuron where the encoding circuit is found with the soma, this is not a requirement. In the case of ganglion neurons of the spiral ganglia, it appears that the encoding circuit is in the first "bead" associated with the input to the soma of the neuron. This is confirmed by the artifacts of the encoding process that have been measured at the synapse with the sensory neuron. The first bead acts as an analog-to-phasic encoder while subsequent beads operate as Nodes of Ranvier, whether they precede, are within, or follow the soma.

In the typical ganglion neuron, the axon is formed as a long thin tube that is tightly wrapped with an electrically insulating material, myelin. The fact that the axon is a long coaxial tube introduces electrical inductance into the circuit. This inductance per unit length complements the capacitance per unit length resulting from the lemma and myelin wrap. When these two parameters are approximately equal, the mode of signal transmission along the axon changes from diffusion to propagation as described in Section 7.3.5. This is a fundamental change of immense importance. Of crucial importance, the action potential continues to propagate along the axon without regard to the electrical potential at the collector terminal of the Activa. Such a condition cannot be achieved by diffusion. Diffusion requires the source to remain at the signal level until the signal reaches the termination of the circuit.

The action potential propagated by a myelinated axon travels much faster than it would by diffusion (an instantaneous velocity of approximately 4400 meters/sec). However, the amplitude of this signal does dissipate with distance and regeneration is required. At each Node of Ranvier, the signal is regenerated to its maximum value and an additional delay is introduced into the overall delay. This situation makes the total delay, measured along the axon, increase by a significant increment at each Node of Ranvier. The average propagation velocity of the ganglion neuron is dominated by this incremental delay. As a result, the average propagation velocity is reduced to a value near 40 meters/sec.

Figure 7.3.2-1 suggests three different potential definitions of latency. The simplest concept measures the latency as the time from some arbitrary event until the peak of an action potential occurs. The peak of an action potential is most easily measured in a clinical environment. However, not all action potentials exhibit the same width and their peak does not represent a significant functional event.

From an engineering perspective, two other latencies can be defined. A simple application-oriented concept measures the latency as the time from some arbitrary event until a level is reached following the start of the action potential. This level is frequently taken as the level defined as 10 percent of the rise of the action potential from its baseline to its peak. This level is easy to determine graphically. However, it also lacks any functional significance.

The most functionally important and reproducible concept of latency measures the time from some arbitrary event until the action potential initially deviates significantly from the baseline. This condition can be defined at either the axon, dendrite or podite of any phasic conexus (neuron or Node of Ranvier). It signifies the change from a feedback condition with a gain of less than 1.0 to the regenerative condition with a feedback gain of greater than 1.0. For the feedback gain of less than 1.0, the axon segment waveform generally looks like an amplified copy of the stimulus to that conexus. For the feedback gain of greater than 1.0, the conexus axon segment waveform is an action potential regardless of the stimulus waveform.

Figure 7.3.4-1 describes the components of latency as measured at the auditory nerve as presented by Young et al. It shows data representing the mean latency of assorted neurons as a function of their best frequency at a stimulus intensity of 25-35 dB above threshold. They defined the acoustic delay of their test set as 0.55 ms. They drew a freehand curve below the high spontaneous rate data points. This curve has been replaced by a more informative estimate of the delay based on the mean velocity of the Rayleigh wave within the cochlear partition of an endothermic animal (dashed line). The curve can be moved without rotation on this linear plot with respect to position on the cochlear partition. However, there is more scatter in the other data sets.

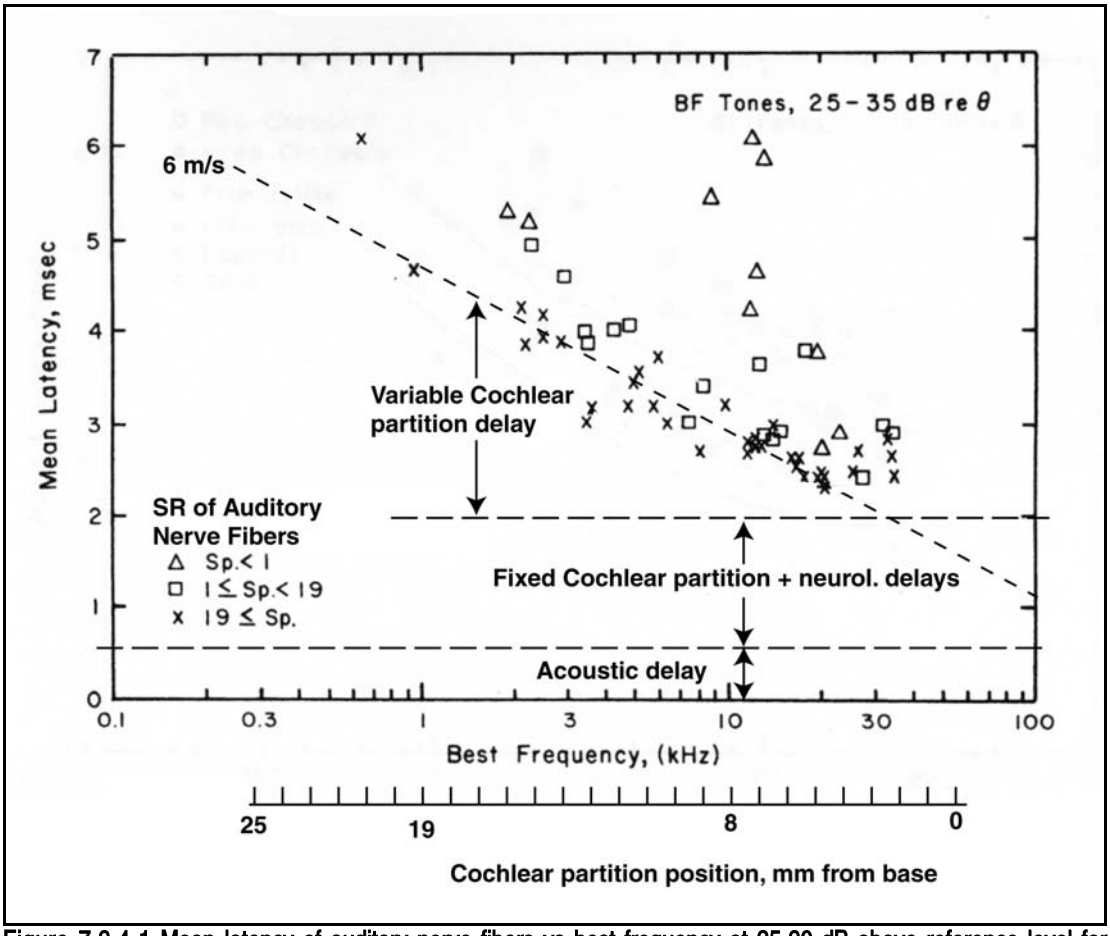

Figure 7.3.4-1 Mean latency of auditory nerve fibers vs best frequency at 25-30 dB above reference level for decerebrate cats. The legend at lower left defines the spontaneous (uncontrolled) rate of neuron firing. The acoustic delay was defined by Young et al. The other delays, and the proposed Rayleigh wave velocity within the cochlear partition are from this work. Modified from Young et al., 1988.

Many authors have described a phase shift in the action potentials collected at the auditory nerve as a function of stimulus frequency without considering the character of that phase shift. A time delay is frequently interpreted as a phase shift. Smolders & Klinke have provided good data and a discussion describing the two components of such phase shifts[35]. However, they did not de-convolve the time delay into acoustic (in air), mechanical (primarily in the

tectorial membrane) and neural components. In the crocodile, the delay component of the phase shift came to 1.49 ms.

Figure 9A in Smolders & Klinke shows a possible second group of delays approximately one millisecond above the main distribution. This delay could be caused by probing a ganglion neuron at a point beyond a Node of Ranvier. Each Node typically introduces a one millisecond delay in the signal stream.

Synchronization and the synchronization index are not clearly defined concepts in hearing. While various mathematical definitions have been offered, they are based on totally empirical interpretations of laboratory data. Synchronization generally refers to arranging some rate associated with one independent source to equal a similar rate associated with a second independent source. The phase-locking of a local oscillator with an incoming signal from an independent distant source is a typical example.

In hearing, phase-locking is used in a narrower sense. It describes the timing of a driven action potential pulse with respect to the generator waveform at an axon causing that pulse. The most frequent concept is to compare the time of the peak in the action potential waveform with the zero crossing of the generator waveform resulting from sinusoidal acoustic stimulation. Less frequently, the time of the peak in the action potential waveform is compared with the zero crossing of the sinusoidal acoustic stimulation. The time of the peak is expressed in angular measure with respect to the generator or stimulation waveform. The time of occurrence of the peak is a function of the intensity of the stimulus and the state of adaptation of the hearing system.

The concept of synchronization is generally used when speaking of generator waveform frequencies below 3000 Hz and most often for frequencies below 600 Hz. For higher frequencies, the synchronization index goes to zero. At higher frequencies a different synchronization index can be defined based on the envelope of the stimulus. Rose illustrates this situation in a montage[36]. Goldberg & Brown provided an early description of a synchronization index in a specific context[37]. Delgutte provided a textual definition in 1980 based on data from acoustic tests that are of limited utility[38]. Javel described two or more different definitions in 1988 based on external electrical stimuli[39].

The low frequency synchronization index is difficult to define for three reasons. First, it involves a variety of mechanisms. Second, it frequently involves artificial external stimulation of a neuron. Third, it only applies to certain types of phasic neurons. Figure 7.3.4-2 from Javel provides the necessary data from a cat auditory fiber responding to a sinusoidal stimulus. Javel provided definitions of synchronization indices based on detailed mathematical manipulations but did not describe the range limits on the definitions. It can be inferred that his definition related to sinusoidal stimulation was restricted to the range of zero to 90 degrees. These definitions are not mutually compatible. Javel did note the theoretical maximum of his synchronization index was pi/4 = 0.78 for a sinusoidal stimulus (p. 250) but 1.0 for a square wave stimulus (p. 275).

Frame A shows a 200 Hz sinusoidal stimulus and an overlaid oscilloscope presentation showing multiple traces of the generated action potentials over an extended period of time. Unfortunately, the individual action potentials are not numbered to show their sequence. They are clearly unstable with reference to a given phase angle of the stimulus. At a 200-Hz stimulus frequency (period of 5.0 ms), the fiber can be expected to show some degree of refractiveness following the generation of each pulse. The effect of this refractiveness will be discussed in conjunction with frame C.

Frame B shows the synchronization index calculated by Javel for the data in frame A. It also shows a moving window average through the data points (solid line). Equally interesting, a dashed line has been added showing the data points support a theoretical description of the synchronization index based on an exponential expression. This is the expected expression for a relaxation oscillator with a recharging interval controlled by an RC network.

In natural situations, regenerative pulse repeaters called Nodes of Ranvier (monopulse oscillators) achieve “synchronization” indices that are nominally 1.0. They generate one output action potential for every input action potential received (with a constant phase angle and a very high degree of reliability). In natural situations, encoding neurons (astable oscillators) can produce more than one action potential per applied stimulus (synchronization indices above 1.0) if the applied stimulus is of sufficiently low frequency (typically below 50 Hz). This condition appears to be outside the range of frequencies that Javel considered in his definitions. In the region of 100 to 500 Hz, encoding neurons typically achieve synchronization indices near unity (or pi/4 depending on the mathematical definition). Above 500 Hz, the output of the encoding neuron depends on the combination of the height of the excitation pedestal (due to integration) and the height of the AC component (reduced by the integrator) applied to it.

Frame C shows how an initial action potential is generated when the stimulus amplitude exceeds the stimulus threshold of that neuron. The static threshold of the neuron is shown as the dotted line labeled T_S. The dynamic

threshold of that same circuit is shown by the dashed line, T_D. The dynamic threshold is the result of internal changes in the potentials applied to the Activa as part of the monopulse oscillation process. It is not the actual action potential generated but it is similar in form to the action potential. Note that after a period of time, the dynamic threshold decreases to the value of the still present stimulus. The result is the generation of a second action potential (not shown). This second pulse may exhibit a lower peak amplitude at the axon because the recharging process may not be complete. However, the result is clear. The positive going stimulus of sufficiently low frequency can cause the generation of more than one action potential during a given cycle. The vector diagram for this situation shows the first pulse occurring the first 90 degrees of the circle but the second pulse occurring much later and frequently in the second quadrant of the circle. The presence of a pulse occurring in the second quadrant causes great difficulty for the definition of synchronization index proposed by Javel for sinusoidal excitation.

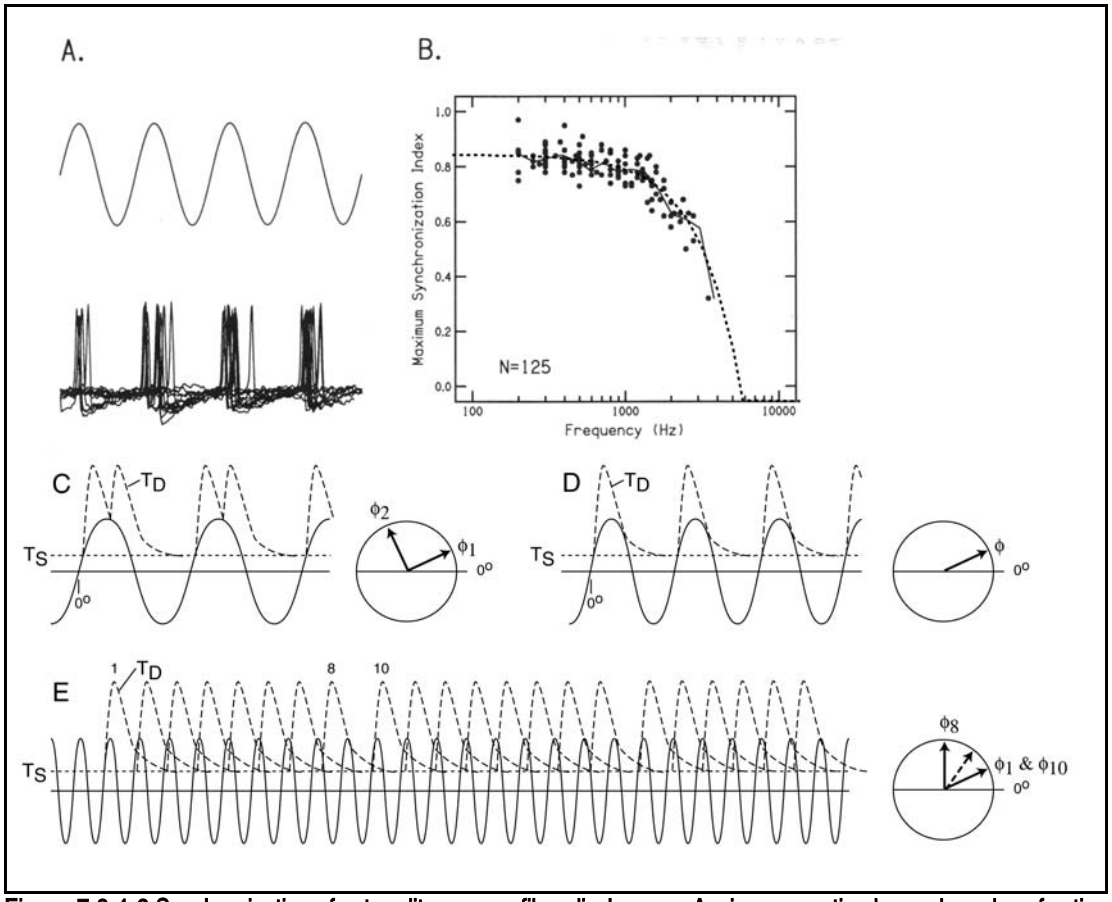

Figure 7.3.4-2 Synchronization of cat auditory nerve fiber discharges. A; sine wave stimulus and overlay of action potentials generated in response to a to a 200 Hz tone stimulus. B; synchronization index as a function of stimulus frequency. Solid line is a moving window average computed by Javel. Dashed line is theoretical exponential curve through data points. C; response of a driven reflex oscillator to a sine wave of frequency far below its refractory frequency limit. D; response of driven reflex oscillator by a sine wave stimulus larger than the static threshold amplitude, T_S, but at less than one half the refractory frequency limit. Dashed lines are the instantaneous threshold of the emitter-to-base circuit. The action potential is generated at a constant phase angle relative to the excitation as shown by the vector diagram at right. E; response of same oscillator to a sine wave stimulus of same amplitude but at twice the refractory frequency limit. Each stimulus pulse after the first encounters a higher instantaneous threshold. Note missing 9th and 18th pulses. The stimulus amplitude did not exceed the dynamic threshold during this interval. The phase diagram shows the variation in angle with pulse number during one set of stimuli. See text. Data from Javel, 1988.

Frame D shows the case more commonly found in the literature, whether due to natural or unnatural stimulation. The stimulus frequency, although higher than in frame C, remains below the refractory frequency limit of the neuron. As a result, each positive going half cycle of the stimulus causes the generation of an action potential. The threshold of

the circuit rises abruptly during generation of the action potential but does not fall to a potential lower than the stimulus during the remainder of the half cycle. Prior to the start of the next half cycle, the dynamic threshold has returned to the level of the static threshold. The result is a synchronization index of nominally unity. One action potential is generated for each positive half cycle of the stimulus. As shown by the vector diagram on the right, the phase angle of each action potential relative to the stimulus is nominally constant at ϕ = K.

Frame E shows the case where the stimulus frequency exceeds the refractory frequency limit. In this case, the dynamic threshold of the neuron does not return to the static threshold before the next positive going half-cycle of the stimulus. As a result, the action potentials are generated at slightly different times, as shown by the increase in the phase angle, ϕ. The phase angle of the first pulse occurs at angle, ϕ_1. The phase angles of pulses two through eight increase gradually until a pulse is actually omitted. Pulse ten then occurs at the same phase angle as ϕ_1. This process repeats indefinitely until the amplitude of the stimulus fails to exceed the dynamic threshold during the positive half cycle.

As shown in frame E, the interval between pulses varies incrementally at this stimulus level and there is the potential for missing pulses. Such a pulse train will generate a PST histogram with pulses grouped around an average pulse-to-pulse interval. If the stimulus frequency is varied in amplitude incrementally, a point will be reached where the synchronization index will be precisely 1.0. At that stimulus value, the pulse-to-pulse groupings will become narrower and the histogram will frequently present a chopped appearance with the pulse-to-pulse spacing equal to the period of the stimulus.

Under clinical conditions, any pharmacological agent that causes the neuron to recharge more slowly than normal will likely result in lowering the synchronization index. Similarly, in the electrophysiology laboratory, any probe adding significant capacitance to the recharging circuit of the neuron will tend to reduce the synchronization index.

If the amplitude of the stimulus in the above figure is significantly reduced, the synchronization index may be impacted drastically.

Figure 7.3.4-3 shows the range of discharge rates achievable in a driven encoding neuron for very small changes in excitation intensity[40]. The sinusoidal stimulus was externally generated and each neuron exhibited a negligible spontaneous firing rate following destruction of the associated sensory neurons. As a result, each neuron exhibited a static action potential threshold of approximately 52 dB relative to the test set reference. For the lowest two stimulus frequencies, the action potential rate reached the stimulus rate within less than 2 dB. The synchronization index went from zero to a nominal 100% for a change of only 2 dB. At 600 Hz, the index went from zero to 100% for a change of only 6dB. The curve for 800 Hz, which is well outside the expected operating range for an encoding neuron, is incomplete. However, the index went from zero to a value near unity for a change of less than 8 dB.

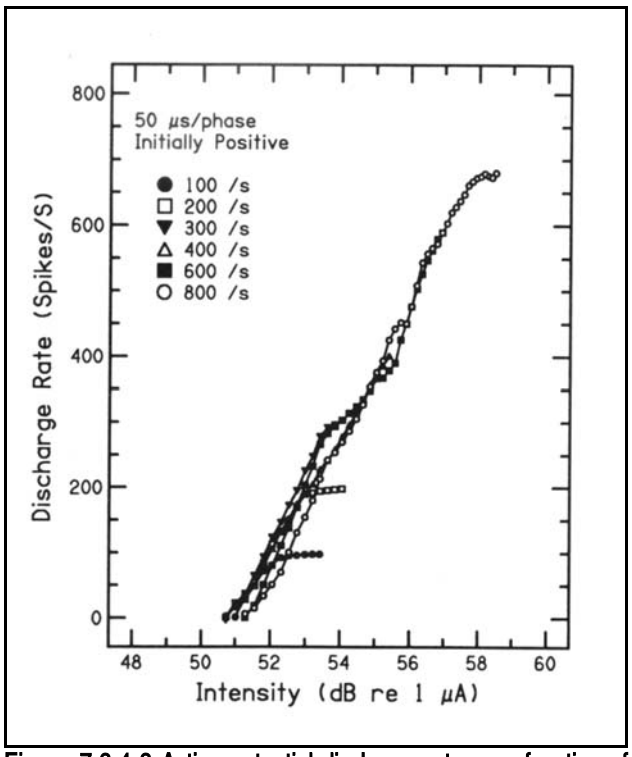

Figure 7.3.4-3 Action potential discharge rate as a function of intensity. The nerve fiber was responding to biphasic electrical pulse trains presented at rates ranging from 100 to 800 pulses/second. From Javel, 1988.

If this figure applied to free running encoder neurons, the illustrated performance would be suggestive of a modulation index on the order of 75% of the carrier frequency near 375 Hz. This is a very high index that would suggest nonlinear encoder performance and the generation of significantly more sidebands. While this nonlinearity may make interpretation of histograms relating to action potentials more difficult, the original modulation is fully recoverable without distortion by a properly implemented phase

modulation decoder.

Javel provided another discussion related to pulse, as opposed to sinusoidal, stimuli (pages 273-6). While his figure 17.15 shows a constant synchronization index, the raw data in figure 17.14 does not support that position. The histograms for stimuli below 47.4 dB show distinctly different discharge phase angles. Even at 51 dB the distribution of phase angles is finite whereas his definition of the synchronization index requires the phase angle to be a constant for an index of 1.0.

7.3.4.3 The introduction of myelin in connection with the axon

As indicated above, a lengthening of the axon of the ganglion neuron relative to the bipolar neuron can introduce capacitance in shunt with the other impedance elements of the output circuit and lead to oscillation in the ganglion circuit. However once a critical level of capacitance is reached, additional capacitance is not desirable. It requires the Activa to switch more current between the input and output circuit to achieve the same level of action potential amplitude. To avoid this problem while achieving maximum axon length, a portion of the axon is wrapped in myelin. This process has the effect of thickening the dielectric between the axoplasm and the surrounding plasma and thereby lowering the effective capacitance per unit length of the axon.

7.3.4.4 The introduction of the Node of Ranvier in connection with the axon

Wrapping a significant part of the axolemma in myelin is an effective way of allowing the axolemma to be increased in length. However, it is not an adequate modification if the action potential is to be projected over distances beyond a few millimeters. In that case, active signal amplification is necessary. This can be provided by analog amplifiers while accepting the degradation of the signal waveform implicit in transmitting a pulse waveform over a relatively simple electronic transmission line, e.g., one without equalization stages to compensate for the normal phase distortion per unit length. The alternate approach is to regenerate the waveform. This actually involves replacing the received signal waveform with an alternate waveform, typically of similar waveshape. This regeneration of the waveform is the purpose of the Node of Ranvier. The process can be repeated indefinitely along the neuron since there is no cumulative waveform distortion in this approach.

7.3.4.5 Signal input via the poditic conduit

Although not a well-developed situation in the hearing literature, there are examples in the broader literature of ganglion cells exhibiting both dendritic and poditic arborizations. Such poditic arborizations suggest the poditic conduit accepts signals. These signals would be treated as out-of-phase with respect to the dendritic inputs. They could therefore subtract from the critical signal amplitude needed to initiate generation of an action potential. Such signal subtraction would normally be considered a stage 2 operation at the input to a stage 3 encoding neuron. If an exceptionally large signal was applied to the poditic terminal, it could be considered inhibitory.

7.3.4.6 Transfer function of the stage 3 encoding circuits

Figure 7.3.4-4 shows an ideal overall transfer function of a stage 3 projection circuit. The left half of the figure describes the transfer function of the encoding circuit. The input excitation can be of either the monopolar or bipolar type. However, the intrinsic absolute bias point is set differently in the two situations. The vertical scales shown in the figure are nominal. The important feature is they are linear with respect to time but not with respect to frequency.

The labels at the lower left refer to the typical parasol ganglion neuron, a neuron optimized for monopolar signal processing. In the absence of any input, the quiescent point of the parasol neuron is near the negative most extent of its operating range. Its action potential generation rate will be near zero under this condition. Upon excitation, it will generate action potentials with a time period between pulses inversely proportional to the excitation potential. The label between the two frames defines the operating point of a midget ganglion neuron, a neuron optimized for bipolar signal processing. In the absence of any input, the quiescent point of the midget ganglion neuron is near the middle of its operating range. If biased near –16 mV, it will generate about fourteen action potentials per second on average (one pulse every 0.07 sec). Upon application of a signal, the action potential discharge rate can be driven up to about 200 pulses per second (one pulse every 0.005 sec) or down to only a few pps (one every 0.14 sec).

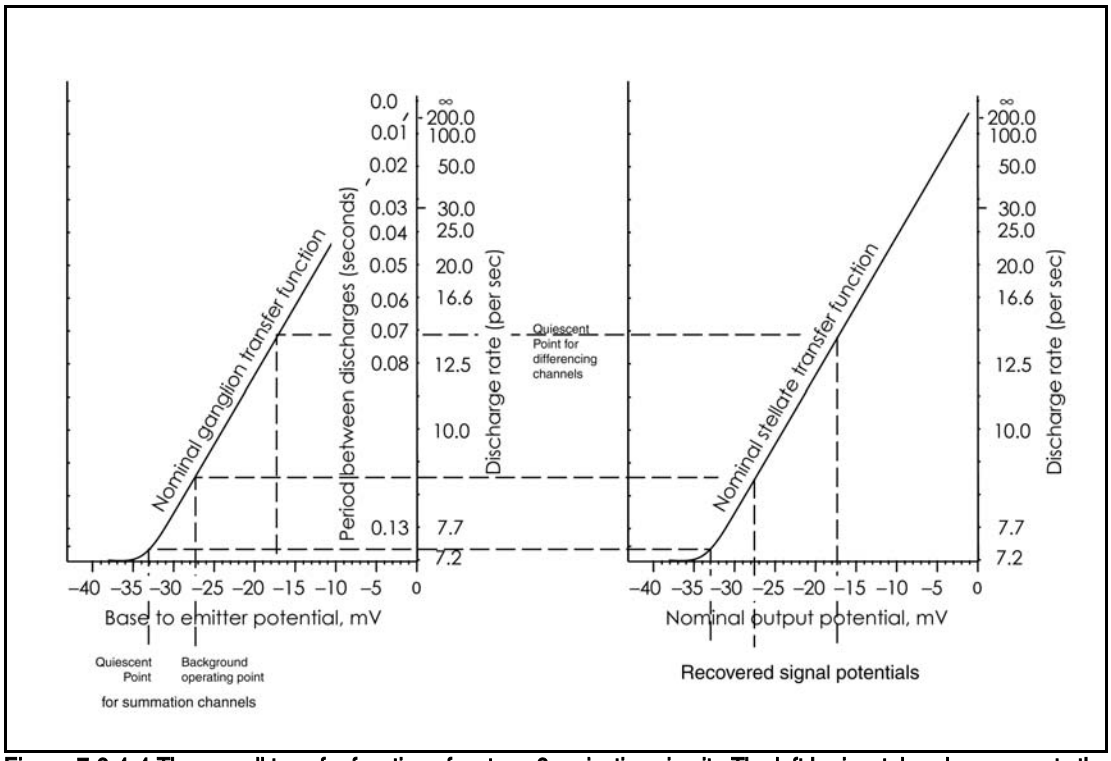

Figure 7.3.4-4 The overall transfer function of a stage 3 projection circuit. The left horizontal scale represents the absolute emitter to base (dendrite to podite) potential of the ganglion encoder circuit. The right horizontal scale represents the equivalent (but relative) voltage scale for the output of a stellite decoder circuit. The entry points for a monopolar input signal are shown at lower left. In the absence of any signal, the quiescent operating point of the parasol type ganglion neuron is shown as –33 mV. The nominal background operating point is shown as –27 mV. Under large signal conditions, the signal extends from near –33 mV to near zero mV. Under ideal conditions, one form of the stellite decoding circuit will reproduce these voltages perfectly as shown by the dashed lines proceeding to the lower right. For a bipolar input signal, the midget ganglion neuron is typically biased to – 17 mV. The excitation can drive this potential over the range of –32 mV to about –2 mV. Under ideal conditions, the pulse rate generated is shown by the vertical scales. These scales can be multiplied by a constant to cover different operating ranges. The pulse interval is linearly related to the excitation potential. The actual pulse frequency is reciprocally related to the excitation. As for the monopolar signal, an ideal bipolar stellite decoder will generate an output potential that is a faithful replica of the input excitation. See text.

7.3.4.7 Correlation with the literature

Tasaki presented an early "Two Stable State Theory" in 1968[41]. His discussion and theoretical foundation did not recognize the negative impedance characteristic of an Activa with a podal impedance. Absent the concepts of an Activa and internal feedback, his electrical circuit, with arbitrary variable resistors, and his explanation of the measured I-V characteristic (figure 7) is less than satisfying. His description of what constitutes an action potential apparently includes any square wave.

As expected from the earlier discussion, the majority of the ganglion neurons of stage 3 are rate-limited to less than 300 action potential pulses per second. This is true of both the auditory and visual systems. This limitation on the maximum acceptable rate of about 300 Hz has been discussed frequently in the literature[42]. However, the discussion has been largely anecdotal and the constellation of neurons examined has been far from comprehensive. On the other hand, special stage 3 neurons associated with the source location subsystems of hearing and the ocular pointing functions of vision are known to operate at up to 550 pps. Johnson and others have recorded pulse rates of up to at least 550 pps in cats[43].

Inoue et al[44]. presented additional data, compatible with the theory presented here, on how the neural response is affected by pharmacological and temperature changes.

Miller et al. have provided recent data on the refractory characteristics of stage 3 neurons in cats[45]. They recorded intercellular signals of low amplitude (a few millivolts) from the auditory nerve following electrical stimulation of the basal turn of the scala tympani. The deviation of their data from a Gaussian distribution in figure 5 shows the limited extent of their data set. Their figure 10 shows the exponential character of the refractory interval clearly. Their introductory discussion notes the variation in the refractory interval among different neurons before settling on a mean value of 330 microseconds. They made an interesting observation that the spontaneous rate of action potential generation was zero in their chemically deafened cats (p. 217). This would confirm the typical spontaneous rate was a result of uncontrolled external noise detected by the sensory neurons.

Pfeiffer & Kim provided very early data on the auditory nerve of the cat following a long experimental period (five years)[46].

Palmer & Evans have provided good data that can be used to quantify the performance of the stage 3 projection neurons in the cat[47]. The data was recorded at either the auditory nerve or the cochlear nucleus in response to a node A stimulus. While they did not specify whether their data applied to the stage 3 neurons at the input or the output of the cochlear nucleus, it can be assumed it applied to the input because of its simple relationship to the stimulus.

Javel and his coworkers have provided very valuable data on the operation of the encoding neurons under a variety of natural and unnatural stimulus conditions. Lacking a theoretical model, their test signals have taken on unusual characteristics and their empirical results have not always been analyzed optimally. Javel has provided a complex probability histogram for the response of a single cell to a biphasic pulse train introduced electrically into the cochlear fluids[48]. The key to interpreting this histogram is to recognize the sub-harmonic relationship between the stimulus frequency and the action pulse frequency.

Delgutte[49] has provided a set of histograms of unique precision that can help define the two classes of signals defined by Liberman in 1978. These histograms tell a much larger story than they were designed to tell. The waveforms shown represent the output of stage 3 ganglion neurons responding to the output from the stage 1 sensory neurons. The acoustic stimuli were synthetic vowels and other complex signals. The material in Delgutte provides a good introduction to the relationship between the vocalization of sound and the action potential pulse frequencies involved. He makes an important observation when speaking of synthetic stimuli. "Unlike natural vowels, the stimuli have only one peak in their spectrum and cannot, in general, be identified by listeners as a specific vowel."

7.3.5 The generic stage 3 phasic signal recovery circuits

The generic stage 3 signal recovery circuits are described physiologically as stellite neurons in this work (Section 7.1.2). As will be discussed below, a variety of stellite neurons can be defined based on the parameters of their electrolytic components. However, they all function as action potential pulse decoders.

Figure 7.3.5-1 illustrates four stellite circuit configurations. The key characteristics of these circuits are the time constant of the RC network associated with the collector circuit, the biasing of the dendrite-to-ground circuit and whether the input to the circuit involves summing (or differencing) of multiple signals.

Frame A describes the operation of the stellite neuron in its principal role, as an envelope detector. It will be shown below that this circuit reproduces the waveform encoded by an earlier ganglion neuron to the degree required for information extraction. The output is provided to the orthodromic circuits associated with the *awareness mode* of hearing. The feature of this circuit is the long time constant associated with its collector circuit. The time constant remains short enough to allow the circuit to reconstruct the original stimulus waveform at frequencies below the integration frequency of 600 Hz (inset). An optimal stellite neuron for envelope extraction provides the performance described on the right in the previous figure. The output amplitude shown at lower right is for a steady-tone stimulus.

Frame B describes the operation of the stellite neuron in its role as a leading action potential pulse detector. This function is primarily in support of the *alarm mode* of hearing operation. It is characterized by a long discharge time constant associated with the poditic impedance. This impedance effectively prevents the circuit from detecting additional pulses after the first because of the high base-to-ground potential.

Frame C describes the operation of the stellite neuron in its role as a detector of binaural delay intervals as explored in this work. This function is primarily in support of the *source location mode* of hearing. In this case, the impedances of the circuit are arranged to begin a long square wave with the receipt of the first pulse via the dendritic input and to terminate that square wave upon receipt of a second pulse from the contralateral channel applied to the poditic input. The length of the square wave is directly related to the angle of the source relative to the sagittal plane of the subject. This square wave can be integrated to provide a signal amplitude directly proportional to this same angle.

Frame D describes the operation of the stellite neuron in a coincidence detection role. This is the operation suggested by Jeffress in his explanation of source location based on binaural coincidence detection. This function is putatively used to support of the *source location mode* of hearing operation. The circuit exhibits a quiescent emitter-to-base voltage that is high relative to the amplitude of either pulse source alone.

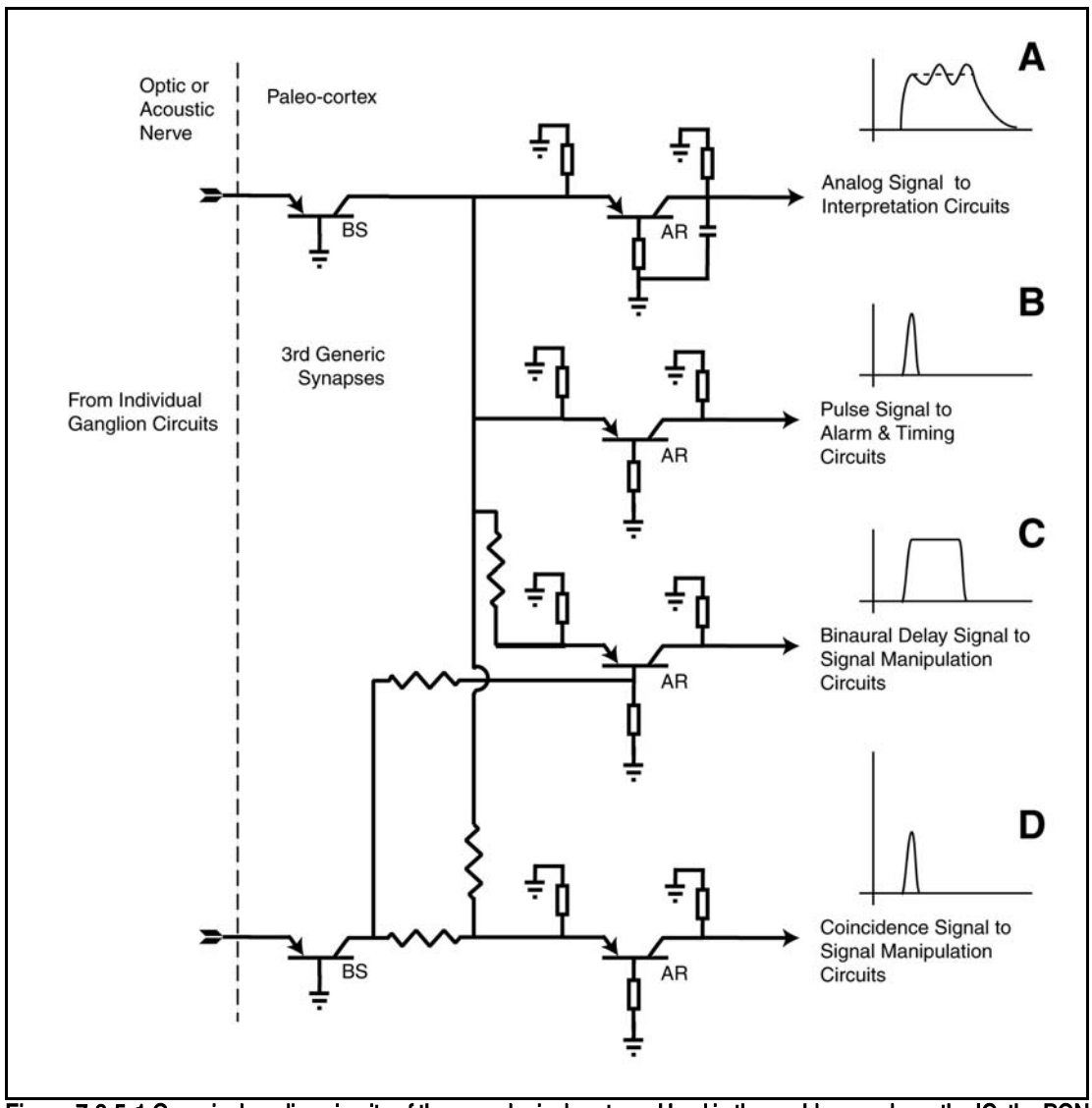

Figure 7.3.5-1 Generic decoding circuits of the neurological system. Used in the cochlear nucleus, the IC, the PGN and many engines of the cerebral cortex. A; the circuit uses an RC combination with a long time constant in the collector circuit to decode time-delay encoded action potential streams for *awareness*. B; the circuit is biased and uses circuitry optimized for detecting the time of occurrence of the first action potential in a possible series of action potentials for *alarm*. It ignores subsequent action potentials. C; the circuit is arranged to produce a long pulse describing the location of the source relative to the sagittal plane for *source location*. D; a coincidence circuit biased to generate an action potential like pulse, ala Jeffress, whenever two action potentials are applied to its input circuitry at approximately the same time.

Circuits A through D are not distinguishable morphologically yet they provide distinctly different functional capabilities.

The circuit at C can be used to process binaural pairs of OHC. Using this feature, individual source locations will be determined for each frequency component of the stimulus sensed by the OHC. This configuration is much simpler and

gives more information than the array of circuits proposed by Jeffress in the 1940's.

By using variants of the above circuits, a wide variety of other output signals can be obtained. Chapter 6 noted the wide variety of pulse trains that have been recorded at the decoding neurons found at the interface of the auditory nerve with the cochlear nucleus. The character of these signals caused Young et al. to describe the laboratory effort in 1988 as in the "stamp-collecting" mode[50]. In the same volume, Oertel et al. (Chap. 10) provided a broad classification of some of these pulse trains based on both temporal plots and inter-spike-interval (ISI) histograms. Their notation ranged from the cardinal type I and type II designations to the fanciful. While they claimed good results in associating specific pulse patterns with the anatomically distinct bushy and stellate cells, their criteria were loose.

Oertel et al. did demonstrate the transition from subthreshold to superthreshold (action potential) generation as a function of electrical stimulation amplitude applied to neurons in the auditory nerve (figs. 8 & 9). Such operation is characteristic of interneurons, not stellite neurons.

7.3.6 The end-to-end transfer function for an awareness mode circuit

[PPA] As noted in Section 7.1.4.1, a type of pulse–position encoding is used that is called tine–delay encoding (TDE) in the neural system. TDE offers many specific features. It does not send any pulses until a stimulus has occurred. It makes the first action potential carry additional information about the starting time of the stimulus. The actual stimulus intensity information is carried as the distance between adjacent pulses.

Frame A of the above figure represents the typical stage 3 circuit assumed in most of the literature. The stage 3 circuit is combined with an optimized stage 2 integrator to reproduce at its output an adequate copy of the analog waveform encoded by the ganglion neuron. Figure 7.3.6-1 describes the signals recorded at different locations along the stage 3 signal path. The letters within the circles refer to the nodes defined in Figure 7.1.2-2 and earlier. Frame A shows the idealized stimulus along with the signal recorded at various locations within the sensory neurons and at node E. The delay labeled w varies with the recording location. Frame B shows the time-delay encoded pulse stream recorded at the first axon segment of the ganglion neuron. Frame C shows the virtually identical pulse stream recorded at a subsequent axon segment following one or more Nodes of Ranvier. The delay labeled y is proportional to the number of nodes passed before reaching the recording location.

Frame D shows the form of the recovered analog signal after a delay labeled z related to the charging time of the integrating circuit. The sawtooth character of the response is due to the balancing of the charging and discharging functions within this circuit. The amplitude rises rapidly initially because of the arrival of more frequent action potentials. The amplitude is sustained during most of the stimulus interval by less frequent pulses. Finally, the output signal decays upon termination of the pulse train.

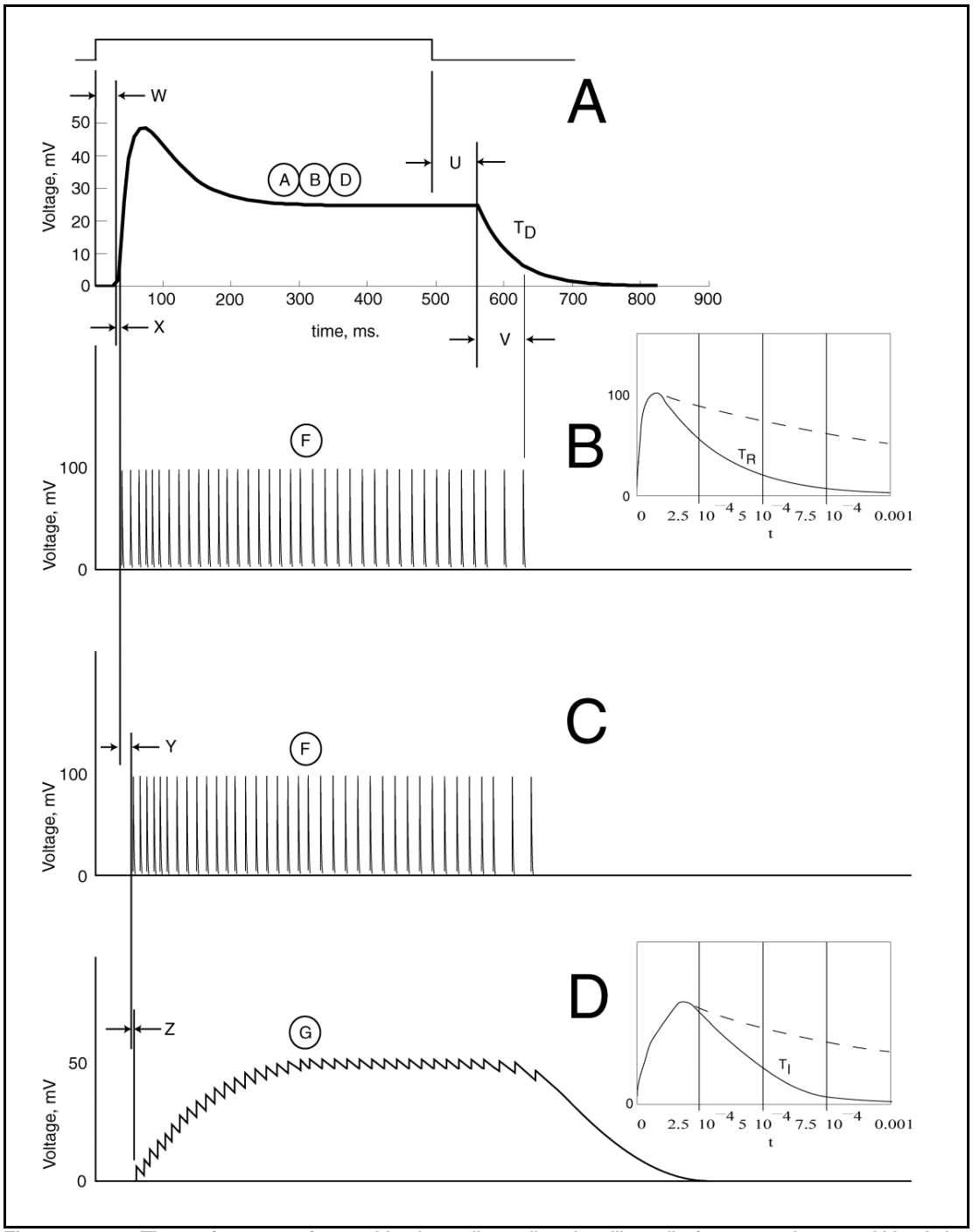

Figure 7.3.6-1 The performance of a combined ganglion cell and stellite cell of stage 3. Letters within circles represent nodes of the system where the waveforms can be observed. A; the stimulus and the resulting analog signal delivered to the ganglion cell. B; the action potential stream produced within the hillock of the ganglion cell and reproduced at Nodes of Ranvier along the length of the neuron. This signal is also delivered to the neurite structure of the stellite cell. C; the analog signal recovered by the stellite cell before any post recovery filtering. w, x, y & z; time delays between various nodes. The value of y depends on the number of Nodes of Ranvier between the source and the point of measurement. u; the delay between the end of the stimulation and the end of the analog waveform created in the sensory neuron.

7.3.7 Providing electrical power to stage 3 neurons

The mechanism powering all neurons is discussed in Section 3.5. Wenthold & Martin have provided material specific to the biochemistry of the stage 3 neurons, with particular emphasis on the role of glutamate and aspartate in their operation[51]. Although their discussion is based on the chemical theory of the neuron, the data is compatible with the Electrolytic Theory of the Neuron proposed here. Their extensive list of references shows a clear role of glutamate and aspartate in the operation of these neurons and the lack of such participation by acetylcholine. Glutamate and aspartate operate as neuro-facilitators rather than the conventional view that they are neurotransmitters, a role filled by electrons rather than chemicals.

Wenthold & Martin also discuss the role of GABA and glycine, and their relatively high concentrations within the cochlear nucleus. Their position is in agreement with this work in describing both GABA and glycine as neuro-inhibitors. Normally, they are the residue of the electrostenolytic process powering the neurons. The excessive buildup of these neuro-inhibitors near a neuron is a clear source of inhibition. The term inhibition has been poorly defined in hearing for a very long time. Kiang (1965, page 124) addresses this awkward term "inhibition" [his quotation marks] in the context of hearing.

Oertel et al have also provided brief descriptive material on their topical application of glutamate and aspartate to neurons within the AVCN and DCN *in vitro*[52]. They did not observe any changes in the operation of the AVCN neurons based on their protocol. However, they did observe changes in the DCN neurons in later experiments under different conditions. Their results appear compatible with this work if the two amino acids are considered neurofacilitators rather than neurotransmitters. They performed similar experiments to determine the role of glycine and GABA on similar neurons *in vitro* (p. 330). Their results appear compatible with this work if the two amino acids are considered neur-oinhibitors rather than neuro-transmitters.

7.4 Reformulating the concept of signal transmission in neuroscience

Neuroscience has had a difficult time understanding the method of signal transmission used in the neural system because of a misconception adopted in the late 19th Century based on the work published by Hermann in 1863. The subject has only been addressed by a hand full of researchers over the last 150 years. Hermann proposed the signals were diffused along the length of the neuron in a manner used by William Thomson (Lord Kelvin) to describe the flow of heat in the 1850's.

This same proposal had been put forward by Thomson to explain how an undersea telegraph cable would work. Cables were built to Thomson's specification and they failed miserably.

> The cable placed between Ireland and Newfoundland in 1858, and designed to Thomson's specifications, required sixteen and one half hours to transmit the 99 word message of Queen Victoria to the New World[53]. The rate was six words per hour compared to the nominal rate of 15 words per minute of the first successful cable based on Maxwell's propagation concept . The Kelvin cable was slower by a factor of about 150:1 and clearly not commercially viable.
>
> Interestingly, Richet documents a variety of other mis-characterizations and miscalculations made by Kelvin culminating in his famous assertion of 1896 before the Scientific Jubilee. "One word characterizes the most strenuous efforts for the advancement of sciences I have made perseveringly during fifty-five years, and that word is Failure."

All subsequent coaxial cables were designed by electrical engineers in accordance with Maxwell's Laws (specifically the GWE described below). These have all performed as designed (beginning in 1863).

> While Thomson's accomplishments were many, he could not accept scientific defeat or the burgeoning work of others. His best remembered quotations from later in his life include: "Radio has no future" and "X-rays are a hoax." He obviously did not consider the general solution of Maxwell's Equations or the emerging understanding of the photon as too important. Thomson fought the Maxwellian concept of propagation until he passed from the scene.

While compatible with the teachings of Thomson, a dominating figure of the 19th Century, Hermann's concept of neural transmission along an axon was, and remains, inappropriate. Up until now, no more detailed description of axon signal propagation has appeared.

In large animals, the distance between individual neurological engines can be considerable. The distance between peripheral elements and the CNS can exceed 10-15 meters. Transmitting a neural signal over these distances by charge diffusion requires prohibitive amounts of energy (power over a period of time) and incurs significant bandwidth penalties.

Signal transmission occurs within the neural system in two forms. The simple diffusion of charge is used over distances of less than one millimeter. Transmission of energy over distances greater than one millimeter is accomplished by an alternate mechanism, propagation.

The unique mechanisms associated with the propagation of neural signals, and described here, have been observed primarily, if not exclusively, in *Chordata*. The purpose of these mechanisms is to achieve the energy efficient transmission of neural signals over long distances essentially error-free. These purposes are best achieved by changing from an analog method of signaling (as used in stage 1, 2, 4 & 5) to a phasic or pulse (frequently described as a digital) mode of signaling as found in stage 3.

This section will explore the mechanisms used in stage 3 to achieve high performance signal propagation over long distances. Understanding the method of action potential propagation in stage 3 neurons requires three conceptual changes:
- replacing previous concepts of the axon as an RC transmission line as proposed by Hermann,
- replacing the concept of a neuron as an active two-terminal device as proposed by Hodgkin & Huxley, and
- replacing the concept of signal transmission by the diffusion of charge as proposed by Thomson.

The phasic signals, consisting of streams of action potentials, are propagated (as opposed to diffused) over typically myelinated axons just as they are within a man-made coaxial cable. The axon exhibits resistance, inductance and capacitance (R, L & C or RLC) just like any coaxial electrical assembly. The equations of Maxwell (known as the GWE) describe this electromagnetic propagation over the neuron precisely.

> A key difference between diffusion and propagation concerns the duration of the signal at the source. In diffusion, the source must be held at the desired potential until the signal has reached the receiving point (generally a fraction of a second within the neural system). In propagation, the source must be held at the desired potential only for a short interval described by the reciprocal of the bandwidth of the channel. This is a much shorter interval (typically milliseconds). As a result, propagation can support signaling at several orders of magnitude higher frequency than can diffusion. The detailed discussion concerning these competing high level concepts is found in Section 7.4.2.

7.4.1 Background related to stage 3 neuron propagation

The operation of stage 3 neural channels has not been presented previously in the hearing literature. To overcome this problem, this section will, of necessity, present a range of material at an academic level before describing its application in the neural system. Of specific importance will be the mathematics associated with the General Wave Equation (GWE) of Maxwell. It provides the framework for discussing all means of signal transmission within the neural system. The various forms of the GWE will be developed as appropriate to the signaling function. While Thomson (Lord Kelvin), Hermann, Cole, Hodgkin & Huxley, Tasaki, Rall and Taylor have offered explanations of how signals were transmitted within the neural system, their explanations were unsuccessful. Only the briefest remarks on these roles will appear below.

When investigating the transfer of neurological signals, all of the methods available must be considered if the correct model is to be obtained. Theoretically, the transfer of a signal can involve conduction (diffusion) through a medium, convection (circulation) within a medium, and propagation through (or along) a medium.

1. Diffusion will be used in the conventional sense used in physical chemistry, the movement of atoms or ions *through* a second material along a field gradient. However, it is important to recognize that the diffusion coefficients of a given material may differ considerably based on the state of matter of the second material. The liquid, liquid-crystalline, crystalline solid, and amorphous solid states are particularly relevant to biology

Conduction as used in electronics and electrolytic chemistry relates to the diffusion of electrical charges from one location to another *through* a second medium. Again, the state of matter involved is critical. In most states, the transfer of charge does not involve the physical motion of heavy ions. The dominant carrier is usually a negatively charged electron, except in some liquid-crystalline or solid-crystalline materials. In those cases, the dominant carrier can be the positive equivalent of the electron, known as a hole. As noted in Section 3.5.4, the hole has the mass of an electron but a different mobility. This mobility is due to an electron moving in a salutatory manner through such

a crystalline material. Bockris & Reddy discuss the motion of holes in great detail without recognizing it is the negative charge that is actually moving[54]. They speak of it as "the non-conforming ion."

2. Convection is the physical transport of energy, or other identifiable feature, by means of the bulk physical motion of the substrate, to which the feature is physically attached, along a gradient.

4. Propagation is a distinctly different form of energy transmission. Propagation is a vector-based mechanism that plays an important role in acoustics and electromagnetics. It does not involve the physical movement of any particle over a substantial distance. In the acoustic environment, it explains the spatial separation of acoustic signals within the cochlear partition. One application in the electromagnetic environment is the propagation of signals along stage 3 neurons. In the electromagnetic environment, this mechanism involves two orthogonal quantities, an electrical field and a magnetic field. In the acoustic environment, the quantities and fields involved are more complex as discussed in Section 4.1.5.

> Propagation in the technical sense defined here plays a major, well documented but previously unexplained, role in the operation of the neural system of all chordate animals. Maxwell's general wave equations will be found to be key to understanding both the operation of the neural signal transmission system and the method of frequency analysis employed within the cochlear partition of the hearing modality.

The scope, and discipline, of electrophysiology is not uniquely defined in the literature. Piccolino has provided a recent historical review of the field of electrophysiology from its beginning with the famous experiments by Galvani (1791) on the legs of the frog[55]. This section is primarily concerned with the electrophysiology of the signaling performed within the neural portion of the cells forming the stage 3 neural system. The electrophysiology of other cell types in other systems is not of concern. Even the electrophysiology of the soma of the neuron, and its internal constituents, are not of concern here.

There has been a general misconception in the biological literature, dating from Hermann in the late 1800's[56], that an electrical transmission line of adequate bandwidth can be composed of only resistors and capacitors. Hermann began an extensive investigation into the responses of nerve using the most primitive of tools (using sulfuric acid as an analog of a biological plasma). He initially reported his work in 1863[57]. While drawing some useful conclusions concerning the chemistry related to neurons, his electrical model was obviously primitive. Many of Hermann's electrical drawings show a familial similarity to some of Maxwell's of the same period[58]. While interesting, the Hermann representations appear bazaar today. Hermann formalized his concept of neural response, based on the Heat Equation of Thomson, while Maxwell, who was sitting nearby, was finalizing his broader General Wave Equations (the GWE). The problem that Hermann (and Thomson) overlooked was that electrons are charged particles. The flow of a current through a conductor induces a magnetic field. Any change in that current induces a change in the magnetic field that is opposed by the inductance of the conductor and its environment. How to handle this induced magnetic field was one of the fundamental (and revolutionary) features of the GWE.

The neuroscience community accepted the Hermann proposal and has long contended that the axons of neurons were completely characterized by only the two parameters, resistance and capacitance. This has been true in spite of the extensive work of Cole in the 1930's and 40's measuring the inductance of axons[59]. Huxley & Hodgkin were aware of the inductances measured by Cole but, like others in the field, chose to ignore the inductance in favor of the simpler analysis based on Kelvin's heat equations.

Thomson's heat equations are based on a first order differential equation and result in exponential functions related to two circuit parameters, typically resistance and a single form of reactance known as capacitance. The first order form supports the mechanism of diffusion. Maxwell's GWE are based on second order differential equations, result in the flow of energy in sinusoidal form. The flow is related to three circuit parameters, resistance, capacitance, and a second form of reactance, inductance. The second order form introduces the mechanism of propagation.

A Hermann cable (a.k.a. Kelvin cable) is frequently labeled an RC cable based on its containing only resistances and capacitances. The more general Maxwellian cable can be labeled an RLC cable.

The proposition that the operation of a neuron can be explained based on the first order differential equation of Thomson is not founded on electrical engineering principles[60] nor supported by subsequent physiological experiments. The discovery of the saltatory nature of the neural signals was particularly damaging. Cole discussed the difficulty of using the diffusion equation to explain neural operation extensively in 1968[61].

Taylor attempted to rationalize some of the many models of cables in the literature through that of Hodgkin & Huxley.

Taylor presented a thorough mathematical review of "Cable Theory," as restricted to an RC cable[62]. He includes a section on the giant axon with an axial wire introduced into it. Taylor does note the following crucial fact ten years after the work of Hodgkin & Huxley. "Since the 1939 papers of Tasaki, in which he demonstrated directly that only the nodes of Ranvier in mammalian myelinated nerve are excitable, it has been abundantly shown and generally conceded that the 'saltatory' theory as propounded by Lillie is correct." This position may have been more controversial than he suggests. However, it remains correct today. He references Tasaki's 1953 paper and provides a caricature of the myelinated axon with Nodes of Ranvier. It is not clear why Taylor did not interpret the complex plane data of Cole as calling for a second order differential equation containing both inductance and capacitance.

Taylor then makes a set of assumptions. "We make the assumptions that the radial currents in the core and external region are to be ignored, that the myelin sheath between nodes has an infinite resistance and negligible capacitance and that the node width is negligibly small but with finite impedance." This statement defines a loss-free line (to be defined below) and not the Hermann cable he continued to use in his analyses.

Goldman & Albus followed with a similar mathematical derivation in 1968[63]. Like Taylor, they relied upon the Equation of Heat rather than the General Wave Equation, although they did introduce "isopotential patches of excitatory membrane" to model Nodes of Ranvier. Like Hodgkin & Huxley, they could not solve rigorously the equations they developed and relied upon dimensional analysis and numerical methods. The velocities presented by Goldman & Albus are calculated using parameters chosen to match the <u>average</u> velocities found in the literature (8-45 meters/sec) and not the phase velocities discussed below.

After nearly 100 years, Rushton re-examined Hermann's proposal and attempted to restate it in the appropriate terms of his day. He presented a series of calculations using dimensional analysis as a tool rather than providing rigorous mathematical solutions. Rushton described signal transmission along an axon using Hermann's model but assigned his interpretation the label "local circuit theory." Piccolino (pg 393) has pointed out that the term local circuit theory does not appear in Hermann's writings.

It is unfortunate that other investigators did not challenge the work of Rushton and suggest a reinterpretation of his views. Replacing the static "local circuit" by the dynamic "local interaction" of electromagnetic fields would have led to an entirely different perspective on neural signal transmission.

Rall provided a short mathematical rationale that distinguishes between signal transfer by conduction versus signal transfer by propagation for the first time in 1977[64]. However, he did not differentiate between projection neurons involving action potentials and other neurons processing electrotonic signals. The matter of myelination is a crucial factor in discussing these two major classes of neurons. Without recognizing the difference between these classes, it is unrealistic to draw conclusions as is done at the end of his rationale. Rall continued to model the signal transmission within an axon of a neuron based on Hermann's cable as late as the 1980's but with poor results[65].

Ritchie reviewed Rushton's concept of the local circuit in Waxman et al. in 1995[66]. While using the term propagation in the vernacular, he made no distinction between conduction and propagation in the technical sense. Nor did he differentiate functionally between the types of neurons represented in his caricatures (figure 4.1). He did report current pulses as a function of location along an axon. Neither he nor Rushton addressed the inductance associated with the axon and measured by Cole.

In summary, this work does not support descriptions of the axon segment based on the RC cable concept. The failure associated with the Hermann (a.k.a. Kelvin) cable is that the signal source must maintain its voltage (or temperature) value until the signal arrives at the far end of the cable by diffusion. The bandwidth of such a cable is proportional to the diffusion velocity divided by the distance. The longer the distance, the lower the bandwidth. As a result, the inter-symbol interval is proportional to the distance. In underwater telegraph cables, the inter-symbol interval became many seconds to minutes. With an inter-symbol delay this long, the bandwidth of the RC cable was unusable. The following sections will show a coaxial structure of the RLC cable type leads to a different mode of signal transmission wherein the inter-symbol delay is given by the reciprocal of the bandwidth of the cable itself.

7.4.2 Replacing the excitable axolemma of Hodgkin & Huxley

The conditions noted by Taylor in 1963 appear to still be true. There is no radial current through the axolemma of a myelinated axon and regeneration of the action potentials occurs at the Nodes of Ranvier.

This work replaces the two-terminal excitable axolemma of Hodgkin & Huxley with the three-terminal Activa formed by the junction between two asymmetrical plasmalemmas (Chapter 3). Because this can be considered a drastic step, some of the problems with the primitive Hodgkin & Huxley neuron are summarized below.

Hodgkin & Huxley presented the results of a particularly intensive study of the axolemma of the third stellate nerve of the squid, *Loligo*, at the midpoint of the 20th Century[67]. Because of the unique relative size of the axon of this nerve, it has come to be known as the giant axon of the small squid *Loligo forbesi* (not the axon of the giant squid). While they only reported on their *in-vitro* experiments related to the axolemma of the neuron, and not the entire neuron, their work has been widely accepted as fundamental to the understanding of the neuron.

The work of Hodgkin and Huxley, supported by Katz and a number of other team members, has taken on a dominant position in the field of neuroscience. The work has become a cornerstone in all pedagogy related to neuroscience. However, the work has not stood the test of time as well in the research environment. Their truncation of the scientific method as they applied it to the overall problem of the neural system has introduced a variety of unstated limitations. It has prevented the introduction of a broad array of scientific and mathematical tools to the challenge of understanding the operation of the neuron (and the axon).

Unfortunately, Hodgkin & Huxley made a series of protocol and procedural decisions that prevent their work from being extended to represent the actual biological situation, or even representing the functional aspects of, the giant axon.

1. As noted by Hodgkin in an introductory paper[68], their approach did not involve the use of the optimal "scientific method." It was highly constrained.

"In order to restrict the field, the review has been confined to the problem of conduction in single fibres, and any consideration of junctional-tissue or the central nervous system has been omitted. Wherever possible, experiments will be discussed in terms of a general hypothesis, which may be regarded as the modern counterpart of the membrane theory of Bernstein (1912) and Lillie (1923). Briefly, the hypothesis is that the action potential depends on a rapid sequence of changes in the permeability to the sodium and potassium ions. It makes use of the observation that potassium is concentrated inside most excitable cells, whereas sodium and chloride are relatively dilute."

Huxley and Hodgkin stressed the importance of removing all neuritic tissue attached to the soma of their neurons before attempting to repeat their experiments. They noted that this effort must be thorough in order to pacify the otherwise unstable neuron (i. e., to deactivate the actual Activa within the soma). Following this cleaning, they were left with an axon that exhibited unusual electrical performance under voltage clamp conditions that they could not completely explain (such as a negative internal resistance now known to be indicative of active semiconducting devices). The technology of their day was unaware of the molecular structure of their axolemma and the fact it was impervious to heavy metal ions but porous in one direction to electrons.

Their constrained analysis prevented them from examining the junctional-tissue of the neuron and discovering the conexus and Activa, the actual source of activity in the neural system.

2. Although not enunciated by Hodgkin & Huxley, their work has been taken to apply to all of the neurons of the biological system. Their selection of *Loligo* appears to have been a poor choice. *Loligo* is not a fish or member of *Chordata*. Significant differences are present between the stage 3 neural systems of *Chordata* and the equivalent stages in *Arthropoda* and *Mollusca*.

3. Subsequently they developed a set of partial differential equations that they did not solve. They did not obtain a closed form solution for either the transient or steady state condition applicable to their problem. Without either of these solutions, they were not able to validate their model or partial equations.

4. When their proposed static mathematical solution, based on lumped-parameter measurements, encountered problems, they used the same measurements in a proposed dynamic solution.

The calculated wavelength of their traveling action potential was a significant fraction of the dimensions of their lumped-parameter test probes. They made no obvious attempt to compensate for this problem.

5. In adopting the lossy RC-based transmission line model to explain the dynamic operation of the axon, they were aware of but discounted the inductance associated with the biological axon.

By adopting the lossy transmission line model, they were forced to consider only conduction as a mode of signal transmission within the neural system. Starting from Maxwell's Equations would have surfaced the propagation mode of signal transmission actually used to transmit signals over appreciable distances in the neural system (at least of *Chordata)*.

6. Their analyses only allowed for continuous (as opposed to switching) operations within the neuron. This forced

them to hypothesize an "independence principle" (pp. 467, 470 & 502) that allowed either sodium or potassium ions (both positive ions) to diffuse through a medium without regard to the electrical field they encountered (movement dominated by the concentration of that ion alone).

These actions of Hodgkin and Huxley have been noted by earlier writers. As Cole noted on page 476, "As to curve-fitting, the procedure and the results of Hodgkin & Huxley (1952b) are entirely unorthodox and are looked at with both amazement and admiration by trained mathematicians." An alternate expression might be "courteous academic consternation" or simply "courteous disbelief." The orthodox goal of a mathematician is to derive a set of mathematically consistent equations that provide incite into the underlying mechanism being studied.

Hodgkin addressed some of the above points in a series of statements in a later paper with Frankenhaueser[69]. As noted in statement (15) of that paper, the resulting template [presented by Hodgkin & Huxley] does not describe any specific fibre but only an undocumented ensemble of fibers. The summarizing comments of Cole concerning "The Melding of Membrane Models" are also pertinent to this summary and should be reviewed[70].

7.4.3 Introduction to the General Wave Equation

It is difficult to review the history of neuroscience concerned with signal transmission while ignoring the role of Maxwell's Equations. James Clerk Maxwell (a contemporary of Thomson and an office-mate of Hermann) published a set of equations in 1863 that can be used to describe a very broad range of physical and electrical problems[71]. One of the solutions to these equations, the General Wave Equation, predicted the advent of radio transmission and other propagation related phenomena (such as the transmission of heat by radiation as an alternative to conduction or convection).

Maxwell developed his General Wave Equations (GWE) in the context of the propagation of acoustic energy before its application to the propagation of electrical signals. However, the coupling between the vectorial elements of the electromagnetic signal and the coupling between the vectorial elements of the acoustic signal are the same. The key feature of the GWE was that any change in an electrical field with respect to time caused a corresponding change in the associated magnetic field with respect to time, and vice versa. The vectorial relationship between these two fields resulted in the propagation of energy in a direction perpendicular to both fields.

The fact of primary importance is that an electrical field changing with time induces a changing magnetic field and that changing magnetic field induces a subsequent changing electrical field. The result is the propagation of a signal in a direction perpendicular to the two fields. No movement of physical particles in the direction of propagation is required.

7.4.3.1 Resolving an inconsistency related to physical chemistry

A cursory scan of Physical Chemistry texts quickly confirms a relevant fact. The field of chemistry does not usually employ the complete version of the General Wave Equation (GWE). Only the simplified forms of Poisson's Equation and the Heat Equation are found. As a result, most of the investigators in neurological research have not been introduced to the GWE, the fundamental equation describing stage 3 signal projection.

A point of confusion has been introduced into the use of Poisson's equation in the study of chemical kinetics. The kinetics of chemical reactions seldom if ever oscillate between two states. As a result, only the first order differential with respect to time is required to explain most kinetic situations. However, the expression on the right frequently exhibits an exponent. It has become common to describe the first order differential equation of kinetics using the term order to describe the highest level exponent on the right. The mathematical community uses the term power, rather than order to describe the value of this exponent. To avoid confusion, it would be preferred if the chemist described the equation for what it was in the language of a mathematician. This notation will be used here. The equations of chemical kinetics are first order ordinary differential equations in various powers of the right-hand term.

This nomenclature quickly surfaces a problem in neuroscience. Not having been exposed to the GWE, many readers will find it difficult to follow the following analyses. A particular problem arises concerning the electrical inductance of an electrically conducting coaxial structure. A positive reactance (such as inductance) does not appear in the first order equations of chemistry. In electrical analogs of chemical processes, only relationships expressible in terms of resistance and capacitance are needed. To describe the operation of a myelinated axon segment, it is necessary to employ a second order differential equation that includes a positive reactance. As noted in Section 7.4.1, the discovery and documentation of the inductance associated with a stage 3 axon by Cole left the community baffled during the 1950's. The inductance data has been ignored ever since.

7.4.3.2 The fundamental GWE

Maxwell's equations have been expressed in integral, differential and matrix form. This makes their application easy in the hands of an experienced investigator. However, they are frequently daunting in the eyes of the uninitiated. Maxwell's General Wave Equation, in its most compact matrix form, can be expressed as;

$$\nabla^2 V = \frac{1}{\nu^2} \cdot \frac{\partial^2 V}{\partial t^2}$$

where del, the inverted delta, is a vector operator but not technically a vector itself. Capital *V* is a vector and nu, ν, is a scalar (that may be a complex mathematical function). This equation applies to any problem involving up to the 2nd differential of the variable, *V*, with respect to any coordinate system required to adequately express the variable.

In differential form, it is usually expressed in Cartesian coordinates as;

$$\frac{\partial^2 V}{\partial x^2} + \frac{\partial^2 V}{\partial y^2} + \frac{\partial^2 V}{\partial z^2} = \frac{1}{\nu^2} \cdot \frac{\partial^2 V}{\partial t^2}$$

The equation describes the sum of the 2nd order differentials of the variable with respect to the three spatial coordinates as equal to the 2nd order differential of the variable with respect to time. In many applications, the equation simplifies significantly when some of the terms in the expanded form of the equation are equal to zero.

1. If the value of the right-hand term equals zero, the equation is known as Laplace's Equation. This form is important in the study of electrostatics and many other problems involving static fields.

2.If the value of the right-hand term is a constant, the equation is known as Poisson's Equation. It applies to more complex electrical field problems that contain a localized concentration of charge, and many other problems.

3. If the value of the right-hand term is proportional to the time and the left-hand term only involves the first order differential with respect to position, the equation is known as Kelvin's Equation or more often, the Equation of Heat Flow. The equation represents the transfer of heat between a stationary source and a sink *by conduction (diffusion)*.

4. The general condition applies when the right-hand term is a second derivative with respect to time. This is the form (the General Wave Equation or GWE) that introduces the dynamic interaction between the variable with respect to both distance and time. This is the form that predicted the propagation of radio and light waves through free space (independent of any aether or other medium) and describes the travel of electromagnetic and acoustic waves through, or along the surface of, a variety of materials.

The GWE is also the form used to describe the operation of electrical filters of arbitrary complexity. Transmission lines are a special class of electrical filters. The coaxial cable is a specific type of transmission line that is of particular interest here.

7.4.3.3 Application of the GWE to neuron operations

To understand the operation of the neural system, it is necessary to move beyond a single concept applicable to all neurons. Different conditions, related to unmyelinated, myelinated and pseudo-myelinated axons, result in different underlying mechanisms. Different mathematical solutions describe these mechanisms.

By closely examining the operation of neurons, in the context of the GWE, it is possible to define two fundamentally different operating modes. One deals with the *conduction* (diffusion) of electrotonic signals (energy) through a bulk medium in the presence of a resistive element and a lumped-constant reactance that is dominated by capacitance. The second mode deals with the *propagation* of phasic signals (energy) largely independent of the medium present (except it may be guided by major discontinuities in the electrical properties of the medium or the surroundings). In this case, the electrical elements (R, L & C) of the cable are distributed. In a well-designed system, the reactances of the capacitive and inductive components of the coaxial cable tend to cancel each other.

The first mode corresponds to conduction in the unmyelinated axon, and in the neurites. When expressed in

mathematical form, this mode corresponds to a first order differential equation such as the Heat Equation. The solutions of these equations are represented by "real" mathematical expressions. The second mode is more complex. When expressed in mathematical form, the mode corresponds to a second order differential equation satisfying the GWE. The solutions of these equations are represented by "complex" mathematical expressions. These expressions introduce the new mechanism of propagation.

7.4.4 The efficient propagation of neural signals using a Maxwellian cable

The successful propagation of an action potential pulse over a long axon requires the generation of the pulse at an impedance level compatible with the propagation medium of the axon, the launch of the action potential pulse onto the medium, and the regeneration of the action potential before it has been attenuated to a value that cannot be recovered by the neurological system. To achieve an acceptably low attenuation coefficient for the propagation medium, the capacitance of the medium must be reduced by myelination. Finally, to avoid excessive attenuation, the signal must be sensed and regenerated within a distance of 2mm or less. Under these conditions, an action potential pulse can be propagated with high fidelity over any distance required.

The diffusion of electrical signals over very small diameter electrolytic conduits with extremely thin outer membranes is very inefficient. First, the speed of diffusion is very low and second, the attenuation of the medium is very high. This is true whether the mechanism employs the physical diffusion of ionized atoms or the transfer of electronic charges between ionized atoms that remain stationary. There is a tradeoff that trades lower bandwidth for lower attenuation. Unfortunately, this is not a desirable tradeoff. A different method of signal transmission is needed.

In order to transmit signals efficiently over long distances within the neural system (distances greater than two millimeters and up to several meters in the context of the neural system), three modifications of the analog neuron were implemented.

- First, the information associated with the analog signals was encoded into a phasic or pulse pattern, usually described as a series of action potentials. The amplitude of these pulses no longer carried any information about the stimulus.
- Second, the relative values of the electrical parameters resistance, capacitance and inductance associated with the axon (henceforth the axon segment) were changed. This was achieved by introducing an insulating jacket (a myelin sheath) surrounding the axon and in intimate contact with it.
- Third, a signal repeater capability was introduced that could regenerate the amplitude of the action potentials without disturbing the spacing between the pulses. This capability was incorporated into an active circuit between pairs of sequential axon segments. This capability and active circuit are known morphologically as a Node of Ranvier.

7.4.4.1 Background–the axon as a transmission line

No physiological models of the neuron extending beyond the conceptual stage have appeared in the recent literature. The most recent computational model of a complete stage 3 axon, based on the simple concept of the RC diffusion cable dating from Thomson (Lord Kelvin) in the 1850's and the two-terminal active neuron dating from Huxley & Hodgkin in the 1950's was diagramed by Finley, Wilson & White[72]. It is a lumped-constant model consisting of 199 computational segments (each segment includes a group of resistive and capacitive elements and miscellaneous voltage sources). They described the model as preliminary in 1988. It is only solvable by computer using an iterative procedure. The solution develops an emulation of the conditions prescribed in advance and using an extensive set of initial conditions. A more effective and accurate model of the axon can be provided by applying the GWE and using less than a dozen parameters based on measured values from the axon.

As already mentioned, many authors have discussed the axon, such as found in a projection neuron, in the context of a transmission line. Section 7.4.1 has presented the technical and historical reasons why the neurological literature has largely overlooked the propagation mode of signal transmission. Figure 7.4.4-1 compares several axon configurations with a man-made coaxial cable.

While man-made cables conventionally employ a metallic inner conductor surrounded by a metallic cylinder as an outer conductor, the neurological cable uses liquid-based conductors for both the central plasma conductor and the outer conductor formed by the surrounding inter-neural matrix (INM). Only a thin layer of the INM is needed surrounding the neuron to provide an electrical path for charge movement. However, the lack of such a continuous liquid path results in the situation in frame C that does not function as a coaxial cable. The laws of electromagnetism show that any coaxial structure exhibits an electrical inductance. In an efficient coaxial cable, the thickness and dielectric constant of the dielectric is chosen to provide a capacitance per unit length matching the inductance per unit length of the cable. In frame D, the dielectric provided by the myelin wrap has deteriorated. As a result, the capacitance per unit length of the axon segment has been drastically increased and the cable is no longer an efficient one. This is a pathological condition in living organisms.

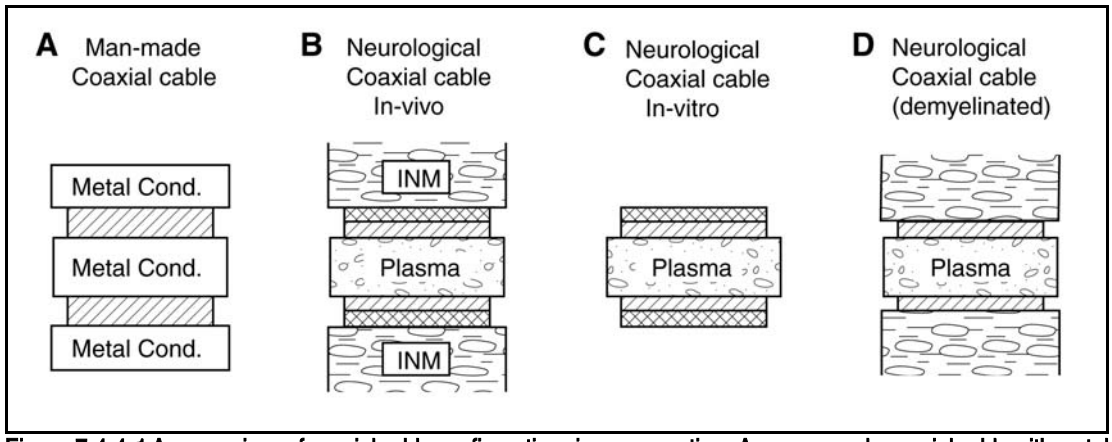

Figure 7.4.4-1 A comparison of coaxial cable configurations in cross-section. A; a man-made coaxial cable with metal conductors and a single dielectric between them. The outer conductors are part of a cylinder. B; an equivalent neurological coaxial cable showing liquid based conductors in the same configuration. The dielectric is composed of the inner layer (hatched) formed by the lemma and the outer layer (cross-hatched) of myelin. C; a neurological coaxial cable removed from its surrounding matrix and no longer functional as a coaxial cable. D; a neurological cable that has been de-myelinated in-vivo that no longer functions as an efficient coaxial cable. INM; inter neural matrix. See text.

as noted earlier, those studying the neuron have long approximated the axon segment using a simple RC ladder network as found in elementary electronics texts. Reliance on these simple ladder network analogs has introduced three major problems.

- They lend false credence to the concept of neural signal transmission by diffusion of the signal.
- They obscure the intrinsic inductance associated with any coaxial conduit.
- They do not lead to realistic values for the electrical elements of the ladder network.

Figure 7.4.4-2 presents the electrical circuit of the typical axon within the larger physiological context of the neural system. The figure is meant to be generic and apply to both the simple ganglion neuron and the more physically extended ganglion neuron consisting of one or more Nodes of Ranvier. In this context, the two titles above the figure are dual and the last Activa on the right may be either a Node of Ranvier or a generic synapse. By referring to the individual zones of the axon, it is possible to avoid confusion. For compatibility with other figures, the Activa on the left is shown being driven by a voltage source, V_s. The poditic impedances, marked Z_b, and the associated collector capacitances (formed by region x) are required if the device is intended to regenerate a pulse signal.

The conduit in the center of the figure is the transmission line of interest. It is myelinated over most of its length but not in regions x and z. The electrostenolytic voltage sources are shown as V_{cc} and V_{ee}. The dashed lines within the conduit represent the reticulum of the axon (or axon segment). The solid lines from the Activas to the reticulum are shown symbolically for convenience. In fact these conductors are formed by the physical concentration of the reticulum as it approaches the Activas. The region labeled x constitutes a lumped constant capacitance associated with the collector circuit of the first Activa. This capacitance is large due to the extreme thinness of the lemma separating the axoplasm from the electrolyte surrounding the axon. Within the area labeled y, the capacitance of the transmission line is distributed and much smaller due to the increased thickness of the lemma/myelin sandwich. The area labeled z constitutes the lumped capacitance of the unmyelinated part of the conduit in the vicinity of the input to the second Activa. Regions x and z will be described as matching sections in the following discussion. They play an important role in transmission line design.

The charge pattern shown along the top of the myelination suggests two pulses are being propagated based on Maxwell's GWE. The counter charge pattern would appear on the inside surface of the axolemma. The accompanying magnetic field loops are shown only partially as solid and dashed lines. The complete loops would extend into the axoplasm and enclose all of the charge on both the outside and inside of the lemma/myelin package.

The segment labeled x is quite variable in length, both intraspecies and interspecies, according to Pannese[73]. He gives an overall range of 28 to 54 microns. The segment labeled y is typically much longer, between one and two

millimeters.

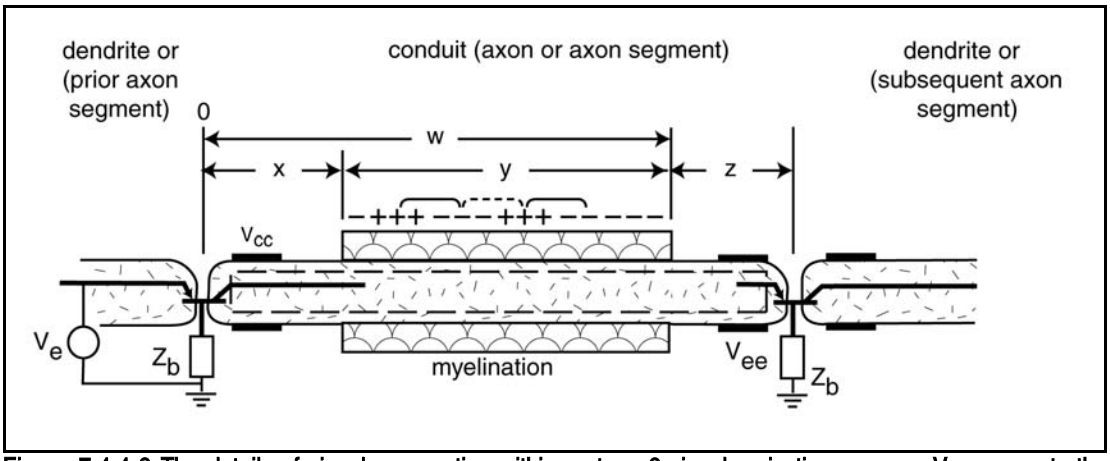

Figure 7.4.4-2 The details of signal propagation within a stage 3 signal projection neuron. V_e represents the originating pulse source. The pulse signal is transmitted by diffusion in regions marked x and z. The region marked x exhibits sufficient capacitance to cause the left Activa to act as a regenerative monopulse oscillator. Pulses are transmitted more efficiently by the propagation method in the region marked y. The plus signs on the outside surface of the myelination represent two propagating pulses separated laterally by more negative regions. An equal but opposite charge pattern appears on the inner surface of the lemma. The arches above the plus and minus signs represent the magnetic fields associated with those charged regions. See text.

The axon segment, in both myelinated and unmyelinated form, is and can be described in detail by the equations for a coaxial cable form of the electrical transmission line. Although not obvious to the uninitiated, every coaxial cable exhibits a finite resistance, capacitance and inductance per unit length. The inductance is an intrinsic feature of a cylindrical transmission line. At the more detailed level, the inductance and one resistance are associated with the longitudinal dimension of the cable while the capacitance and a second resistance are associated with the transverse dimension of the cable.

Figure 7.4.4-3 illustrate the equivalent circuits representing a coaxial axon segment, without considering any matching sections except in frame (D). (A) shows the typical lumped-parameter representation of a short section of a transmission line in unbalanced form. (B) shows the same representation in balanced form. In the ideal case, and within the operating range of the axon, the values of the resistive elements are such that the voltage across R and the current through G can be ignored. The dominant factors are the reactive voltages across the inductors and the reactive currents through the capacitive element. The effective incremental network is shown by the heavier lines. To more accurately represent the physical length of a real axon, it is more appropriate to describe it by using the emphasized network on the left replicated on an incremental basis. The symbol for such a distributed network of a real axon is shown in (C) It describes the electrical performance of the real axon over the distance between its terminal components.

The network in (C), representing the section Y in the previous figure, has a characteristic impedance that is seldom well matched to the driving source. This leads to electrical inefficiency. To avoid this problem, good design practice calls for the introduction of a "matching filter" section between the transmission line and the source and between the transmission line and the following sink. These matching sections are lumped parameter networks similar to that in (D). These filters are similar to one half of the filter shown in (A) but with slightly different parameter values. They represent sections X and Z in the previous figure.

Several significant features should be noted for such an ideal circuit.

1. No significant resistive elements appear in the distributed equivalent circuit of the ideal axon. The longitudinal resistance, R, is very low and the radial conductance through the axolemma and myelination, G, is equally low. The circuit does not dissipate significant electrical power.

2. An actual axon segment consists of two portions, the extended middle section described by the distributed equivalent circuit, and the "matching" end segments which are best modeled using a circuit similar to the lumped

constant model.

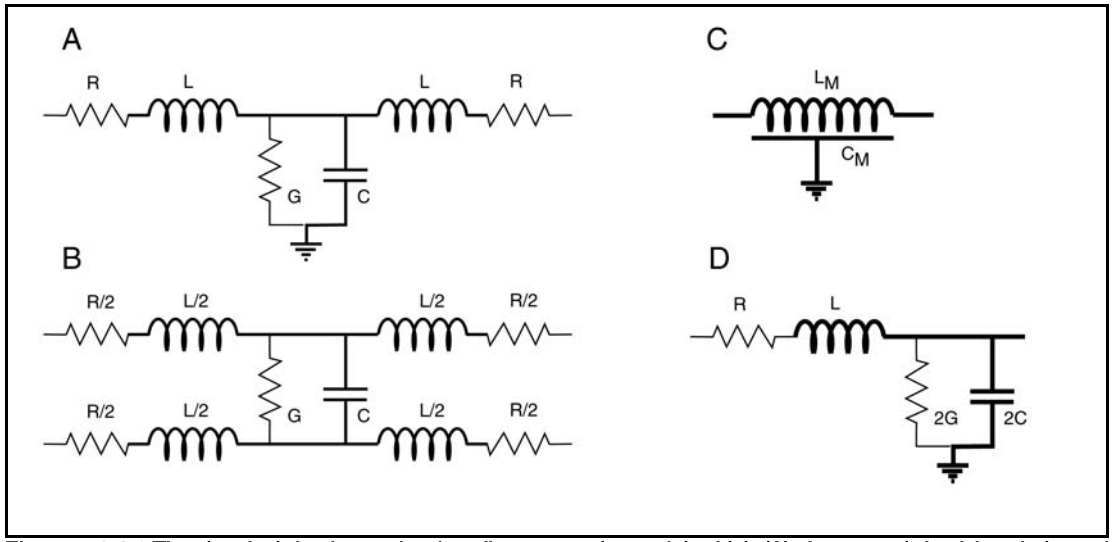

Figure 7.4.4-3 The electrical circuits used to describe an axon (a coaxial cable). (A); the general circuit in unbalanced lumped-parameter form. (B); the same circuit drawn in balanced lumped-parameter form. In efficient cables, the conductive currents passing through the resistive elements are negligible compared to the displacement currents through the inductive and capacitive elements. As a result, a simpler notation is available. (C); the simplified distributed network based on the dominant displacement currents. It forms an efficient propagation medium. (D); the half-section used to terminate either end of the line in (C) based on the component values in (A).

3. The signal propagation velocity along the axon is dominated by the ratio of the inductive to capacitive components per unit length.

4. The loss in signal amplitude along the axon is very low in the ideal case.

5. The group velocity is equal to the phase velocity of the axon segment.

These features of a real axon differ considerably from the Hermann cable model. The real stage 3 axon segment is not, and cannot be described as, an RC network.

Both the inductance and the capacitance of a coaxial cable can be calculated from the physical dimensions of the cable and the appropriate dielectric constant, (ε), and permeability constant, (μ). It must be noted, the equation for the capacitance of a cylindrical structure cannot be calculated from an equivalent pair of flat plates of equivalent area and mean separation. The equation for the mutual inductance of a coaxial cable is different from the equation for the self inductance that is related to the inductance of a straight solid conductor. The total inductance of a cable is the sum of the mutual inductance and the self inductance of the cable. The equations of a coaxial line can be found in any text on transmission line theory.

By optimum choice of the inductance, capacitance and two resistance values, the coaxial cable formed by the axon segment can be made nearly "loss-free." Here, the expression loss-free does not relate to minimum attenuation but to minimum differential phase shift (group velocity in the language of acoustics). Four additional parameters can be calculated from the parameters of a coaxial cable.

- A characteristic impedance, Z_o. It is important in how a separate circuit drives and how a receiving circuit terminates the transmission line.
- The phase velocity of signal propagation, v_p along the transmission line.
- The attenuation constant of the line per unit length, α.
- The phase constant of the line per unit length, β.

Under the loss-free condition, the phase constant is zero and the group velocity equals the phase velocity and the phase velocity of the coaxial cable can be easily calculated. These calculations quickly demonstrate the purpose of myelination. Myelination is used to establish the "loss-free" condition for axon segments of finite diameter.

As noted by Schwan, the *in-vivo* capacitance of an axon may differ from its value in air due to the complex impedance of the INM that normally surrounds it[74]. This variation may aid in rationalizing some of the capacitance values found in the literature.

The existence of an inductance associated with every myelinated coaxial neuron negates all of the equations found previously in the biological literature for such a neuron. The mathematical description of a real axon segment requires recognition of the inductance of that segment.

Besides documenting the existence of an inductance associated with an axon, Cole notes that: "Every element of the circuit, except the membrane capacity C, changes with the potential difference across the membrane." However, these variations are small under operational conditions (pulse amplitudes of less than 150 mV).

7.4.4.2 Propagation over the ideal axon

Figure 7.4.4-4 presents the calculated value for these impedances for various size axons. The values are for both unmyelinated and myelinated neurons based on the membrane dimensions and for a permittivity assumed to be equal to 3.0 for discussion. As calculated, 100 layers of myelin membrane cause a change in capacitance of about 12:1. Note the significant change in these values as a function of axon radius. The unmyelinated values shown intersecting the gray bar are typical of the values to be expected in the experiments of Hodgkin & Huxley. These values are clearly not typical of the 1-5 micron radius applicable to stage 3 projection neurons in *Chordata*.

Chiu & Ritchie measured the capacitance of normal and unmyelinated axonal segments in mammals (rabbits)[75]. Although they did not provide the radius or length of their segments, they described an increase of 20 +/– 2.6 times in the capacitance after demyelination from an initial total value of 3 +/– 1.2 pF. The capacitance ratio of 20:1 would suggest a myelination consisting of about 150–200 BLM layers in their specimen.

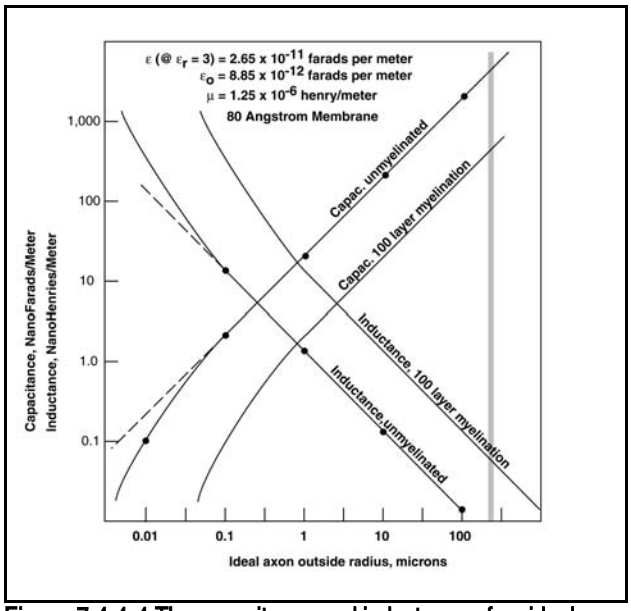

Figure 7.4.4-4 The capacitance and inductance of an ideal axon segment. R = G = 0. The vertical gray bar represents the radius of the typical *Loligo* axon without surrounding tissue.

Figure 7.4.4-5 shows the characteristic impedance, Z_0, of an ideal axon segment based on standard coaxial line equations (scale on the right). The propagation velocities shown in the figure (scale on the left) represent ideal transmission lines.

A major problem with using the giant axon of *Loligo* as a surrogate for a chordate projection neuron is seen immediately. The characteristic impedance of that size axon is very low if it is stripped of its surrounding neurons. As a result, it is extremely difficult for the conexus of the neuron to excite it. While it can support the transmission of a signal by diffusion, it may not be able to support it by propagation. While the giant neuron of Loligo makes a good motor signal processing (stage 6) neuron, it makes a very poor stage 3 signal propagation neuron. The giant axon of *Loligo* is not analogous to the stage 3 propagation neurons found in *Chordata*.

The figure also predicts propagation velocities much higher than reported in the neurological literature. However, the literature reports average velocities (including any delay introduced by Nodes of Ranvier) and not the phase velocity along an axon segment.

Section 7.4.5.2 will show the nominal phase velocity of a typical axon is 4400 meter/sec. This measured phase velocity of 4400 meters/sec is 300 to 1000 times faster than the speeds calculated by Taylor and Hodgkin. They were trying to make their Kelvin/Hermann-based approach agree with the average velocity of a neural signal traveling between two identical points relative to a chain of Node of Ranvier and axon units, instead of the phase velocity within an axon segment. The models of Taylor and of Hodgkin do not predict (or relate to) the actual phase velocity

of an axon segment.

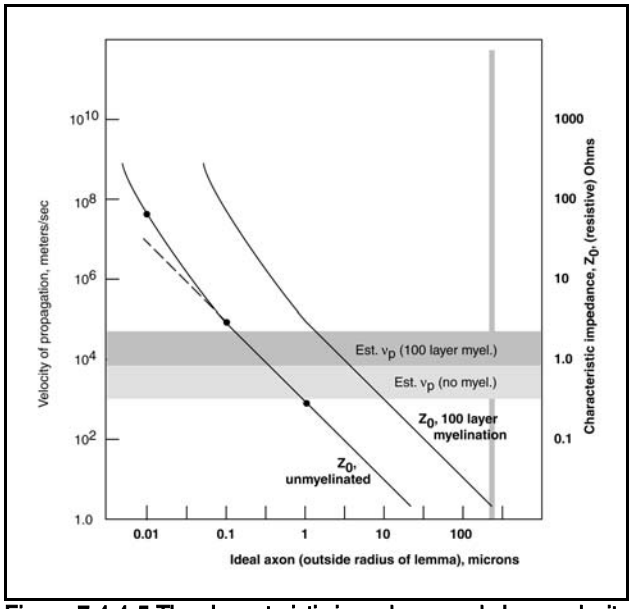

Figure 7.4.4-5 The characteristic impedance and phase velocity along an axon. Upper solid line, a typical myelinated axon. R = G = 0. The phase velocity does not vary significantly for typical biological dielectrics. Bottom, the estimated values are for a real but unmyelinated axon. The characteristic impedance is relative to the square root of L/C. The vertical gray bar represents the radius of the typical axon of *Loligo*.

7.4.4.3 The variation in reactance over a lossy coaxial cable–a real axon

Figure 7.4.4-6 shows actual impedance measurements by Cole on the squid axon after undefined preparation procedures. Caution should be observed here. The data was collected under pathological, *in-vitro, conditions*. Cannulation changed the effective conductance of the fluid within the axon. The plasma was frequently replaced by sea water to simplify the instrumentation procedure. Such a change would have a significant change in the conductance of the internal fluid. Cole describes the empirical derivation of the expected impedance on pages 36-37 (without considering any potential inductance) and then notes the considerable consternation in the community when the axon was found to exhibit considerable net positive (inductive) reactance at low frequencies. Pages 78-79 describe conceptual discussions aimed at avoiding the obvious. The coaxial axon exhibits significant inductance.

Cole presented the data in a nonstandard form in his original work. By using conventional filter theory and complex plane plotting conventions (positive reactance at the top), the revised figure can be used to evaluate the nature of the impedance measured on a lossy axon based on conventional filter theory.

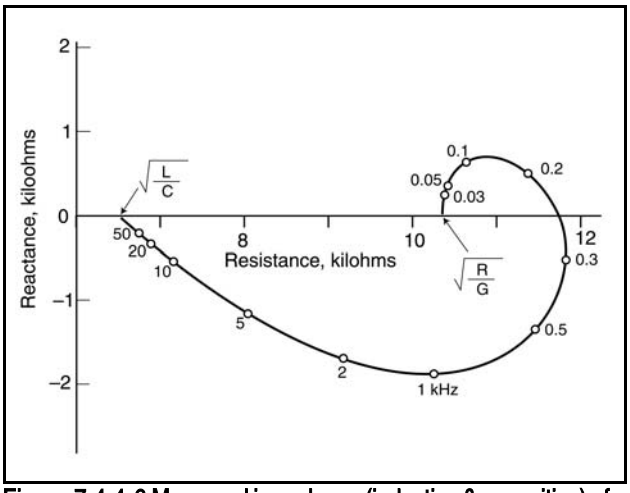

Figure 7.4.4-6 Measured impedance (inductive & capacitive) of a real axon after unspecified preparation procedures. Replotted from Cole, 1968, and annotated. Positive reactance values show a net inductive reactance. The locus crosses the horizontal axis at three frequencies. A high frequency dominated by the ratio of L/C, a very low frequency dominated by the ratio of R/G, and an intermediate point describing the ideal (lossy) cable.

The equation for the characteristic impedance can be useful in interpreting the complex impedance plane measurements of Cole. However, it must be noted first that the equation only applies to a transmission line that is terminated at each of its ends using an impedance equal to this characteristic impedance. If the cable is not properly terminated, measurements such as Cole made will depend on the precise position along the axon where they are made. The measured values will reflect this inadequate termination by exhibiting a voltage standing wave ratio, VSWR, along the line. This parameter is an indicator of the error in termination. In the case of a real axon, the adequacy of the termination is currently unknown. However, a matching filter is usually required between the myelinated portion of the axon and the active circuits at each end of each axon segment. Such a matching filter is usually formed by the unmyelinated portion of the axon segment, segment z. This matching section was destroyed by the cannulation used by Hodgkin & Huxley and by Cole.

7.4.5 The propagation velocity of a real stage 3 axon

Excellent data on the phase velocity of signal propagation by an axon is available. The same data shows the time delay associated with each Node of Ranvier.

7.4.5.1 Historical Background –propagation velocity of axons

Based on his "local circuit theory," Rushton developed an empirical relationship between the average value of signal propagation in a myelinated neuron and its diameter. Rushton's calculations showed that the conduction velocity in an axon should be related to the square root of the axon diameter. Until the discovery of saltatory conduction in nerve fibers in the late 1950's, Rushton's approach was not challenged within the community. In fact, Ritchie presented it again in 1995 in parallel with other material taking a different approach. Ritchie[76] pointed out this prediction has not proven accurate in the laboratory. In hindsight, Rushton was calculating the end to end or average velocity of a signal along an uninterrupted axon without considering the effect of any series inductance or shunt capacitance. His solution does not apply to the propagation of a pulse over a transmission line.

In 1962, Fitzhugh presented a quite different analysis of the problem. He assumed saltatory conduction and models the axon as consisting of an excitable membrane, using the Hodgkin-Huxley membrane model, at each Node of Ranvier with a section of cable between them. The cable consisted of only resistors and capacitors. The membrane was the conventional two-terminal network of the time. Although Fitzhugh spoke of a delay at each node, he did not incorporate such delay in his model. The equations he presented contained more than twenty adjustable parameters, six of which were of unknown physical significance[77]. Four of the six were complex algebraic functions of time. Fitzhugh was unable to solve the equations and resorted to numerical calculation based on circuit element values given by Tasaki in 1955. While his figures are still reproduced today, they should be discounted.

Frankenhaeuser & Huxley[78] presented a paper using the same mathematical framework for the excitable membrane as Fitzhugh and listed 15 caveats applying to their evaluation of the same differential equations. They did not solve the equations but converted them to the difference form to accommodate a digital computer.

A frequently referenced paper followed in 1968 by Goldman & Albus[79]. This paper adopted the same set of partial differential equations as used by both Fitzhugh and by Frankenhaeuser & Huxley. It did not incorporate the notion of saltatory transmission by projection neurons. They continued the previous approach of depending on dimensional analysis to accredit the equations and then proceeded to convert them to numerical difference equations for evaluation via a general purpose digital computer. They included a crucial comment. "This treatment of course, produces no information as to the exact form of the solution nor can any actual conduction velocity values be obtained."

These four analyses must be considered exploratory by current standards. They did not adopt equations for a real transmission line and they did not treat the Node of Ranvier as an active, three terminal, site. Lacking a solution to their simultaneous differential equations, there is no way to prove their equations have been formulated properly and are represented by the proper initial conditions.

7.4.5.2 The measured propagation velocity of an axon *in-vivo*

Huxley & Stampfli [80] presented a figure in 1949 that described both the phase velocity and the average velocity of the signal traveling along an axon *in vitro*. The data was limited by the instrumentation of the day. Although not as accurately calculable as in the next figure, the curves are consistent with the phase velocity of 4,400 m/sec and the regenerator delay of 0.19 msec found there. The signal waveforms are all monophasic.

Smith et al. have provided some data that updates the Huxley and Stampfli results[81]. The first three figures of Smith et al. describe real test configurations and real results. However, the mathematical models used to create figures 5-4 and beyond do not represent the propagation of a real signal along a real axon. No attenuation constant or phase constant was introduced into their equations. Bostock has presented additional data[82,83] but a similar caution applies. Most of his voltage waveforms were computer-generated.

Figure 7.4.5-1 is from Smith et al. It is reproduced here with a series of dashed lines and a heavy vertical arrow added by this author. The specimen was a rat spinal root axon *in-vivo*. (A) was obtained by launching a pulse along an axon using the test configuration of Rasminsky & Sears[84] and measuring the voltage profile at 0.1 mm intervals using a probe next to the outside of the Schwann cell surrounding the axon. Usually, the detected signal was due to displacement currents. The leakage current component of the interneuron where it is myelinated is exceedingly low. It is possible the waveforms contained a conductive component for the probe positioned in the perinodal space. The signal levels were so low that considerable data processing was used to obtain these waveforms, typically averaging

128 individual traces at each location. (B) was obtained by taking the trace-to-trace differences after averaging. This process emphasizes the major changes occurring in the areas of the Nodes of Ranvier. These waveforms were then used to construct the contour map in (C).

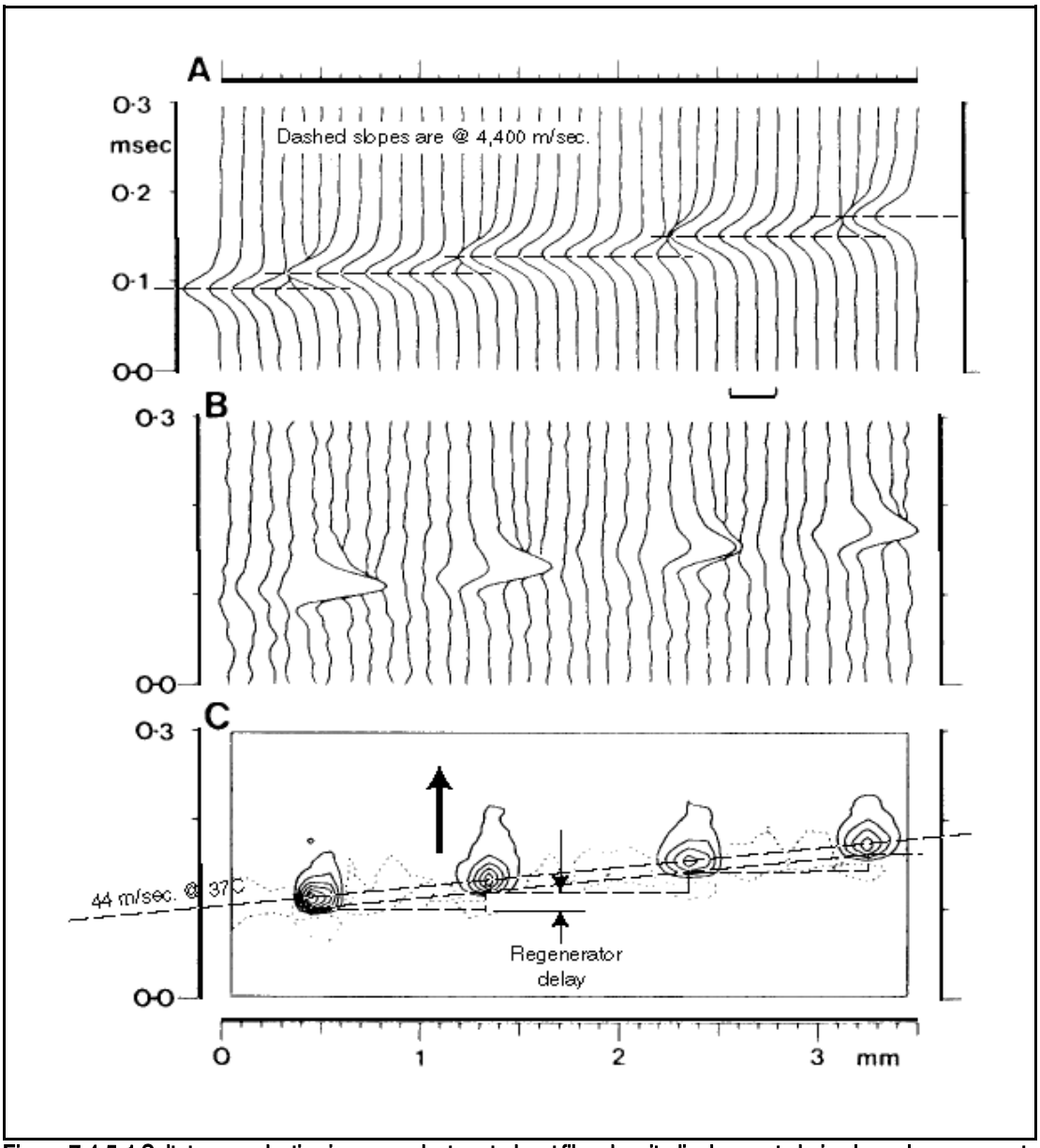

Figure 7.4.5-1 Saltatory conduction in a normal rat ventral root fiber: longitudinal current, derived membrane currents and membrane current contour map, plotted to same distance and time scales, with dashed lines and arrowheads added by this author. A, Averaged longitudinal currents (n=128) recorded at 100 micron intervals along the root (calibration bar: 4 microamps.). B, Membrane current records calculated by subtracting adjacent records of (A). C, Membrane currents re-plotted as a contour map. Inward currents are indicated by continuous lines, outward currents by dotted lines. Contour interval: 0.5 nA/100 micron electrode displacement, 37C. Dashed lines relate to signal velocities in the neuron, see text. Modified from Smith et al. (1982)

The focus of each contour group represents the best estimate of the location of the Node of Ranvier (along the horizontal axis). It also represents the time of occurrence of the peak amplitude of the signal at that location relative to the signal at the previous measurement point. Note that the best estimate of the node position is in fractions of a

millimeter in this presentation whereas the actual axial node dimension is in microns. The probes used had a nominal diameter of 100 microns. The contour map is a particularly compact form for interpreting the information obtained. However, it obscures some features of the raw data. The grouping of the waveforms in (A) is very important. In (C), overlaying a sloping line through the peaks of the contours to obtain an average velocity for the neural signal over a distance of several nodes is possible. The overlay shown corresponds to an average velocity of 44 meters/sec., a number consistent with the literature for a myelinated axon of about eight microns overall diameter. The peaks of the contours represent the peak of the newly regenerated action potential at each node. A second dashed line can be drawn slightly below this line and with the same slope. This second line is shown as intersecting the skirt of the contour at approximately the 10% amplitude point. It is meant to represent the average velocity line measured at the point where the threshold level of the regenerator circuit is exceeded. This is the point where the integrated current from the transmission line of the previous axon segment has resulted in a voltage exceeding the threshold voltage.

Looking again at (A), one sees a quite different picture. A similar dashed line drawn through the peaks of each of the individual groups of measurements is very nearly horizontal. At the scale shown, this overlay shows the phase velocity of the signal within a given axon segment is immensely faster. At the scale of the drawing, the phase velocity is clearly at least 30 times faster and probably 100 times faster than the average velocity in (C). The dashed lines in (A) are drawn at 1% of the average velocity slope passing through the nodes in (C), e. g. 4400 m/sec. Although these lines appear horizontal, they are not. Pending further experimentation, the phase velocity of the signal within an individual axon segment of a myelinated neuron of about eight microns overall diameter will be taken as 4,400 meters/sec. This measured value is at least a factor of 100 times the accepted average velocity associated with a myelinated neuron of this size. If dashed lines, again apparently horizontal, representing this phase velocity are introduced into (C) as the velocity between nodes, there is a considerable delay left unaccounted for at each node. This delay is the pulse regenerator delay associated with the charging time of the regenerator conexus that reproduces the action potential. The delay derived from the graph is approximately 0.19 msec. at each node. The fundamental conclusion is obvious. The average velocity in a myelinated neuron is not related to the phase velocity within the axon segments. The delay associated with the phase velocity within each axon segment is negligible. The average velocity is calculated from the average axon segment length divided by the pulse regenerator delay at the associated Node of Ranvier. In this case, the average projection velocity is very near 44 meters/sec (compared to 4400 meters/sec for the phase velocity).

Rasminsky and Sears have provided similar data for a demyelinated ventral root nerve[85]. Even in this condition, their data shows propagation velocities of 500 to 600 meters/sec or higher (in some cases, much higher by scaling).

Both Huxley & Stampfli and Smith et al. calculated an average velocity for their data but neither group addressed the obviously much higher phase velocity in their data.

7.5 The use of statistical and graphical tools in hearing research

Recording stage 3 signals and preparing histograms from them can provide excellent and detailed performance data concerning the hearing modality. The histograms corroborate many of the circuit diagrams, mechanisms and features of hearing described in previous chapters. The importance of documenting the precise location of the measurements (within a millimeter) is highlighted by the delay of between 0.7 and 1.0 ms encountered at each active conexus, whether it is at a synapse, at a Node of Ranvier or within a soma.

While neural signals related to a given stimulus are not stochastic, their complexity has led frequently to the use of statistical methods as an aid to interpretation. These techniques are useful as a first order guide to the underlying mechanisms. Recognizing that the pulse streams associated with stage 3 neural signaling are time-delay encoded is key to understanding these pulse streams. With this understanding, the stage 3 phasic signals can be traced back to their analog origins.

Three methods of graphical presentation have proven particularly useful in hearing research. They are reviewed in Section 7.5.1; the peristimulus interval (PST) histogram, the inter-pulse interval (IPI) histogram and the regularity analysis of Bourke. The problem is that none of these presentations gives a complete description of the relevant phasic signals. They are only useful when interpreting highly simplified and stylized stimuli, generally constant amplitude sine wave bursts. Even in this situation, both the frequency of the sine wave and its intensity significantly impact the information displayed in the graphic.

The PST histogram is particularly sensitive to the Riemann folding of the original record. If the selected interval is not a multiple of the period of the stimulus frequency, the stimulus envelope and the resulting action potential pulse stream, it will not be stationary in the mathematical sense. The result will be an artificially high “spontaneous rate” caused by smearing the implicit information associated with at least one of these across the interval of the histogram. This is a particular problem with the action potential pulse rate since this parameter is not controlled directly by the

investigator.

The pattern of action potential generation in a specific neural channel in response to a stimulus is very complex. The pattern depends on:

1. The processing mode supported by the channel.
2. The distance from the sensory neurons along the neural channel.
3. Whether the channel is a summing, a differencing or a more complex channel.
4. The amplitude profile of the stimulus.
5. The frequency content of the stimulus amplitude-profile.

There are two major problems inherent in the use of histograms in hearing research. The first relates to the fact that once the data is convolved into a histogram, it cannot be de-convolved in support of additional research. While it can be argued that a rate histogram of the PST type shows information that a continuous temporal recording may not, the opposite is also true. This is clearly shown but not highlighted in figure 8.13 of Gulick et al[86]. Their PST histograms clearly show the periodicity of the pulses following the first pulse but overlook the statistical probability that the second pulse in the pulse train of their temporal recordings may not occur because of threshold considerations.

The second problem is more critical. The conventional histogram frequently takes the *rate* of action potential generation as a fundamental feature of the neural system. This is not the case. The fundamental parameter is the time interval between pulses, not the pulse rate. If the ordinate of the histogram is replotted using an equal time interval instead of an equal frequency interval, a more appropriate histogram will be obtained (Section 7.5.1.4).

Less critical is the tendency by investigators to overlook all of the variables folded into a single histogram. Javel has provided a good tutorial on the analytical techniques associated with the histograms used in hearing research[87]. Gulick et al. have also provided a good first order review of histograms for pedagogical purposes (pages 174-181). However, they do not discuss or show the dependence of the histogram on the intensity of the stimulus. Neither do they demonstrate that their proposed reciprocal relationship between the CF of a signaling channel and the repetition rate of the action potentials of that channel (following the first) holds below 500 Hz.

7.5.1 Applying statistical methods in hearing research

The complexity of the temporal signals applied to the hearing modality and the complexity of the temporal response of the modality, as recorded at different points, has caused many types of graphical data presentations to be tried. A logical approach to interpreting these signals has been to employ graphics from the field of statistics. These graphs are excellent for surfacing various features of a temporal data stream during exploratory research. However, their effective use requires a variety of compromises and certain *a priori* knowledge. In order to advance to the applied research phase in hearing, it is important that a more formal framework of histography be established. Section 7.5.1.4 will use this framework to reinterpret some of the previously reported histograms of hearing.

Kiang made the first extensive use of histograms when he explored the operation of hearing in the cat (1965). His discussion was entirely empirical and no theoretical discussion of the attributes and limitations of the histogram was provided. He did not provide any block diagram or schematic of hearing in the cat. While Kiang's explicit discussion of the PST form of data presentation was good, it suffered in three areas. Although he shows a finite pulse interval in an example in figure 3.3, his analysis was limited to the impulse situation. Second, it failed to note the folding of the original data that is inherent in the presentation. This folding obscures significant features in the data as discussed in detail by Smith & Brachman[88]. Third, as he noted using the term N_1 to describe the response recorded at the round window, "While the N_1 recordings are relatively stable from click to click, the time pattern of spike discharges fluctuates considerably for identical stimuli that are well above 'threshold'."

A histogram is a specialized graph used in statistics. In hearing, a more complex folded histogram has been most often used. It is based on sampling a function of time (of very long duration relative to the pulse-to-pulse interval of the data and relative to the period of a series of repetitive stimuli). While the histogram has been commonly used in hearing, no treatise could be found describing the features and limitations of the typical, uniquely-folded, histogram.

The National Institute of Standards & Technology (USA) has provided an elementary description of a simple histogram in an online handbook[89] (Section 1.3.3.14). It does note the majority of histograms are used to display univariate data. Young et al. reiterated the points made by NIST and expand slightly on the subject[90]. NIST provides a 4-plot test (Section 1.2.3) to insure the data at hand is univariate and adequately understood.

The histogram is a method of displaying a univariate relationship between a set of samples using a two-dimensional

graph space. The variable is displayed along the abscissa in quantized form and the number of samples in the set associated with a specific quantization is shown using the ordinate scale. In the case of hearing, the abscissa is most often a time interval subdivided into a set of equal duration time bins.

It is very clear, based on both the variables associated with the P/D Equation, the method of action potential encoding, and the time delay introduced by the slow velocity of neural transmissions, that the action potential signals recorded at the auditory nerve and later in the neural system are not univariate. More than six variables are involved. To use a histogram effectively in applied research related to hearing, it is mandatory that all of these variables be controlled and described as part of the documentation accompanying the univariate presentation.

At the pedagogical level, it is often suggested the histogram is useful in hearing because it is able to display the character of a stochastic process. While this may be a feature of the histogram, the histogram is not restricted to displaying stochastic processes. This work has shown that the signals within the hearing modality are not stochastic, unless the exciting stimulus is stochastic (or the stimulus level is so low the hearing modality is reporting the internal noise level of the neurological system itself).

After a brief introduction to the basic peri-stimulus-time (PST) histogram, four distinct types of histograms will be used in this chapter, an extended PST histogram (E-PST), a folded PST histogram (F-PST) a conforming PST histogram (C-PST), and an inter-pulse interval (IPI) histogram. A dual form of the IPI histogram designed to accommodate the presence of two invariate data sources will also be used.

7.5.1.1 The extended PST histogram

The most basic past assumption in hearing has been that the action potential pulses resulting from a stimulus were all the results of a single underlying process, i. e. a univariate data set. This is generally not true. Figure 7.5.1-1 illustrates a variety of situations encountered in the PST histogram, including those described above. (A) shows the four basic types of signals that can be applied to the auditory system. The impulse on the left is the basic function of mathematics. It exhibits a finite area, defined by zero width and an infinite height. A real pulse is shown on its right. A real pulse exhibits a finite area defined by a finite (but minimal) width and a height. It need not be square. The third case shows a pulse of long duration, and includes a real rise time and fall time. The fourth is the sinusoidal excitation. These four types can be combined so as to represent any conceivable acoustic stimulus waveform using the rules of Fourier Analysis.

(B) shows a typical impulse stimulus and the resulting generator waveforms at the output of the sensory neuron under five different conditions of stimulus energy (area). Note the mathematical latency is measured from the point where the response departs the horizontal axis. The latency, L1, of the generator waveform consists of two components in hearing experiments. The first component describes the time for the acoustic impulse to travel from the source to the sensory neuron. This latency can be tens of milliseconds long because of the speed of the surface acoustic wave within the cochlear partition. The second component describes the time for the sensory neuron to respond to the stimulus. The latency of the sensory neuron is a function of the integrated area of the impulse. This latency can also be milliseconds long. The amplitude of the generator response of the sensory neuron is also a function of the integrated area of the impulse.

In many experiments, the generator waveform is only recorded at some point along the auditory nerve after it has been encoded as a stage 3 signal. The time for the encoded signal to travel from the sensory neuron to the point of recording may also be multiple milliseconds.

The extended interval between the stimulus and the response at the point of recording is seldom reported when a histogram is presented.

(C) shows the action potentials generated in response to the earliest (and tallest) generator waveform in (B). The generator potential is shown dashed for reference. The first action potential is delayed by an interval, δ, consisting of two components. The first component is the delay associated with the encoding neuron. The second component is the delay associated with the time for the signal to travel through the spiral ganglia and arrive at a given location along the auditory nerve. The following pulses in each group are generated after delays proportional to the intensity of the initial generator waveform. They eventually stop when the remnant of the action potential no longer exceeds the threshold level of the stage 3 encoding neuron.

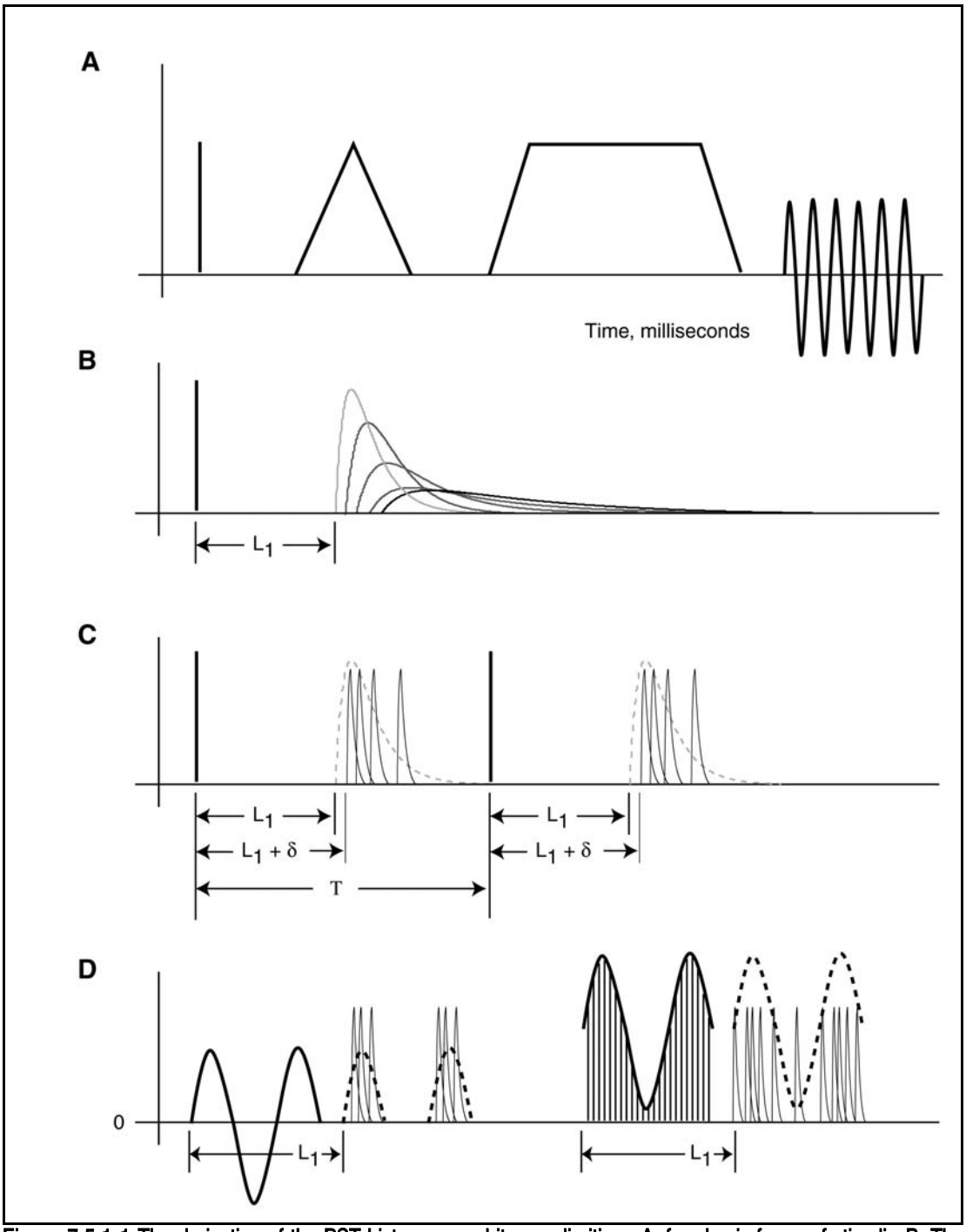

Figure 7.5.1-1 The derivation of the PST histogram and its peculiarities. A; four basic forms of stimuli. B; The responses of a sensory neuron to an impulse. C; the parameters of the responses of the auditory neurons to two simple acoustic impulses. D; the typical response of the sensory neuron and the following ganglion cell to a sine wave. By combining these forms, the generator waveforms and the action potential patterns associated with any stimulus can be described.

If a sequence of equally spaced acoustic impulses is presented to the ear, each impulse will generate a group of action potentials transmitted along an axon within the auditory nerve. If the time interval between the impulses is too short, the second group of action potentials will attempt to encroach on the time span of the first group. To the naive, this may cause the action potential stream to appear continuous. On the other hand, the ganglion neuron cannot generate action potentials below a minimum spacing determined by its refractory period. Thus, the overall action potential stream may show artifacts due to this refractory period.

When a low frequency sinusoidal waveform is presented as a stimulus as in (D, left), the sensory neuron generates an output waveform that tracks the positive excursion of the waveform. The latency, L, has been shown expanded here for ease of interpretation. This generator waveform causes the stage 3 ganglion neuron to generate one or more action potentials during the positive half of the sinusoidal waveform. Laboratory results have shown that the sensor neuron does not generate an output during the negative excursion of the stimulus. In the absence of a response, the stage 3 action potential generator is also dormant. (D, right) shows a more complex stimulus. In this case, the low frequency tone is modulated on a higher frequency carrier. The output of the sensory neuron follows the excursion of the lower frequency tone, which is always positive. As a result, the action potentials are generated throughout the cycle of the low frequency tone.

Frames (C) and (D) clearly establish that a histogram of the data collected only during the duration of the stimulus (the peri-stimulus time interval) is of little value in hearing. Because of the latency, the response may only occur after the stimulus has ceased. A second problem is the often significant decay characteristic in the stage 1 generator waveform following the driven response. This results in a difficulty with the common name for a hearing histogram, a peri-stimulus-time histogram (PST). To actually capture the response, the interval of the histogram must actually be extended beyond the interval of the stimulus. Thus, a conventional PST histogram is more appropriately labeled an extended PST histogram (E-PST) since the abscissa typically extends beyond the termination of the stimulus. Both of these problems support the use of an *extended* PST histogram (E-PST) where the total period extends from about 6 ms to as much as 30 ms beyond the termination of the stimulus. Alternately, the mathematical delay between the response and the stimulus can be specifically reported.

7.5.1.2 The folded PST histogram

In hearing, stage 3 signals are frequently recorded in response to low stimulus levels. For many reasons, the action potentials produced by stage 3 encoding may be irregular in occurrence or in inter-pulse spacing. To alleviate these problems, it is conventional to record the responses to a repetitive sequence of stimuli and correlate the responses by summing the data occurring within specific intervals following each of the individual stimuli. The result is a folded (and typically extended) PST histogram (F-PST). By referencing the start of each stimulus, the resulting F-PST typically displays the first action potential of the response with high confidence. However, later pulses may not be presented as well since they may not occur synchronously with the bin spacing used in the histogram. As a result, the subsequent action potentials may be recorded in bins adjacent to the expected bin. This smearing of the data is one source of a high spontaneous rate (an average count observed across the bins of the histogram) in the resulting graphic representation.

Figure 7.5.1-2 provides a collage of responses used to form a folded PST histogram in hearing. The top row is divided into two frames to illustrate tones significantly above and below the integration frequency of the sensory neuron (typically 600 Hz in humans). The second row shows the generator response at the pedicle of a sensory neuron expected for these two types of stimuli. The values, Δ_1, indicate the delay associated with the specific stimulus. Note the significantly longer delay associated with the low frequency response of an OHC neuron near the apex compared to the similar OHC high frequency response near the base of the cochlear partition. The dashed line indicates the effective threshold level of the encoding neuron following the sensory neuron.

The third line shows the two stage 3 responses expected from the above stimuli. Note the two-pulse groups on the right, where the refractory period of the encoder is less than one-half the period of the stimulus and the generator potential remains above the effective threshold. The period between the two pulses in each group is not harmonically related to the stimulus frequency. This period reflects the intensity of the stimulus during that half cycle.

The original stimulus record is shown in the next row using a longer time line. The frequency used to form each pulse may be at any frequency. The complete time line is n-times the length of the folded samples shown above. The next row shows the nominal stage 3 record (with pulses in groups of nine). If the total record is divided into T segments and each segment is divided into bins no wider than one half the interval between the individual pulses, the record can be transformed using a Riemann fold as illustrated at the bottom left. Note the multiple scales provided below the histogram. The mathematical process can be considered a time-shifted summation. This process results in a count in each bin which is the sum of the counts in each bin with the same number before shifting the time interval

at the cut points. Note the ordinate describes the number of pulses in a given bin and not the number of pulses per unit time. For pulses (1) of equal spacing, (2) that spacing equal to the bin spacing, and (3) the phase of the pulses occurring at the center of the bin sampling interval, the count per bin will be as shown.

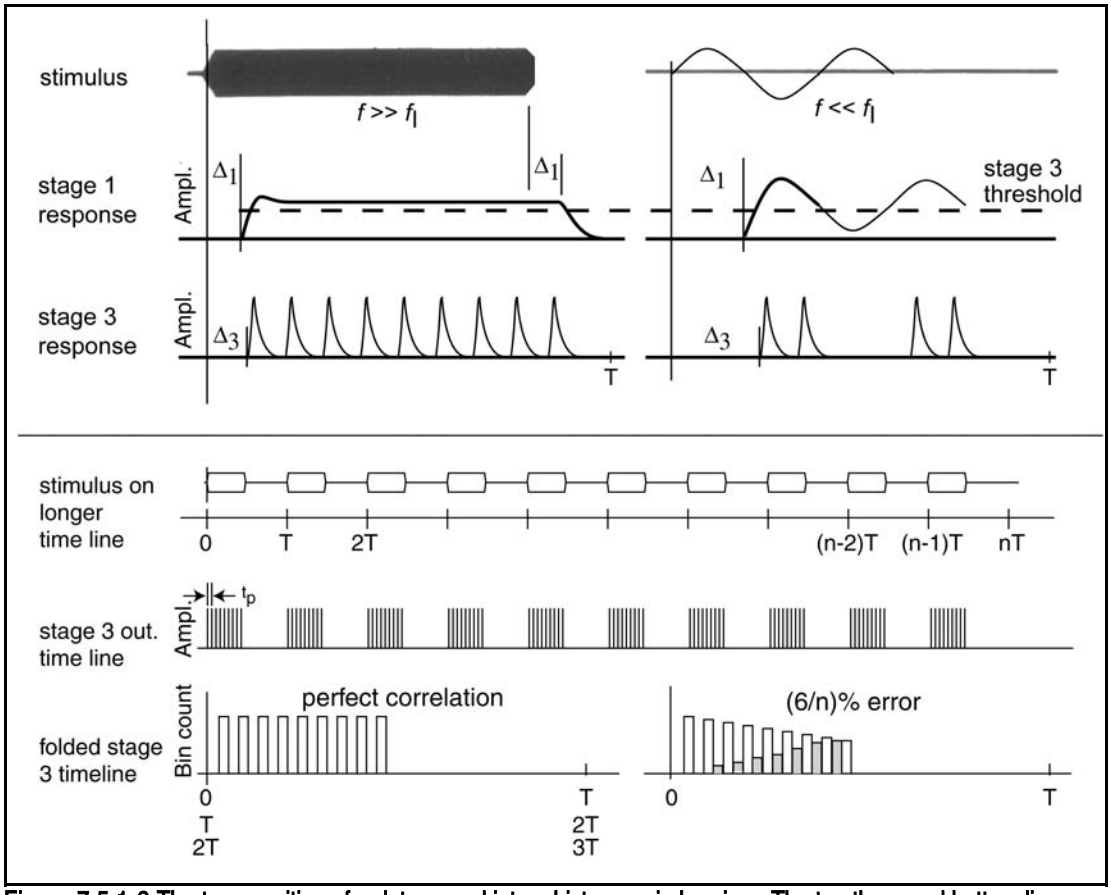

Figure 7.5.1-2 The transposition of a data record into a histogram in hearing. The top three and bottom lines are divided into left and right frames. The bottom line shows the sensitivity of a folded expanded PST histogram (the conventional type) to a sampling error where tp is not a submultiple of n•T. Left; the pulses all fall into bins separated by a fixed time interval. Right; the pulses fall into different bins depending on when they were collected. See text.

If the interval, T, is not a multiple of the pulse spacing, t_p, a more complicated situation occurs. As more and more segments are convolved into the histogram, a growing fraction of the pulses will appear in the wrong sampling bin. The figure shows an error of 6% of the interval T. For fold level of n, the error is a minuscule (6/n)% of the total record length.

The consequences of this error have been large in the literature. When the pulse interval, tp, has been a sub-multiple of the interval, T, the figure on the left has arisen. This response has been described as that from a "chopper neuron" since at least 1974[91]. It is in fact the ideal pattern of a neural channel reporting a constant amplitude stimulus of specific intensity. No chopping of the stimulus or of the generator potential has occurred. When the pulse interval, t_p, which is a function of the stimulus intensity, has not been a submultiple of the interval, the figure on the right has arisen. This figure, which can be obtained from the same neuron, has been attributed to an entirely different class of neurons.

While the use of names like chopper, chop-S, chop-T, onset, etc. may be convenient in pedagogy and discussions using the vernacular of hearing research, they should be avoided in favor of more specific descriptions of the signals forming the histograms.

As in many similar applications outside of hearing, attempting to correlate the data from more than 100 individual

recordings is generally not productive. The performance of the system becomes limited by the stability of the overall test configuration. A better solution is to increase the signal-to-noise ratio of the individual recordings. This can frequently be achieved by switching from recording signals from interneural probes to recording signals from intraneural probes (including using patch-clamp techniques). Intraneural signals typically exhibit both a signal amplitude 100 to 1000 times higher than those obtained with extra-neural probes, and a much lower noise component.

7.5.1.3 Developing the conforming PST histogram

Past histograms have been based on the assumption of linearity in the hearing system. These assumptions are not supported by the available data. Javel noted in 1986 that the discharge rate of stage 3 neurons in response to an external stimulus is highly distorted when plotted using a linear ordinate. Figure 7.5.1-3 reproduces his figure 6. He shows (left) that using a logarithmic ordinate allows pulse rates as low as 1-2 pps to be shown on the same scale with rates of 200 pps or more[92]. He also shows (right) that the data from a wide variety of stage 3 neurons can be superimposed through normalization to show a generic response limited primarily by the spontaneous rate of the individual neuron. This composite response is linear (has a slope of one) at intensities below 45 dB. However, at higher intensities, its slope decreases until saturation is reached near 100 dB. His best neurons exhibited an action potential generation rate ranging from about 1-2 pps to more than 200 pps.

As shown in Section 7.4, the stage 3 encoding process (time delay as a function of stimulus amplitude) is quite linear. However, the cumulative performance of the system from an acoustic stimulus to stage 3 action potential pulse generation is highly nonlinear. The nonlinearity is dominated by the output current-to-voltage conversion at the pedicle of the stage 1 sensory neurons.

While Javel did not provide any justification for his normalizing procedures, it appears they are at least partially justified by the adaptation capability of the sensory neurons and potential test protocol differences. By striving to reduce the spontaneous rate, the generic response can be expected to represent nominally performing stage 3 neurons over an intensity range of about 80 dB. This range covers both the phonotopic and mesotopic regimes of hearing. It consists of the instantaneous dynamic range of the sensory neurons of stage 1 (about 35 dB), and the nominal adaptation range of the same neurons of at least 40 dB.

The generic response shown is virtually identical to the logarithmic current-to-voltage characteristic of the stage 1 sensory neuron (Section 5.5.1).

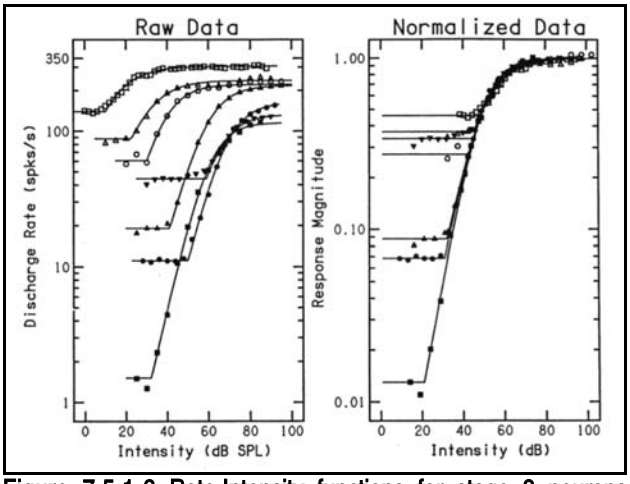

Figure 7.5.1-3 Rate-Intensity functions for stage 3 neurons responding to an external stimulus plotted using logarithmic coordinates. Different symbols represent different fibers measured at their CF and fitted with curves using a least-squares procedure. By normalizing the scale using a logarithmic ordinate, the saturation due to the diode in the collector load of the sensory neuron is clearly seen. From Javel, 1986.

7.5.1.4 Comparing the C-PST and the non-conforming PST histograms

Section 7.3 has shown that the linearity of the stage 3 encoding mechanism is between the time interval between action potential pulses and the excitation applied to the encoding neuron. The linearity is not between the frequency of the generated pulses and the excitation.

Figure 7.5.1-4 shows the difference between plotting a histogram using an ordinate that is linear with respect to frequency during the temporal interval and one using an ordinate that is linear with respect to the time interval between pulses (and nonlinear with respect to the instantaneous frequency). The figure on the left is from Kiang[93]. It shows the conventional peristimulus time interval histogram (PST or PeST) recorded from a channel that is occupied by one tone signal with a characteristic frequency of 18.5 kHz at –55 dB when a suppressing tone is introduced at a frequency of 21 kHz at –15 dB for 50 ms. Such tests are frequently used to explore suppression mechanisms in hearing[94]. Historically, the data has been difficult to interpret. Based on this work, the data appears to be acquired from a differencing channel neuron based on a probe contacting the auditory nerve or some later point in the auditory system.

The frame on the right shows the same nominal data but with the ordinate linear with respect to the time delay between adjacent action potential pulses. The result is a nonlinear scale with respect to instantaneous pulse frequency.

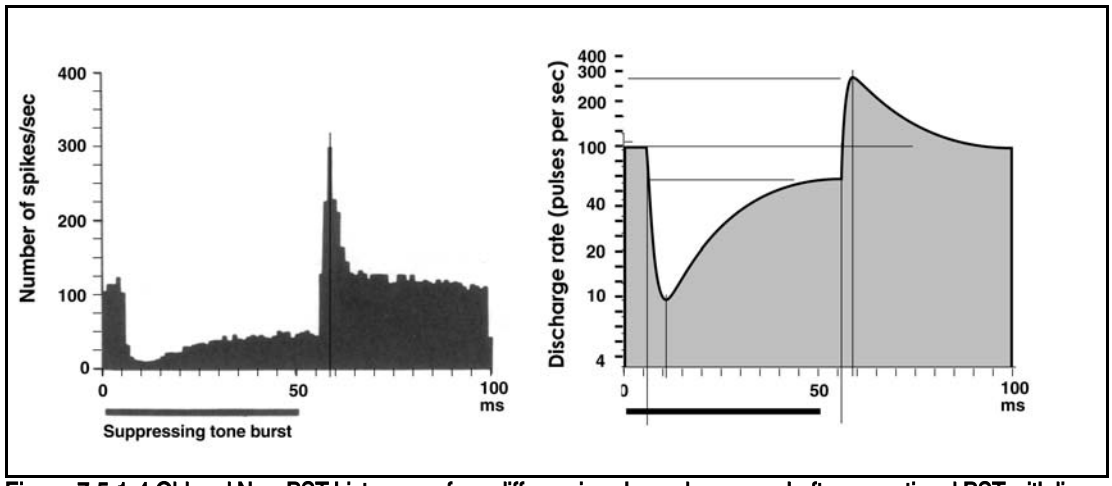

Figure 7.5.1-4 Old and New PST histograms for a differencing channel neuron. Left; conventional PST with linear ordinate. Right; conformal PST with 'linearized ordinate. Both figures show the effect of a second tone burst subtracting, for a 50 ms interval, from the pulse rate in the channel due to an initial tone burst at a different frequency. The intrinsic latency of the process (6 ms) and the clinical latency (12 ms) are more clearly shown in the conforming PST histogram. The transient performance, along with the effect of saturation, are also more clearly shown in the conforming PST. See text. Original data from Kiang, 1965.

The difference between the two presentations is considerable. The nonlinear discharge rate scale on the right is linear with respect to the time intervals involved (as developed in Section 7.3.4). By replotting the envelope of the data on the left, the actual transient characteristics of the circuits are clearly seen. The curves are composed of simple exponentials. The overall waveform on the right would be more symmetrical if the intensity of the first tone was reduced. The amount of reduction cannot be estimated without knowing the spontaneous rate (SR) of the channel in the absence of any stimulation. Kiang gave the SR in a separate figure as 64 pps.

The ordinate of any period histogram used in hearing must be linear with respect to time differences rather than instantaneous frequency differences if a faithful reproduction of the encoded signal is to be portrayed.

Quantitative analysis is aided considerably by the new histogram scaling and new information about the operation of the circuit becomes available. The transients associated with the start of the suppressing tone, and the recovery after the end of the suppressing tone are clearly seen. In both cases, a fixed delay of about six milliseconds is encountered. These delays are followed by a five-millisecond on-risetime and a three-millisecond off-risetime.

7.5.1.5 The inter-pulse interval (IPI) and dual IPI histograms

The PST form of histogram reports a count in each bin associated with the selected period. This is a very useful form for portraying data that appears at sub-multiples of the overall histogram period. However, it frequently obscures other data occurring at non-synchronous intervals. This data becomes smeared across the overall period of the histogram and contributes to the "spontaneous rate," the apparent background count associated with PST histograms. To avoid this limitation of the PST histogram, an alternate formulation of a histogram is often used. This formulation uses the same original record but determines the interval between each pair of action potentials and reports the number of times the same interval occurs. The resulting IPI (sometimes called the inter-spike interval, ISI) histogram presents a probability, along the ordinate, that a pulse following a given pulse will occur within any time interval displayed along the abscissa. The cumulative probability is 100% that a pulse will follow the first pulse prior to the maximum interval displayed on the histogram.

In this formulation, the abscissa can be a linear continuous scale. However, the data is of limited precision and it is common to subdivide the abscissa into equal width bins and collect the data into those bins to improve the legibility of the histogram.

The resulting IPI histogram highlights the period associated with the stimulus repeat cycle, the period of any frequency components associated with the stimulus, the period of any prominent but uncontrolled frequency components in the response and the period associated with the action potential pulse stream itself. Depending on the complexity of the stimulus profile, some of these periods may not be relevant to a specific histogram.

Javel presented a figure (11) in 1988 that clearly shows the character of IPI histograms resulting from very simple stimuli at 70 dB SPL[95].

The major problem with the iPI histograms is they normally measure all time intervals from a common starting point, either the start of the stimulus or the first pulse following the start of the stimulus. The results frequently depend on the reference.

A single IPI histogram can be used in exploratory research to uncover the presence and temporal properties of action potentials. However, it does a poor job of elucidating the underlying character of the data. In hearing, two separate sources of univariate data contribute to the action potential streams recorded at the auditory nerve. As a result, it is necessary to define and plot two distinct histograms to illustrate the properties of these data sets.

To be maximally useful in the analysis of the electrophysiology of hearing, the interval between the start of the stimulus and the occurrence of the first action potential (based on its mathematical beginning rather than the clinical peak) should be recorded. This information describes the total delay associated with the acousto-mechanical portion, stage 0, of the system, plus the delay associated with the P/D Equation of the stage 1 sensory neurons, plus the propagation delay associated with stages 2 & 3.

Of equal importance is the interval between the first pulse and the second pulse (under the assumption that the stimulus is a constant amplitude tone burst at a frequency far above the integration frequency of the stage 1 neurons).

Finally, the interval between subsequent pairs of pulses beginning with the second pulse is of interest. These values should be very similar under the constant stimulus amplitude condition (unless adaptation is playing a role).

Manipulating the above information requires more complex data reduction techniques than used generally in the past. However, the results greatly clarify the performance of the system and are easily obtained using modern computer capabilities.

Plotting the resulting two sets of histographic data on a single dual IPI histogram is straight forward if annotation is provided to highlight the dual character of the presentation.

7.5.1.6 The use of the C-PST and dual IPI histograms

Figure 7.5.1-5 provides a collage of conforming PST and dual IPI histograms along with values from a regularity analysis. The purpose of this set is to illustrate the variation in histograms obtained from a single neuron as a function of stimulus intensity.

> A dual IPI histogram is used because two distinctly different relationships need to be documented. A simple IPI histogram is not appropriate in this situation.

Row A shows the stimulus on a record that can be interpreted in two ways. It can be assumed it was applied over an interval of T seconds, or that it was applied repeatedly over an interval of k•T seconds.

Row B shows the extended PST histogram on the left, a compound IPI histogram in the middle and values from a regularity analysis of the Bourke type on the right. Bourke developed a comprehensive analysis that presented the mean and standard deviation of the values in the PST and IPI histograms on a bin-by-bin basis[96]. Abrupt changes in these parameters highlight the presence of multiple underlying mechanisms.

For no stimulus, the extended PST histogram shows what appears to be a stochastic process due to random noise. However, the spontaneous rate may also include an average bin count due to the presence of action potentials in the recorded data that had inter-pulse periods that were not related to the interval T. Under stochastic conditions, the equivalent IPI histogram shows a constant probability for any time interval (horizontal line) down to a minimum interval determined by the bandwidth of the neuron and/or test instrumentation. However, if there are uncontrolled but regularly occurring non-stochastic signals present, this IPI histogram will show that fact (dashed lines).

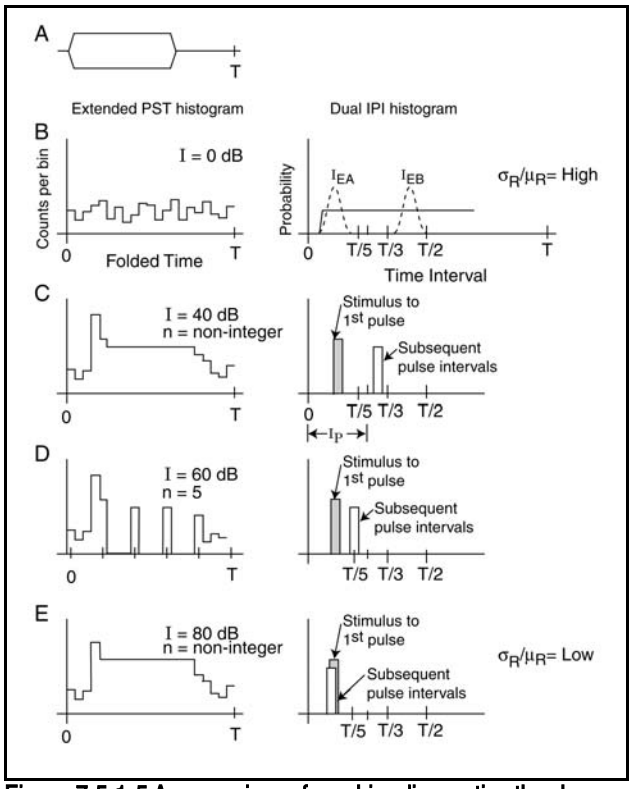

Figure 7.5.1-5 A comparison of graphics discounting the chopper concept. Row A; the stimulus. Row B; the histogram shows a typical SR in the absence of stimulus. The IPI shows the period of potential sources of extraneous signals. Row C; the histogram shows conventional data. The dual IPI shows the P/D delay and the pulse interval between subsequent action potentials. Row D; the histogram in D shows the action potential pulse stream can be made synchronous with the duration of the histogram by adjusting the stimulus intensity. The result has been labeled chopping. In all other respects the histogram is the same as that in C and E. The decreases in both first pulse delay and pulse-to-pulse interval as a function of stimulus intensity is seen in rows C, D & E. Row F; the case of a stimulus frequency well below the actionpotential pulse frequency. See text.

The regularity analysis for a stochastic background results in a high value of the standard deviation of the inter-pulse interval divided by the mean inter-pulse interval. However, these individual values are poorly defined. Figure 3(A) of Young et al. suggest a value of 13 ms (equivalent to 77 Hz) for μ_R and 0.3 for the ratio of σ_R/μ_R near threshold based on their experiments. 77 Hz may be the vascular pulse rate of their sedated cat.

Row C shows the extended PST histogram displaying a nominal characteristic reflecting an initial set of action potentials occurring at a fixed interval after the start of the stimulus. This delay is a function of stimulus intensity. For the remainder of an interval equivalent to the stimulus duration, the PST displays a lower but still high count per bin reflecting the presence of many action potentials occurring at intervals that are not synchronous with the interval T. After a period equivalent to the stimulus duration, the response returns to the spontaneous rate following a decay characteristic. The compound IPI histogram shows two features. The first is a high probability of an action potential occurring following the start of a stimulus by a significant delay time (shaded bar). This delay time incorporates several individual delays as discussed in this chapter. The unshaded bar shows the inter-pulse interval between subsequent pairs of pulses beginning with the first pulse. As noted when discussing the PST histogram, this interval is not typically a sub-multiple of T (n is not an integer). The regularity of this stimulus condition is lower than that in B.

Row D shows a situation that occurs at a given stimulus intensity (shown here as 60 dB). At this intensity, the action potential pulse rate is a sub-multiple of the interval T. At this higher intensity, the stimulus-to-first-pulse interval shown in the IPI histogram has been reduced (the shaded bar has moved to the left relative to the arrowhead). The extended PST histogram shows a unique characteristic. Following the initial pulses signaling the start of the stimulus duration, subsequent action potentials occur at intervals that result in their accumulation in specific bins of the PST histogram. The result is a stationary PST histogram showing equally spaced bars. Young et al. have described this result as characteristic of a specific type of neuron within the cochlear nucleus that they defined as a "chopper." Their labeling suggests this neuron is uniquely processing the signals delivered to it. In fact, this feature is characteristic of a wide variety of neurons when driven at a specific signal level. There is no mechanism associated with the neuron that is "chopping" the signal represented by the PST histogram. The action potentials are merely being created with an inter-pulse period that is a sub-multiple of T.

Row E shows the similar presentations for an even higher intensity stimulus. The IPI histogram shows the first pulse starting even earlier than in the previous rows and the pulse-to-pulse interval smaller than in previous rows. However, the pulse-to-pulse period is no longer an integer sub-multiple of the interval T. The PST histogram has lost its unique appearance and returned to the more common appearance of row C. The regularity of the pulse-to-pulse pattern has reached a very low value because of the dominance of the pulses caused by the high intensity stimulus over any extraneous pulses related to the spontaneous rate.

Row F shows the unusual condition where the stimulus frequency is well below the action potential pulse frequency. At sufficiently high stimulus intensity, two pulses are generated per (rarefaction) half-cycle of the stimulus. No pulses are generated during the compression portion of the stimulus cycle. The situation has been unexplainable in the past and the phenomenon has generally been labeled "peak-splitting." However, the height of peak P_1 is not reduced with the appearance of peak P_2 in the general case[97]. Because of the low stimulus frequency, the stimulus at the input terminal is still above threshold at the end of the refractory period of the encoding neuron and the neuron proceeds to generate a second action potential. The spacing between P_1 and P_2 in Johnson's histograms is typically one millisecond and is independent of the stimulus frequency.

This figure demonstrates that the form of the neural response following stage 3 encoding is a complex function of the frequency and intensity of the stimulus. The encoded pulse stream may represent the envelope of a high frequency stimulus, or it may describe the actual phasic equivalent of the analog stimulus.

A problem with any histogram is the loss in detail relative to the stability of the system over the duration of the actual data collection record, particularly if the bin-spacings are not related to the inter-pulse period of the action potentials. Javel provided data illustrating this problem, although the titling of his figure could be more precise[98]. The figure shows a period histogram on the left and an interval histogram on the right with a duration of nominally eight periods. The latter is not an inter-pulse interval histogram.

The above figure forms the basis for interpreting the PST histogram collage by Johnson[99]. His collage shows the variation in the tone-based histogram over a wide range of frequency and intensity, including the two-pulse pattern at very low frequencies. Several investigators have attempted to relate the second pulse in the two-pulse pattern to the opposite half cycle of the stimulating tone rather than to the encoding scheme of the stage 3 ganglion neurons.

A more sophisticated regularity analysis has been developed in the paper by Young et al. to describe the pulse data they collected from the auditory nerve[100]. If their data was re-analyzed to separate the pulse-to-pulse data from the start-of-stimulus to first pulse data the utility of their analysis would be increased.

Javel presented a set of histograms (his figure 3) in 1980 that highlighted the problem of duration selection[101]. As Kiang observed, it is almost inevitable that some non-synchronous pulses will be generated due to extraneous uncontrollable inputs. The result is a finite SR level in the resulting histogram.

7.5.2 Highlighting the graphical interpretation of hearing performance

Histograms are easily prepared from any point in the neural system where the axons of stage 3 encoding neurons are accessible. This chapter has provided the background necessary to interpret many of the histograms presented in various pedagogical essays. Figure 7.5.2-1 provides a widely reproduced group of stylized recordings from somewhere in the medial geniculate nucleus[102]. Unfortunately, this group does not show the spontaneous rate of the neuron associated with each histogram and it provides no information about the period of the histogram in relation to the action potential pulse rate present when creating the histogram. It can only be assumed the ordinate scales are linear with respect to the discharge rate. Several of the frames suggest they are IPI type histograms. In general, the durations of the histograms are longer than that of a precisely defined peristimulus time interval histogram.

It is critically important that the precise location of the neuron providing the recording be defined, particularly whether the axon involved is arriving at the engine, leaving the engine or is an associative fiber remaining within the engine.

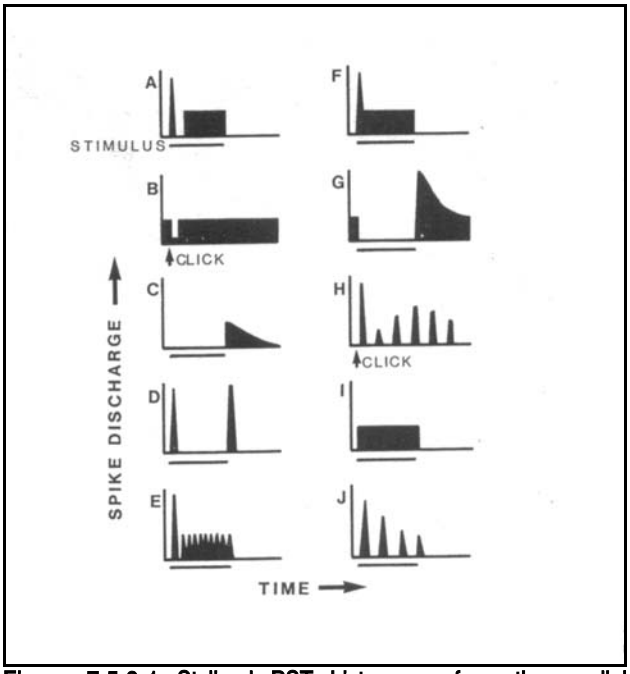

Figure 7.5.2-1 Stylized PST histograms from the medial geniculate nucleus. Frames B & H are based on single clicks repeated at a time interval equal to the length of the histogram. Note the complex response in H. See text. From Keidel, 1974.

It is also highly important that the actual temporal records forming the underlying interval histogram and the final PeST-histogram be retained so that changes occurring during the recording interval can be studied. Only with this knowledge can the data be accumulated in a manner that can be interpreted in the future.

Lacking the above information, only speculative, and frequently conflicting, comments can be made concerning the probable character of these histograms.

7.5.2.1 Eliminating distortion from characteristic frequency graphs

The characteristic frequency of a sensory neuron is typically obtained by measuring the action potential stream at the output of the spiral ganglia associated with that neuron. Obtaining faithful data at this point requires the system prior to that point to be linear. Unfortunately, this condition is never met for large changes in the stimulus intensity. The characterization can be obtained in two ways. In the first, it is obtained by holding the acoustic stimulus intensity constant and recording the variation in pulses as a function of stimulus frequency. In the second, it is obtained by adjusting the intensity of the stimulus as a function of frequency while maintaining the pulse frequency constant.

In the first method, the external stimulation is held constant. However, the actual stimulation of the sensory neurons is a variable with respect to frequency and the adaptation mechanism of the neuron attempts to compensate for that variability. The actual stimulation can be kept constant using the combined transfer function of all of the acousto-mechanical elements of the ear. The result is the actual characteristic frequency plot of the sensory neuron.

In the second method, the large variations in stimulus intensity are also compensated by the adaptation amplifier (to the extent of its ability). The extent of this compensation can be very large. As a result, the reported characteristic frequency graph is highly distorted. The typical characteristic frequency graph shows a distorted representation of the characteristic frequency of the sensory neuron, known as the tip section, and a distorted representation of an extended region known as the tail section.

Careful attention to the design of the protocol is needed if precise frequency characteristics of a given neuron are to be obtained. Phillips describes the methods of acquiring the data as described above and the terms involved more specifically[103].

7.5.2.2 Reinterpreting histograms using conforming ordinate scales

Several investigators have provided extensive sets of PST and IPI histograms. Additional understanding of the hearing performance of the subject animals can be obtained if their PST data is replotted on a conforming histogram (Section 7.5.1). Where the data is still available in raw form, it would also be useful to perform a regularity analysis to highlight additional features of the data.

Palmer & Russell have provided extensive sets of IPI histograms from the stage 3 afferent neurons of the auditory nerve of the guinea pig[104]. Much of the data was collected at frequencies below the integration frequency of broadband (IHC) sensory neurons. Their method of stimulation was not specified in detail but probably involved a sealed auditory canal based on their earlier work. Their introduction notes the recorded action potentials in response to low frequency stimuli were not probabilistic. In fact, they were quite deterministic.

Anderson et al. have provided histogram data on the squirrel monkey[105]. The histograms were prepared to stress the change in phase of the data in the histograms as a function of frequency. Their protocol involved an open auditory canal. The data also provides an estimate of the time delay (latency) between the stimuli and the response at the selected auditory nerve fibers.

Rose et al[106]. have provided additional, conventional (non-conforming) histogram data, with the overlaying stimuli, by the same group as above. Close examination of the histogram data shows it does not go to zero in the presumed rectified regions. If their histograms are replotted using conforming ordinates, the overlays can be moved up to superimpose with the resulting histograms. The ratio of amplitudes, R_A, used in the reconstructed analog waveforms, varied with the intensities used due to compression at the pedicle of the IHC sensory neuron. As a result, the analog waveforms overlay their histographic data when plotted using a conforming ordinate scale. There is no suggestion of rectification. Rose et al. arrive at many conclusions supported by this work, including the deviation of the cochlear partition from a pure Hankel function in the low frequency region (page 695). They also note, by footnote 3, the significance of their expression "locked to the cycle" when discussing the relationship between the action potentials generated and the low frequency stimulus.

Smoorenburg et al[107]. have continued the work described above by Rose et al. but using the cat. Their figure 15 is

similar to that shown for Rose but it also includes histograms for only a single tone. These histograms when replotted using a conforming vertical scale, show a sinusoidal character that can be overlaid by the stimulus waveform. The experiments of Smoorenburg et al. were designed to find frequency components in stage 3 signals that did not exist in the different frequencies present in the stimuli. While they knew these cross modulation products had been recorded from neurons of the auditory nerve, they focused on recording stage 3 signals from the anteroventral cochlear nucleus (AVCN). They did not determine whether their signals were recorded at the terminus of the auditory nerve or at the origins of the stage 3 neural paths proceeding to other orthodromic engines.

Johnson has provided a large set of period histograms for individual auditory fibers in the cat when using stimuli introduced into a closed ear canal[108]. It is difficult to determine from his text whether he was working with OHC or IHC sensory neurons at low frequencies. His stated purpose was to study the relationship between the average spontaneous discharge rate and the synchronism between the time of stimulus and the time of the resultant action potentials. While his conclusion was that more investigation was required, his data is useful in other contexts.

His histograms demonstrate the excellent operation of the adaptation circuit of the sensory neurons, with adaptation becoming active at approximately 50 dB below his reference level of 115 dB SPL. Low frequency roll-off of the overall cumulative auditory frequency response, up to the auditory nerve, began at about 500 Hz. At his lowest frequencies and highest stimulus levels in the figure, a second group of action potential pulses are recorded approximately one millisecond after the peak in the first group (regardless of the stimulus frequency). These pulses are not due to a harmonic in the generator potential. They are cause by the input to the stage 3 encoder remaining significantly above threshold following a majority of the refractory interval of the encoder.

7.5.2.3 Adding a regularity analysis to the conforming PST histogram

Shofner & Young[109] and Young et al[110]. produced several papers in the 1980's of significant value (particularly for their data content) obtained from decerebrate cats. They included an expanded analysis of the action potential pulse stream using a PeST histogram and a separate graph of the mean and standard deviation of the pulse count on a bin-by-bin basis. While the pulse counts were not plotted using a conforming vertical axis, the statistical graphs highlighted the presence of multiple underlying mechanisms. The analysis showed that a single pulse stream could exhibit a "chopped" appearance at certain stimulus intensities but not at other intensities.

Many other insights into the operation of stage 3 propagation neurons can be obtained by reinterpreting these papers based on the theory of this work.

7.6 Advanced stage 3 data related to the cortex and speech perception

As noted earlier, stage 3 signals can be recorded from many areas of the auditory system since stage 3 circuits are used to interconnect all of the signal processing and signal manipulation engines of the neural system. The signals exhibit ever greater complexity and ever less tonotopicity as they are recorded higher in the neural system. Exploring this complexity is beyond the scope of this volume.

The types of signals found in the auditory cortex are diverse and suggest the signal processing carried out prior to the signals arriving at the cortex js very complex. Evans & Whitfield have identified a variety of signal types within the auditory cortex of an alert cat[111]. They have also provided a list of similar investigations, primarily with anaesthetized cats.

McAlpine et al. have recently presented a series of histograms recorded within the inferior colliculus (IC) of guinea pig at low stimulus intensities[112]. Although involving complex test protocols, the histograms of their figure 4 clearly show the stimulus was not rectified within the sensory neurons or anywhere else prior to the IC. They also show the compression of the signal by the sensory neurons as a function of the stimulus level. Their peak action potential rate was only 65 pps and rates as low as 20 pps are shown. Their figure 5 shows similar results, except for phase shifting within the signaling channels (but no rectification). The pulse rate went as high as 130 pps.

The complexity of the information stored in the saliency map (Section 8.5) strongly suggests a more complex form of information transfer is used between the map and the frontal lobe of the CNS. It appears the information is transferred using a word-serial/bit-parallel format. Information would be transferred bidirectionally over separate parallel paths (duplex transmission). To intercept a single complete data-word in the laboratory would require the use of multiple, simultaneous, strategically-placed probes.

Table of Contents

7 Stage 3 Signal Projection 293
7.1 Introduction 293
7.1.1 The "stellite neuron" versus the stellate neuron 294
7.1.2 The "fundamental" stage 3 signaling path 296
7.1.3 Background 297
7.1.4 Types of coding used in hearing and other sensory systems 298
7.1.4.1 Terminology specific to coding/modulation 298
7.1.4.2 Specific background related to coding/modulation 299
7.1.4.3 Signals associated with summing and differencing channels 300
7.2 The morphology, cytology and topology of stage 3 projection neurons 301
7.2.1 The morphology and cytology of the stage 3 neuron 302
7.2.2 A defining morphological feature of a stage 3 ganglion neuron 303
7.3 The physiology and operation of stage 3 pulse and hybrid neurons 304
7.3.1 The generic stage 3 phasic neurons as relaxation oscillators 305
7.3.1.1 The interneuron and Node of Ranvier as regenerators 305
7.3.1.2 The detailed circuitry and operation of the Node of Ranvier 307
7.3.2 The Action Potential (AP) vs pseudo action potentials 308
7.3.2.1 Details of the generic action potential waveform 309
7.3.2.2 The effect of temperature on the action potential 310
7.3.3 Electrical operating conditions in the absence of feedback 311
7.3.4 The encoding (ganglion) neurons 311
7.3.4.1 Operation of the ganglion neuron 311
7.3.4.2 Characteristics of ganglion neurons 312
7.3.4.3 The introduction of myelin in connection with the axon 317
7.3.4.4 The introduction of the Node of Ranvier in connection with the axon 317
7.3.4.5 Signal input via the poditic conduit 317
7.3.4.6 Transfer function of the stage 3 encoding circuits 317
7.3.4.7 Correlation with the literature 318
7.3.5 The generic stage 3 phasic signal recovery circuits 319
7.3.6 The end-to-end transfer function for an awareness mode circuit 321
7.3.7 Providing electrical power to stage 3 neurons 323
7.4 Reformulating the concept of signal transmission in neuroscience 323
7.4.1 Background related to stage 3 neuron propagation 324
7.4.2 Replacing the excitable axolemma of Hodgkin & Huxley 326
7.4.3 Introduction to the General Wave Equation 328
7.4.3.1 Resolving an inconsistency related to physical chemistry 328
7.4.3.2 The fundamental GWE 329
7.4.3.3 Application of the GWE to neuron operations 329
7.4.4 The efficient propagation of neural signals using a Maxwellian cable 330
7.4.4.1 Background–the axon as a transmission line 330
7.4.4.2 Propagation over the ideal axon 334
7.4.4.3 The variation in reactance over a lossy coaxial cable–a real axon 335
7.4.5 The propagation velocity of a real stage 3 axon 336
7.4.5.1 Historical Background –propagation velocity of axons 336
7.4.5.2 The measured propagation velocity of an axon *in-vivo* 336
7.5 The use of statistical and graphical tools in hearing research 338
7.5.1 Applying statistical methods in hearing research 339
7.5.1.1 The extended PST histogram 340
7.5.1.2 The folded PST histogram 342
7.5.1.3 Developing the conforming PST histogram 344
7.5.1.4 Comparing the C-PST and the non-conforming PST histograms 344
7.5.1.5 The inter-pulse interval (IPI) and dual IPI histograms 345
7.5.1.6 The use of the C-PST and dual IPI histograms 346
7.5.2 Highlighting the graphical interpretation of hearing performance 348
7.5.2.1 Eliminating distortion from characteristic frequency graphs 349
7.5.2.2 Reinterpreting histograms using conforming ordinate scales 349
7.5.2.3 Adding a regularity analysis to the conforming PST histogram 350
7.6 Advanced stage 3 data related to the cortex and speech perception 350

List of Figures 3/19/13

Figure 7.1.1-1 Top level block diagram of hearing and the ubiquitous presence of stage 3 295
Figure 7.1.2-1 Top level description of the stage 3 signal path 296
Figure 7.1.2-2 The circuit diagram of the fundamental stage 3 neural path 297
Figure 7.1.3-1 The structure of action potential streams when encoded 301
Figure 7.2.1-1 The axon segment as a multi-terminal electrolytic cell 303
Figure 7.2.1-2 A Node of Ranvier isolated in living tissue by dissection. 303
Figure 7.3.1-1 Development of the generic stage 3 neuron 306
Figure 7.3.1-2 The electrolytic circuit of the generic stage 3 encoding neuron 307
Figure 7.3.2-1 The features of the action potential at a Node of Ranvier 310
Figure 7.3.2-2 Measured action potentials as a function of temperature 310
Figure 7.3.4-1 Mean latency of auditory nerve fibers vs best frequency 313
Figure 7.3.4-2 Synchronization of cat auditory nerve fiber discharges 315
Figure 7.3.4-3 Action potential discharge rate as a function of intensity 316
Figure 7.3.4-4 The overall transfer function of a stage 3 projection circuit 318
Figure 7.3.5-1 Generic decoding circuits of the neurological system 320
Figure 7.3.6-1 The performance of a combined ganglion cell and stellite cell of stage 3 322
Figure 7.4.4-1 A comparison of coaxial cable configurations 331
Figure 7.4.4-2 The details of signal propagation within a stage 3 signal projection neuron 332
Figure 7.4.4-3 The electrical circuits used to describe an axon (a coaxial cable) 333
Figure 7.4.4-4 The capacitance and inductance of an ideal axon segment 334
Figure 7.4.4-6 Measured impedance (inductive & capacitive) of a real axon 335
Figure 7.4.5-1 Saltatory conduction in a normal rat ventral root fiber 337
Figure 7.5.1-1 The derivation of the PST histogram and its peculiarities 341
Figure 7.5.1-2 The transposition of a data record into a histogram in hearing 343
Figure 7.5.1-3 Rate-Intensity functions for stage 3 neurons responding to an external stimulus 344
Figure 7.5.1-4 Old and New PST histograms for a differencing channel neuron 345
Figure 7.5.1-5 A comparison of graphics discounting the chopper concept 346
Figure 7.5.2-1 Stylized PST histograms from the medial geniculate nucleus 348

SUBJECT INDEX (using advanced indexing option)

acetylcholine 323
acoustic environment 325
action potential 293, 294, 296-298, 300-302, 308-322, 324, 327, 328, 330, 336, 338-342, 344-350
Activa 293, 296, 302, 303, 305-312, 315, 317, 318, 326, 327, 331, 332
adaptation 314, 344, 346, 349, 350
adaptation amplifier 349
alarm mode 319
amplification 305, 317
attention 349
auditory nerve 297-300, 313, 315, 316, 319, 321, 323, 339, 340, 342, 344, 346, 348-350
average velocity 296, 334, 336, 338
awareness mode 319, 321
axon segment 296, 302-307, 313, 321, 326, 328, 330-335, 338
axoplasm 302-304, 308, 309, 311, 317, 331
bilayer 309
broadband 297, 349
Brownian motion 308
cable theory 326
calibration 337
chopper neuron 343
chord 299, 308
coaxial cable 324, 329-333
cochlear nucleus 294, 298, 302, 312, 319-321, 323, 346, 347, 350
cochleotopic 298
coding/modulation 298, 299
colliculus 294, 350
common-base 307
compensation 349
computation 326, 336
computational 330
conduction velocity 336
conexus 296, 297, 301, 302, 305-308, 313, 327, 334, 338
conforming PST histogram 340, 344, 345, 350
decoder 317, 318
diode 303, 306, 307, 310, 344
dynamic range 298, 344
electromagnetic propagation 324
electrostenolytic process 323
encoder 296, 304, 312, 316, 318, 342, 350
extended PST histogram 340, 342, 346, 347
GABA 323
ganglion neuron 296, 303, 304, 311, 312, 314, 317-319, 321, 331, 342
Gaussian 319
General Wave Equation 324, 326, 328, 329
glutamate 323
group velocity 333
Hankel function 349
Hermann cable 325, 326, 333
hole 324
hydronium 303
impedance measurements 335
independence principle 328
inferior colliculus 350
instantaneous velocity 297, 312
interneuron 305, 336
IPI 338, 340, 345-349

IPI histogram 340, 346, 347
ISI 321, 345
liquid-crystal 303
liquid-crystalline 307, 324
local circuit 326, 336
locomotion 301
masking 319
medial geniculate 348
mesotopic 344
modulation 298, 299, 316, 317, 350
monopulse 302, 305, 314, 315, 332
monopulse oscillator 332
myelin 302-304, 306, 307, 312, 317, 326, 330, 331, 334
myelinated 297, 302-304, 309, 310, 312, 324, 326, 328, 329, 331, 332, 334-336, 338
Myelination 302, 326, 330-334
N1 339
neurite 302, 312, 322
neurites 294, 311, 329
node A 319
node E 321
node E' 297
Node of Ranvier 293, 296, 298, 303-307, 309-314, 317, 330, 331, 334, 336-338
noise 298, 299, 311, 319, 340, 344, 346
OHC 297, 311, 320, 342, 350
P/D equation 340, 346
patch-clamp 304, 307, 312, 344
peak-splitting 348
pedestal 314
phase velocity 333-336, 338
phase-locking 314, 349
phylogenic tree 298
poda 307
poditic 296, 302, 304, 312, 317, 319, 331
propagation velocity 303, 312, 333, 336
pseudo-action potential 309
pulse-to-pulse 300, 311, 316, 339, 346-348
pyramid neuron 294
Rayleigh wave 313
refractory period 311, 342, 348
residue 323
saliency map 350
signal-to-noise 344
signal-to-noise ratio 344
simple neurons 302
spiral ganglia 294, 297, 298, 302, 312, 340, 349
SPL 346, 350
stage 0 346
stage 1 ..... 295, 298, 319, 324, 342, 344, 346
stage 2 ..... 296, 300, 312, 317, 321
stage 3 ..... 293-309, 311, 312, 317-319, 321-325, 327, 328, 330, 332-334, 336, 338, 340, 342, 344, 348-350
stage 4 ..... 295, 296
stage 6 ..... 301, 334
stellate 294-296, 302, 304, 321, 327
stellate cell 294
stellate neuron 294, 296, 304
stellite 294-296, 298, 300, 302-304, 309, 318-322
stellite neuron 294-296, 304, 319, 320
superior colliculus 294
synapse 298, 302-305, 307, 312, 331, 338
synchronization index 314-317
tectorial membrane 314

topology 300, 301, 304
type 1 305
type 2 305
type B 297
type I 297, 298, 321
type II 297, 321
type N 295, 297
verification 305
voltage clamp 327, 328, 336
word-serial/bit-parallel 350

Endnotes

1. Carpenter, M. Sutin, J. (1983) Human neuroanatomy, 8th Ed. Baltimore, MD: Williams & Wilkins page 644
2. Young, E. Robert, J-M, & Shofner, W. (1988) Regularity and latency of units in ventral cochlear nucleus: *J Neurophysiol* vol. 60, no. 1, pp 1-29
3. Lewis, E. & Henry, K. (1989) Transient responses to tone bursts *Hear Res* vol 37(3), pp 219-239
4. Schwartz, A. (1986) Auditory nerve and spiral ganglion cells: morphology and organization *In* Altschuler, D. Hoffman, D. & Bobbin, R. *ed.* Neurobiology of Hearing: The Cochlea NY: Raven Press pp 1-21
5. Brown, M. & Ledwith, J. (1990) Projections of thin (type-II) and thick (type I) auditory-nerve fibers into the cochlear nucleus of the mouse *Hear Res* vol. 49, pp 105-118
6. Evans, E (1972) The frequency response and other properties of single fibres in the guinea-pig cochlear nerve *J Physiol* vol 226, pp 263-287
7. Geisler, C. (1998) From sound to synapse. NY: Oxford Univ. Press page 17 and chapter 12
8. Harrison, J. & Howe, M. (1974) Anatomy of the afferent auditory nervous system of mammals *In* Keidel, W. & Neff, W. *eds.* Auditory System. NY: Springer-Verlag Chapter 9
9. Brown, M. & Ledwith, J. (1990) Projections of thin (type-II) and thick (type I) auditory-nerve fibers into the cochlear nucleus of the mouse *Hear Res* vol. 49, pp 105-118
10. Whitfield, I. (1978) The neural code *In* Carterette, E. & Friedman, M. *eds.* Handbook of Perception. NY: Academic Press Chapter 5, pp 163-184
11. Panter, P. (1965) Modulation, Noise and Spectral Analysis. NY: McGraw-Hill pgs 1 & 604
12. Perkle & Bullock (1973) Approaches to coding *In* Schmidt, F & Melnechuk, T. *eds. Neuroscience Research symposium Summaries*, vol. 6. Cambridge, MA: MIT Press
13. Hind, J. Anderson, D. Brugge, J. & Rose, J. (1967) Coding of information pertaining to paired low-frequency tones in single auditory nerve fibers of the squirrel monkey *J Neurosci* vol 30, pp 794-816
14. Gelfand, S. (1998) Hearing NY: Marcel Dekker pg 184
15. Abbas, P. & Miller, C. (2004) Biophysics and physiology *In* Zeng, F-G. Popper, A. & Fay, R. *eds* Cochlear Implants: Auditory Prostheses and Electrical Hearing NY: Springer Chapter 5
16. Hodgkin, A. & Huxley, A. (1952) A quantitative description of membrane current and its application to conduction and excitation in nerve. *J. Physiol.* vol. 117, pp 500-544
17. Yost, W. (2000) Fundamentals of Hearing, 4th Ed. NY: Academic Press pg 289
18. Ottoson, D. & Svaetichin, G. (1953) The electrical activity of the retinal layer *Acta Physiol Scand* vol 29(1), pp 31-39
19. Waxman, S. Kocsis, J. & Stys, P. (1995) The Axon. NY: Oxford University Press
20. Tasaki, I. (1982) Physiology and electrochemistry of nerve fibers. NY: Academic Press. pp. 37-61
21. Siegel, J. (1992) Spontaneous synaptic potentials from afferent terminals in the guinea pig cochlea Hear Res vol 59, pp 85-92
22. Steriade, M. Jones, E. & Llinas, R. (1990) Thalamic oscillations and signaling. NY: John Wiley, pp 132-133
23. Goldbeter, A. & Moran, F. (1988) Dynamics of a biochemical system with multiple oscillatory domains as a clue for multiple modes of neuronal oscillations *Euro Biophys J* vol 15(5), pp 277-287
24. Fulton, J. (2004) Biological Vision: A 21st Century Tutorial. Victoria, BC, Canada: Trafford pp 65-70
25. Gray, T. (1954) Applied Electronics. NY: John Wiley & Sons pp 819-825
26. Mueller, P. & Rudin, D. (1968) Resting and action potentials in experimental bimolecular lipid membranes *J Theor Biol* vol 18, pp 222-258
27. Mueller, P. & Rudin, D. (1968) Action potentials induced in biomolecular lipid membranes *Nature* vol 217, pp 713-719
28. Schwarz, J. & Eikhof, G. (1987) Na currents and action potentials in rat myelinated nerve fibres at 20 and 37C. Pflugers Archives-European Journal of Physiology, vol. 409, pp. 569-577
29. Schwarz, J. & Eikhof, G. (1987) Na currents and action potentials in rat myelinated nerve fibres at 20 and 37 Celsius. *Pflugers Arch.* vol. 409, pp. 569-577
30. Hodgkin, A. & Huxley, A. (1952) A quantitative description of membrane current and its application to conduction and excitation in nerve *J Physiol* vol 117, pp 500-544
31. Abas, P. & Miller, C. (2004) Biophysics and physiology *In* Zeng, F-G. Popper, A. & Fay, R. *eds.* Cochlear Implants: Auditory Prostheses and Electric Hearing NY: Springer pp 161-164
32. Mueller, P. & Rudin, D. (1968) Op. Cit. *Nature* vol. 217, pg 714
33. Mueller, P. & Rudin, D. (1968) Op. Cit. *J Theor Biol* vol. 18, pg 237
34. Golding, N. & Oertel, D. (1996) Context-dependent synaptic action of glycinergic and GABAergic inputs in the dorsal cochlear nucleus *J Neurosci* vol 16(7), pp 2208-2219
35. Smolders, J. & Klinke, R. (1986) synchronized responses of primary auditory fibre-populations in *Caiman crocodilus* (L.) to single tones and clicks *Hear Res* vol. 24, pp 89-103
36. Rose, J. (1959) (1959) Organization of frequency sensitive neurons in the cochlear nuclear complex of the cat *In* Rasmussen, G. & Windle, W. *eds.* Neural Mechanisms of the Auditory and Vestibular Systems. Springfield Il: Charles C. Thomas Chap 9 pg 123
37. Goldberg, J. & Brown, J. (1969) Response of binaural neurons of dog superior olivary complex to dichotic tonal stimuli: some physiological mechanisms of sound localization *J Neurophysiol* vol 32, pp 613-636
38. Delgutte, B. (1980) Representation of speech-like sounds in the discharge patterns of auditory-nerve fibers *J Acoust Soc Am* vol 68(3), pp 843-857
39. Javel, E. (1988) Acoustic and electrical encoding of temporal information *In* Miller, J. &. Spelman, F. *eds.* Cochlear Implants: Models of the Electrically Stimulated Ear. Englewood Cliffs, NJ: Prentice Hall pg 285
40. Javel, E. (1988) Basic response properties of auditory nerve fibers *In* Altschuler, R. Hoffman, D. & Bobbin, R. *eds.* Neurobiology of Hearing: The Cochlea NY: Raven Press. Chapter 13, pg 284
41. Tasaki, I. (1968) Nerve excitation: A macromolecular approach. Springfield, Ill: Charles C. Thomas also in Tower, D. (1975) The basic neurosciences, vol. 1 NY: Raven Press pg. 177-195
42. Carlyon, R. & Deeks, J. (2002) Limitations on rate discrimination *J Acoust Soc Am* vol. 112(3), pt 1, pp 1009-1014
43. Johnson, D. (1980) Op. Cit. pg 1116
44. Inoue, I. Kobatake, Y. & Tasaki, I. (1973) Excitability instability and phase transitions in squid membrane under internal perfusion with dilute salt solutions. Biochem. Biophys. Acta. vol. 307, pp. 371-377
45. Miller, C. Abbas, P. & Robinson, B. (2001) Response properties of the refractory auditory nerve fiber *JARO* vol 2, pp 216-232

46. Pfeiffer, R. & Kim, D. (1972) Response patterns of single cochlear nerve fibers to click stimuli: descriptions for cat *J Acoust Soc Am* vol. 52(6) pt 2, pp 1669-1677
47. Palmer, A. & Evans, E. (1982) Intensity coding in the auditory periphery of the cat: responses of cochlear nerve and cochlear nucleus neurons to signals in the presence of bandstop masking noise *Hear Res* vol. 7, pp 305-323
48. Javel, E. (1988) Acoustic and electrical encoding of temporal information *In* Miller, J. &. Spelman, F. *eds.* Cochlear Implants" Models of the Electrically Stimulated Ear. Englewood Cliffs, NJ: Prentice Hall Chapter 17
49. Delgutte, B. (1980) Representation of speech-like sounds in the discharge patterns of auditory-nerve fibers *J Acous Soc Am* vol. 68(3), pp 843-857
50. Young, E. Shofner, W. White, J. Robert, J-M, & Voigt, H. (1988) Response properties of cochlear nucleus neurons in relationship to physiological mechanisms *In* Edelman, G. Gall, W. & Cowan, W. *eds.* Auditory Function: Neurobiological Bases of Hearing. NY: John Wiley & Sons Chapter 9, pg 307
51. Wenthold, R. & Martin, M. (1984) Neurotransmitters of the auditory nerve and central auditory system *In* Berlin, C. Hearing Science. Philadelphia, Pa: Taylor & Francis Chapter 10, pp 342-369
52. Oertel, D. Wu, S. Hirsch, J. (1988) Electrical characteristics of cells and neuronal circuitry in the cochlear nuclei *In* Edelman, G.
53. Richet, P. (2007 in Eng, 1999 in French) A Natural History of Time. Chicago, Il: University of Chicago Press pg 198
54. Bockris, J. & Reddy, A. (1970) Modern Electrochemistry, vol. 1. NY: Plenum Chapter 5
55. Piccolino, M. (1998) Animal electricity and the birth of electrophysiology: the legacy of Luigi Galvani *Brain Res Bull* vol. 46, no. 5, pp 381-407
56. Hermann, L. (1905) Lehrbuch der Physiologie, 13th ed. Berlin. See also Hille, pg. 27
57. Ludimar Hermann, *Untersuchungen über den Stoffwechsel der Muskeln ausgehend von des Gaswechsel derselben* (Berlin, 1867). The results reported in this book are extended and summarized in the revised third edition of Hermann's textbook, *Grundriss der Physiologie des Menschen* (Berlin, 1870), esp. 233-239. The *Grundriss* was published first in 1863 .
58. Lenoir, T (1987) Models and Instruments in the Development of Electrophysiology, 1945-1912 *In* Historical Studies in the Physical Sciences, Vol. 17. Berkeley: University of California Press pp 1-54 *Also available on the web in 2003* http://www.stanford.edu/dept/HPST/TimLenoir/Publications/Lenoir_ModelsInstruments.pdf.
59. Cole, K. (1968) Membranes, Ions & Impulses. Berkeley, CA: University of California Press pp 77-87
60. Kraus, J. (1953) Electromagnetics. NY: McGraw-Hill pp. 417-444
61. Cole, K. (1968) Membranes, Ions and Impulses: A Chapter of Classical Biophysics. Los Angeles, CA: University of California Press, pp 77-103
62. Taylor, R. (1963) Cable Theory *in* Nastuk, W. *Ed.* Physical Techniques in Biological Research. NY: Academic Press
63. Goldman, L. & Albus, J. (1968) Computation of impulse conduction in myelinated fibers; theoretical basis of the velocity-diameter relationship *Biophys Journal* vol. 8, pp 596-607
64. Rall, W. (1977) Core conductor theory and cable properties of neurons. Chapter 3 *In* Handbook of Physiology, Section 1, Vol. I, Kandel, E. *ed.* pg. 60
65. Rall, W. (1989) Cable theory for dendritic neurons *In* Koch, C. & Segev, I. eds. Methods in neuronal modeling: From synapses to networks. MIT Press pp 9 - 92
66. Ritchie, J. (1995) Physiology of axons *In* Waxman, S. Kocsis, J. & Stys, P. The Axon. NY: Oxford University Press pp 68-73
67. Hodgkin, A. & Huxley, A. (1952) A quantitative description of membrane current and its application to conduction and excitation in nerve *J Physiol* vol 117, pp 500-544
68. Hodgkin, A. (1951) The ionic basis of electrical activity in nerve and muscle *Biol Rev.* Vol. 26, pp 339-409
69. Frankenhaeuser, B. & Huxley, A. (1964) The action potential in the myelinated nerve fibre of Xen opus laevis as computed on the basis of voltage clamp data *J. Physiol.* vol. 171, pp 302-315
70. Cole, K. (1966) The melding of membrane models *Ann NY Acad Sci* pp 405-408
71. Ramo, S. & Whinnery, J. (1953) *& subsequent additions.* Fields and Waves in Modern Radio. NY: John Wiley & Sons
72. Finley, C. Wilson, B. & White, M. (1988) Models of neural responsiveness to electrical stimulation In Miller, J. &. Spelman, F. *eds.* Cochlear Implants" Models of the Electrically Stimulated Ear. Englewood Cliffs, NJ: Prentice Hall Chapter 5
73. Pannese, E. (1994) Neurocytology. NY: Thieme, pg 60
74. Schwan, H. (1963) Determination of biological impedances *In* Physical Techniques in Biological Research NY: Academic Press pp 323-406
75. Chie, S. & Ritchie, J. (1980) Potassium channels in nodal and internodal axonal membrane of mammalian myelinated fibers *Nature* vol. 284, pp 170-171
76. Ritchie, J. (1995) Physiology of axons. *In* The Axon. Waxman, S. Kocsis, J. & Stys, P. Ed. NY: Oxford Univ. Press pg. 84
77. Frankenhaeuser, B. & Huxley, A. (1964) The action potential in the myelinated nerve fibre of Xenopus Laevis as computed on the basis of voltage clamp data. J. Physiol. (London) vol. 171, pp. 302-315
78. Frankenhaeuser, B. & Huxley, A. (1964) Op. Cit.
79. Goldman, L. & Albus, J. (1968) Computation of impulse conduction in myelinated fibers; theoretical basis of the velocity-diameter relation. Biophysical Journal, vol. 8, pp. 596-607
80. Huxley, A. & Stampfli, R. (1949) Evidence for saltatory conduction in peripheral myelinated nerve fibres. *J Physiol* Vol. 108, pp. 315-339. [Also at Stampfli, R. (1981) Overview of studies on the physiology of conduction in myelinated nerve fibers. *In* Demyelinating Disease: basic and clinical electrophysiology, Waxman, S. & Ritchie, J. *ed.* NY: Raven Press pp. 11-23]
81. Smith, K. Bostock, H. & Hall, S. (1982) Saltatory conduction precedes remyelination in axons demyelinated with lysophophatidyl choline *J Neurol Sci* vol. 54, pp 13+
82. Bostock, H. (1982) Conduction changes in mammalian axons following experimental demyelination, *in* Culp, W. & Ochoa, J. *eds.* Abnormal Nerves and Muscles as Impulse Generators. NY: Oxford University Press pp 236-252
83. Bostock, H. (1993) Impulse propagation in experimental neuropathy. *In* Peripheral Neuropathy, 3rd. Dyck, P. & Thomas, P. *eds.* Philadelphia: W. B. Saunders pp. 109-120
84. Rasminsky, M. & Sears, T. (1972) Op. Cit.
85. Rasminsky, M. & Sears, T. (1972) Internodal conduction in undissected demyelinated nerve fibres. *J Physiol* vol. 227(2), pp 323-350
86. Gulick, W. Gescheider, G. & Frisina, R. (1989) Hearing. NY: Oxford University Press pg 177
87. Javel. E. (1988) Acoustic and electrical encoding of temporal information *In* Miller, J. &. Spelman, F. *eds.* Cochlear Implants" Models of the Electrically Stimulated Ear. Englewood Cliffs, NJ: Prentice Hall Chapter 17
88. Smith, R. & Brachman, M. (1980) Operating range and maximum response of single auditory nerve fibers *Brain Res* vol 184, pp 499-505
89. NIST/SEMATECH e-Handbook of Statistical Methods, http://www.itl.nist.gov/div898/handbook/
90. Young, F. Valero-Mora, P. & Friendly, M. (2006) Visual Statistics. NY: John Wiley & Sons pp 183-213
91. Keidel, W. (1974) Information processing in the higher parts of the auditory pathway *In* Zwicker, E. & Terhardt, E. *eds.* Facts and Models in Hearing. NY: Springer-Verlag pg 216+

92. Javel, E. (1986) Basic response properties of auditory nerve fibers In Altschuler, R. et al. Op. Cit. Chapter 13, pg 221
93. Kiang, N. (1965) Discharge patterns of single fibers in the cat's auditory nerve. Cambridge, Ma: MIT Press monograph #35, pg 113
94. Moore, B. (1995) Hearing. NY: Academic Press pg 86-88
95. Javel, E. (1988) Physiological and psychophysical correlates of temporal processes in hearing *Hear Res* vol 34, pp 275-294
96. Bourke, T. (1976) Electrical responses of neural units in the anteroventral cochlear nucleus of the cat (PhD Thesis) Cambridge, MA. MIT Press
97. Johnson, D. (1980) The relationship between spike rate and synchrony in responses of auditory-nerve fibers to single tones *J Acoust Soc Am* vol 68(4), pp 1115-1122
98. Javel, E. (1986) Op. Cit. pg 218
99. Johnson, D. (1980) The relationship between spike rate and synchrony in responses of auditory-nerve fibers to single tones *J Acoust Soc Am* vol. 68(4), pp 1115-1122
100. Young, E. Robert, J-M. & Shofner, W. (1988) Op. Cit.
101. Javel, E. (1980) Coding of AM tones in the chinchilla auditory nerve; implications for the pitch of complex tones *J Acoust Soc Am* vol 68(1), pp 133-146
102. Keidel, W. (1974) Op. Cit.
103. Phillips, D. (1988) Introduction to anatomy and physiology of the central auditory nervous system *In* Jahn, A. & Santos-Sacchi, *eds.* Physiology of the Ear. NY: Raven Press pp 407-429
104. Palmer, A. & Russell, I. (1986) Phase-locking in the cochlear nerve of the guinea-pig and its relation to the receptor potential of inner hair-cells *Hear Res* vol 24, pp 1-15
105. Anderson, D. Rose, J. Hind, J. & Brugge, J. (1970) Temporal position of discharges in single auditory nerve fibers within the cycle of a sine-wave stimulus frequency and intensity effects *J Acoust Soc Am* vol. 49(4), pt 2, pp 1131-1139
106. Rose, J. Hind, J. Anderson, D. & Brugge, J.(1971) Some effects of stimulus intensity on response of auditory nerve fibers in the squirrel monkey *J Neurophysiol* vol 34, pp 685-699
107. Smoorenburg, G. Gibson, M. Kitzes, L. Rose, J. & Hind, J. (1976) Correlates of combination tones observed in the response of neurons in the anteroventral cochlear nucleus of the cat *J Acoust Soc Am* vol 59(4), pp 945-962
108. Johnson, D. (1980) The relationship between spike rate and synchrony in responses of auditory-nerve fibers to single tones *J Acoust Soc Am* vol. 68(4), pp 1115-1122
109. Shofner, W. & Young, E. (1985) Excitatory/inhibitory response types in the cochlear nucleus . . . . *J Neurophysiol* vol 54(4), pp 917-939
110. Young, E. Robert, J-M. & Shofner, W. (1988) Op. Cit.
111. Evans, E. & Whitfield, I. (1964) Classification of unit responses in the auditory cortex of the unanaesthetized and unrestrained cat *J Physiol* vol 171, pp 476-493
112. McAlpine, D. Jiang, D. Shackleton, T. & Palmer, A. (1998) Convergent input from brainstem coincidence detectors onto delay-sensitive neuron in the inferior colliculus *J Neurosci* vol. 18(15), pp 6026-6039